
NASA CONTRACTOR REPORT




NASA CR



NASA CR-461

# DEVELOPMENT OF EPITAXIAL STRUCTURES FOR RADIATION RESISTANT SILICON SOLAR CELLS

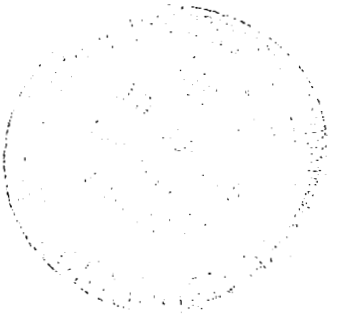

Prepared under Contract No. NAS 5-3559 *by*
TEXAS INSTRUMENTS, INC.
Dallas, Texas
*for Goddard Space Flight Center*

NATIONAL AERONAUTICS AND SPACE ADMINISTRATION - WASHINGTON, D. C. - MAY 1966

NASA CR-461

# DEVELOPMENT OF EPITAXIAL STRUCTURES FOR RADIATION RESISTANT SILICON SOLAR CELLS



Prepared under Contract No. NAS 5-3559 by
TEXAS INSTRUMENTS, INC.
Dallas, Texas

for Goddard Space Flight Center

NATIONAL AERONAUTICS AND SPACE ADMINISTRATION

For sale by the Clearinghouse for Federal Scientific and Technical Information
Springfield, Virginia 22151 – Price $4.00

TEXAS INSTRUMENTS INCORPORATED
Semiconductor-Components Division
Post Office Box 5012
Dallas, Texas 75222

# Technical Summary Report
# on
# Development of Epitaxial Structures
# for
# Radiation Resistant Silicon Solar Cells

This report was prepared by Texas Instruments Incorporated under Contract No. NAS5-3559 for the Goddard Space Flight Center of the National Aeronautics and Space Administration. The work was administered under the direction of the Thermal Systems Branch of Goddard Space Flight Center with Dr. P. H. Fang acting as Project Manager.

## FOREWORD

This is the final report of the contract program which started October 1, 1963 and continued, by supplemental extensions, through June 30, 1965. The report was prepared by the Materials Technology Branch, Semiconductor Reserach and Development Laboratory, Semiconductor Components Division, Texas Instruments Incorporated, Dallas, Texas on NASA contract No. NAS 5-3559.

Mr. Kenneth Bean was the project engineer; principal contributors to the research studies were Dr. Earl Alexander and Mr. Stacy Watelski; theoretical analysis as given in Appendix I was provided by Dr. Murray Bullis and Dr. Walter Runyan. Others contributing to the research, computer routines, and report preparation were Mr. Paul Gleim, Mr. Jimmie Sherer, Mr. Ronald Wackwitz, and Mr. Richard Yeakley. All cells were fabricated under the supervision of Mr. Robert Cole and Mr. Raymond Vineyard of the General Products Department, Semiconductor Components Division. Mr. Robert Haire, Mr. Richard Kinsey, and Mr. Rick Strecker were contract administrators.

DEVELOPMENT OF EPITAXIAL STRUCTURES

for

RADIATION RESISTANT SILICON SOLAR CELLS


## ABSTRACT

Experimental silicon drift-field solar cells were produced by means of advanced epitaxial and diffusion technology. Three different approaches were used for producing the drift-field structures and two different procedures were used for cell fabrication. Drift-field structures built by a single-epitaxial-deposit-and-diffusion technique and fabricated into cells by an improved procedure represent the best combination of methods by which a drift-field solar cell may be produced. Excellent reproducibility of cell characteristics and over-all high process yields establish the production feasibility of this procedure to build drift-field solar cells.

A variety of drift-field structures were made, some of which produced cells more resistant to bombardment by one MeV electrons than are ordinary n-p solar cells. A number of sample cells fabricated near the end of the contract period from near-optimum drift-field structures exhibited high current values in the unirradiated state. On the basis of a theoretical analysis of

drift fields which was made, these sample cells when irradiated should show superior radiation resistance.

The theoretical analysis, which took into account the variation of mobility with concentrations, suggests that the ratio of the impurity concentrations in the drift field should not exceed three orders of magnitude. Furthermore, the width of the drift-field probably should not exceed 25 microns. Low carrier lifetime prevents improvement of over-all collection efficiency by use of significantly thicker deposited layers. Longer wave length response was enhanced in some instances by wider drift fields and by higher initial lifetime (e.g. by use of Lopex* silicon or gettering), but the available power after irradiation apparently was not improved.

A method developed for determining the concentration profile in a drift-field structure represents an important advance in cell evaluation.

---

* Texas Instruments Incorporated Tradename.

TABLE OF CONTENTS

LIST OF ILLUSTRATIONS AND TABLES

LIST OF ILLUSTRATIONS AND TABLES

LIST OF ILLUSTRATIONS AND TABLES

# I. INTRODUCTION

## A. Objective

The objective of this program was the development of technology, supported by working models, to prove the production feasibility of an improved radiation-resistant silicon solar cell. The improvement in radiation resistance was to be achieved by building in, by means of silicon epitaxial techniques, a drift field on the base side of the cell junction. The drift field was to be of sufficient magnitude to reduce substantially the effect of lifetime degradation, due to radiation damage, on cell efficiency.

## B. Scope of Work

Achievement of the program involved development and evaluation of various processing and measuring techniques. A large number of epitaxial depositions were made, using the various approaches described in III.C., to provide material for the experiments with diffusion, glassy-layer gettering techniques, and measurements, and for deliverable sample solar cells. This report discusses these various experiments and processing techniques. Sample solar cells were fabricated, insofar as it was possible, using the standard fabrication process so that the epitaxial cells could be directly compared to standard cells without the drift field. Cell characteristics are given for the various sample cells. During the course of the contract period, a concentration gradient profiling method was developed. Description and uses of

this method are found in IV.B. Fairly late in the contract period, it became feasible to make an analysis of drift fields allowing for mobility variations with impurity concentration. This theoretical work, showing the influence of mobility variations on drift field enhancement in silicon junction devices, is attached as Appendix I and referred to in II.

## II. THEORY

The damage introduced in solar cells by high energy electron and proton bombardment results primarily in lifetime degradation. Reduced lifetime in turn lowers the number of photo-generated carriers that diffuse to the junction and contribute to cell output current before recombination. If a proper polarity electric field is present normal to the p-n junction, a carrier will move with a higher velocity than by diffusion alone. Hence, with such a field, carriers can still be collected even if their lifetime has been materially reduced.

An analysis of drift fields was carried out during the contract period and is included in this report as Appendix I. The analysis allows for the variation of carrier mobility with impurity concentration. With the exception noted in the appendix, all previous analyses have neglected the mobility variation. Included in Appendix I, which is entitled "Influence of Mobility Variations on Drift Field Enhancement in Silicon Junction Devices," are the means by which drift-field structures can be optimized to a specified design value of electron lifetime (or integrated flux density).

## III. EPITAXIAL DEPOSITION

This section discusses the experimental procedures and equipment used in building the epitaxial drift-field structures.

### A. Material, Apparatus, and Procedures

#### 1. Substrate Preparation

Two separate procedures were used, depending on the fabrication procedure being followed (See VI).

a. For Fabrication, Procedure I

Boron-doped silicon crystals approximately 2.5 cm in diameter were grown in the [111] direction and sliced parallel to the (111) plane. The slices, 0.058 cm thick, were cut to 1-cm x 2-cm rectangles and lapped on both sides to a thickness of 0.048 cm using 1800 grit aluminum oxide abrasive. The rectangular blanks were then mounted on one side and etch polished with a planar-type etchant (modified CP-4) to a final thickness of 0.038 cm. In a few instances the blanks were polished mechanically rather than by a chemical etch.

b. For Fabrication, Procedure II

Boron-doped silicon crystals were grown in the [111] direction, centerless ground to $3.020 \begin{smallmatrix} + .000 \\ - .005 \end{smallmatrix}$ cm, and sliced parallel to the (111) plane. The slices, 0.056 cm thick, were lapped on both sides (as above) and chemically polished in a rotating teflon cylinder to a final thickness of 0.031 cm. These round substrates were trimmed to standard 1 cm x 2 cm cells after contact application (See VI).

2. Deposition Apparatus and Conditions

Epitaxial deposition of silicon was accomplished by the reduction in hydrogen of high-purity silicon tetrachloride at temperatures from 1180° to 1250°C (emissivity-uncorrected pyrometer readings). A deposition cycle consisted of loading the substrate(s) into the reactor, purging the reactor with helium or forming gas, heating the substrate(s) in hydrogen to about 1200°C, etching* a few microns of silicon from the surface with a mixture of hydrogen, hydrogen chloride and/or silicon tetrachloride, depositing the required thickness of silicon, cooling the reactor and contents in hydrogen to near ambient temperature, flushing the reactor with helium or forming gas, and removing the epitaxial slices.

Both horizontal and vertical epitaxial reactors were used. The flow system for the reactors is shown in the photographs of Figure 1 and indicated schematically in Figure 2. Both systems are equipped with variable leaks for regulation of flow of the dopant gas (diborane in hydrogen) into the reactant gas stream.

Epitaxial silicon growth rates were nominally two microns per minute. Thickness and resistivities of the epitaxial layers were measured as described in III.D.

B. General Considerations

As indicated in II., a change in impurity concentration of from about two to four orders of magnitude in the

---

* Vapor etching of the silicon substrate immediately prior to epitaxial deposition has been shown[1] to be highly desirable for the production of near-perfect crystal structures.

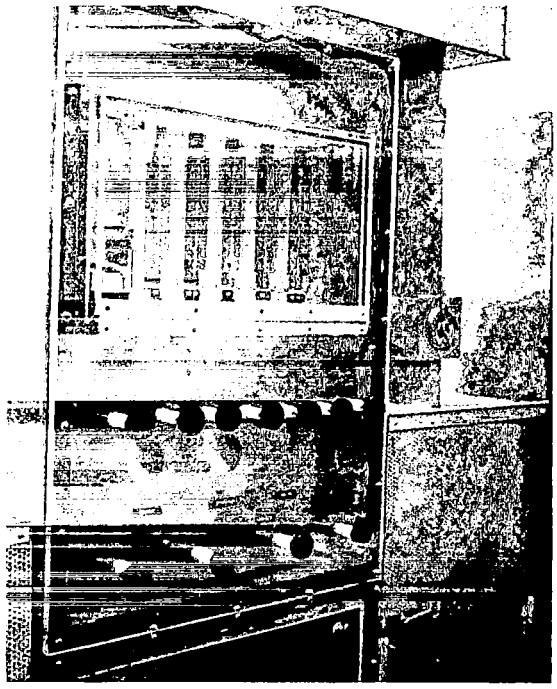

Epitaxial Control Panel and Reactor Enclosure

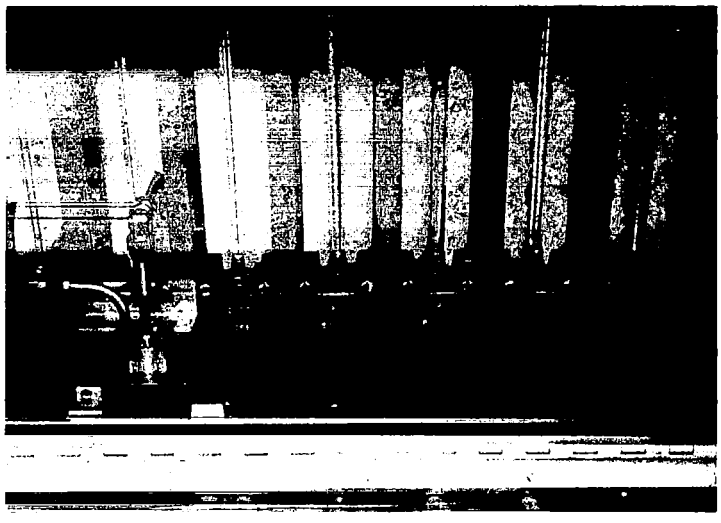

Gas Flow Metering Portion of Control Panel

Fig. 1

EPITAXIAL SYSTEM

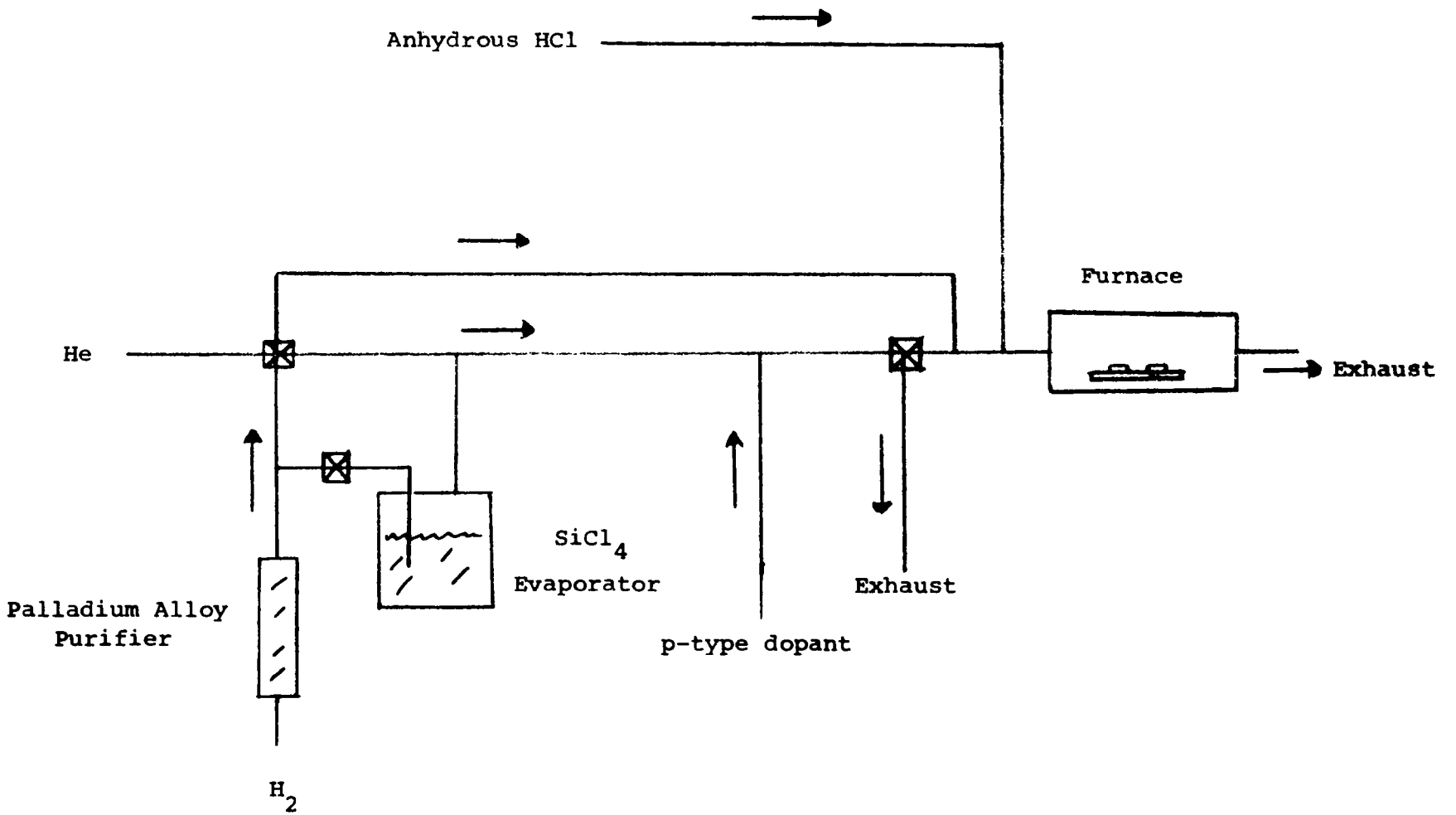


Figure 2

base region must occur within a short distance of the junction. Epitaxial techniques are suited for producing such changes in concentration within a crystal, but there are some limitations that must be observed.

Doping concentrations available vary from between $10^{14}$ to $10^{15}$ impurity atoms/cc of silicon (determined by the purity of the starting silicon tetrachloride and reactor and feed system cleanliness) to between $10^{19}$ and $10^{20}$ atoms/cc, determined by the ability to grow high perfection films.

Impurity adsorption in the growth chamber and feed lines makes it somewhat difficult to decrease the concentration during a reasonable length growing cycle by more than two orders of magnitude (See Fig. 3a). The reverse process, that of starting growth at a very low impurity concentration, has only the time constant associated with the time to transport the impurity element from a metering valve to the growth site.

Various competing reactions occurring during deposition, which transport silicon and impurities previously deposited (or from the substrate) back into the growth chamber often make production of lightly doped films on heavily doped substrates difficult. The severity of the problem, shown schematically in Fig. 3b, depends somewhat on the type of impurity used and the abruptness of the desired transition.

Since epitaxial silicon normally is grown at temperatures from 1100° to 1300°C, appreciable diffusion of the impurities occurs during deposition, which can in many cases alter the concentration profile (see Fig. 3c). For

Fig. 3 - Variations in Doping Level

a.

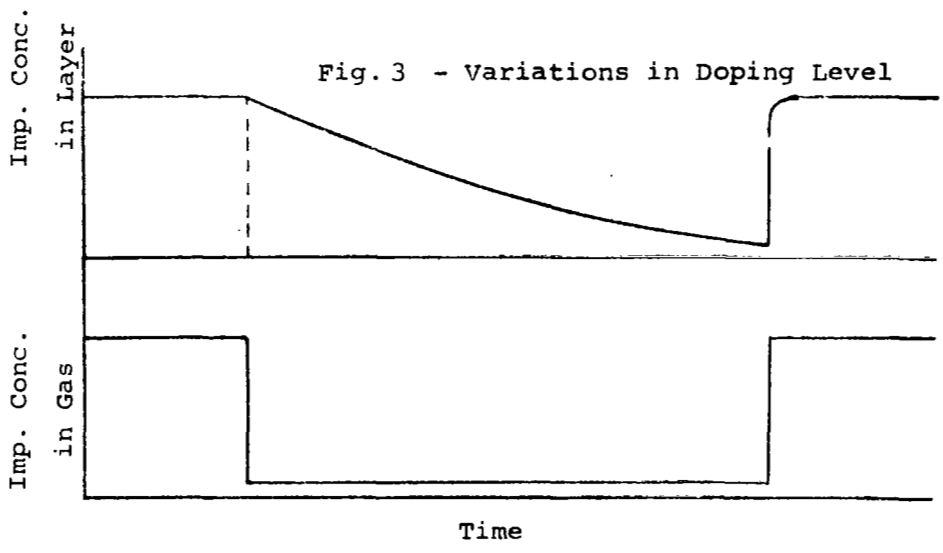


b.

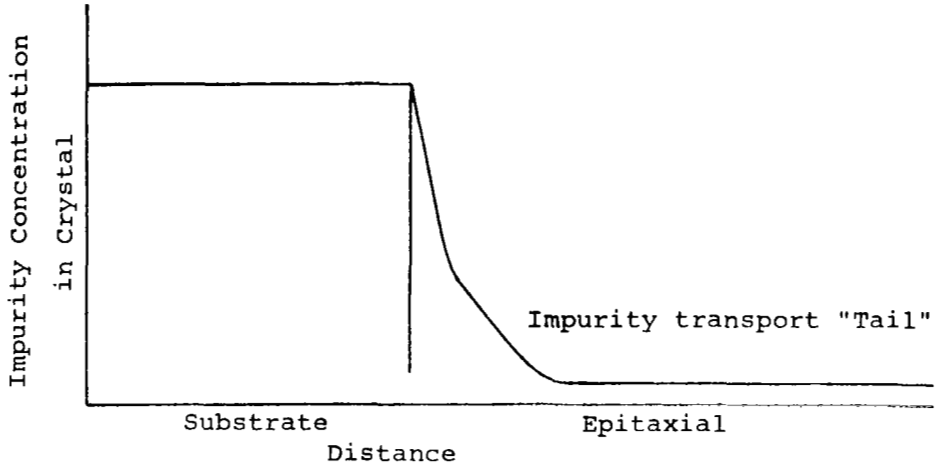


c.

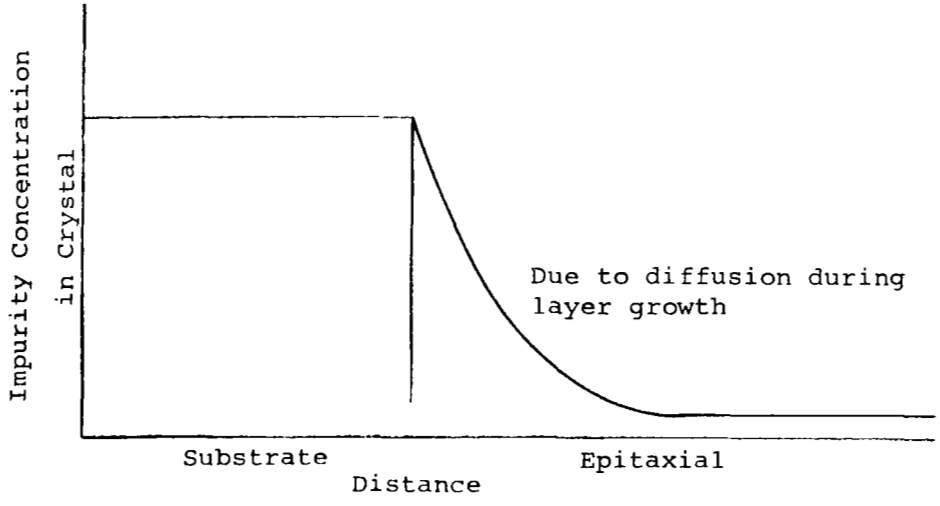

the present objective, the development of an epitaxial drift-field base, this did not pose a problem, since allowance could be made in the subsequent drift diffusion step (IV.A).

The problem of determining the concentration profile actually occurring in the structure is involved and subject to error. A significant advance, however, in determining the profile is reported in IV.B.

Epitaxial films of thicknesses from less than one micron to more than 100 microns can be grown, but the number of crystalline imperfections in the thicker deposits usually is higher.

Carrier lifetime in the deposited film is difficult to measure, but normally is quite low, e.g., between 0.1 to 1.0 microseconds. The cause of this low lifetime in epitaxial materials is not fully understood, but may be attributed in part to accidental transition metal doping.

## C. Approaches Selected for Formation of Epitaxial Drift-field Base

Three specific means which were used to introduce drift fields into epitaxial layers will now be considered. Although the resistivities and thicknesses of the layers in the examples do not correspond to the "optimum" fields described in II, the examples are nonetheless illustrative of the techniques by which the drift fields may be made.

1. Epitaxial Deposition Followed by Diffusion

If a substrate thick enough for mechanical strength (100 to 150 microns or thicker) with an initial doping concentration level of $4 \times 10^{19}$ atoms of boron/cc of silicon ($\approx 0.003\ \Omega$-cm) has a 30 micron layer of silicon with $1.5 \times 10^{15}$ boron atoms/cc ($9\Omega$-cm) added to it, the concentration profile after a fifteen minute growing cycle at 1250°C is as shown in Fig. 4a and is due only to diffusion.

Calculation of the doping profile as a result of diffusion from a concentration step (with the same impurity element on both sides of the step) proceeds from an equation of the form:[2]

$$N(x,t) = \left(\frac{N_1 + N_0}{2}\right) + \left(\frac{N_0 - N_1}{2}\right) \operatorname{erf}\left(\frac{x}{2\sqrt{Dt}}\right)$$

where $N_0$ and $N_1$ are the concentrations on either side of the step, $\pm x$ is the distance from the step, t is the diffusion time, D is the diffusion coefficient for boron in silicon, and the last factor denotes the error function of the argument $(x/2\sqrt{Dt})$.

Now, if an additional 7.5 hours heating cycle at 1250°C is added to the growing cycle, the profile assumes the form shown in Fig. 4b. By this time the substrate impurities have diffused out nearly to the surface and are distributed over a 30 micron distance. An n-type diffusion from the front then produces a cell with approximately the required gradient. By far the majority of cells produced in this contract (See VII.A) were prepared by this simple approach of a single epitaxial deposition followed by diffusion.

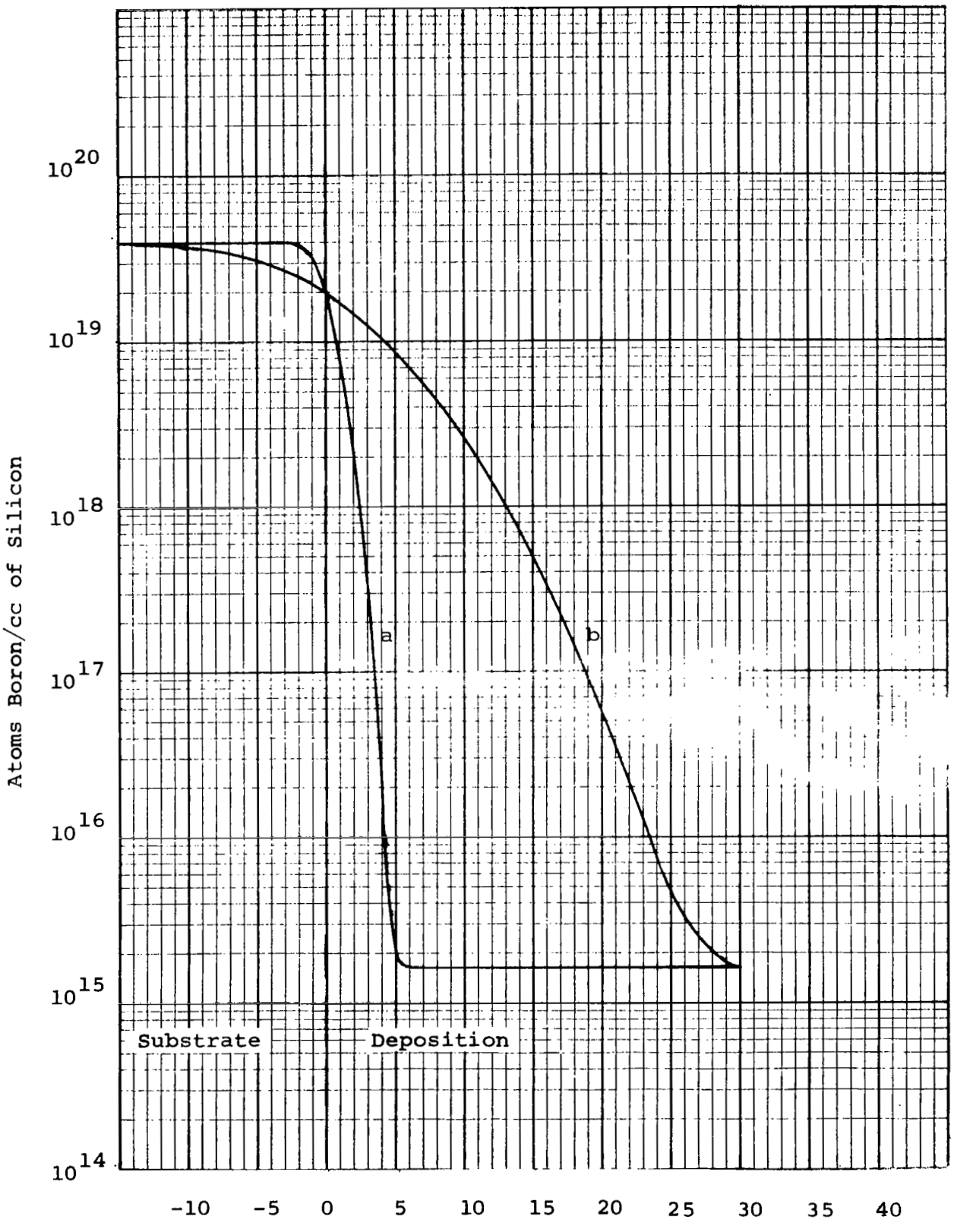


Fig. 4 - Concentration Profile Due to Diffusion

2. Two Epitaxial Layers Followed by Diffusion

Another approach, somewhat more complex, involves the use of two epitaxial reactors and a heavily doped substrate. Here the substrate, doped to about 0.001 Ω-cm, would have a 0.1 Ω-cm layer deposited on it, and then, after removal to another reactor, would have an additional layer of about 10 Ω-cm material deposited thereon. The concentration profile, for the case of two 25-micron, thirty-minute deposits and a three hour diffusion, all at 1250°C, is shown in Fig. 5. Such a profile is an approximation to the distributions which are obtained by the first approach (III.C.1.). This procedure has the virtues of still being relatively simple, much faster than a diffusion from the backside, and avoiding the problem of dope hangover due to adsorption on reactor walls (III.B.). Where the substrate is not so heavily doped, and in certain other instances, it is possible to make the desired two-layer structure by using only a single epitaxial reactor. For such cases, following the first deposition, a few minutes of "purging" in hydrogen helps sweep away the dopant in the reactor prior to the second deposition. Several cells were made from epitaxial structures formed by this two-layers-and-diffusion approach.

3. Dope Programing During Epitaxial Deposition

With sufficiently short feed lines, carefully designed deposition chamber, and a reasonable (but lower) deposition temperature, impurity concentration apparently can be programed down over about four orders of magnitude during epitaxial deposition. Figure 1 of III.A.2. showed

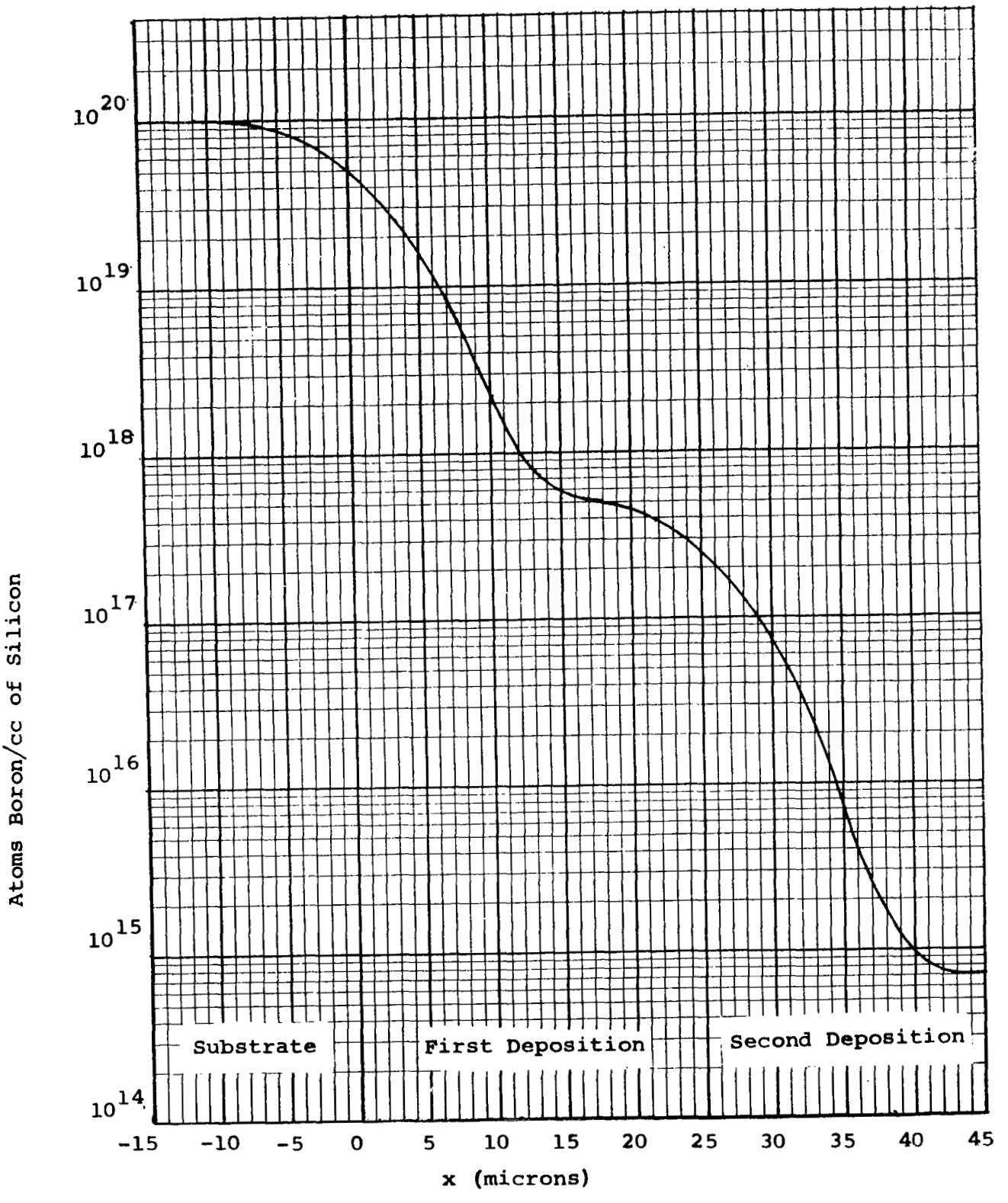


Fig. 5 - Impurity Distribution for a Double Epitaxial Layer

a feed system which has short lines and a dope valving system capable of being motor driven to change the dope gas flow over the required number of orders of magnitude.

For various reasons, this third approach was never fully implemented in this solar cell contract. However, experience gained from some otherwise-unrelated epitaxial work in the laboratory permit the discussion of relative merits of the various epitaxial approaches in the next section. Approximations to this third approach were made by manually adjusting dopant flow in stepwise decrements during deposition. Figure 6a shows a ten-step adjustment of dope gas flow during a 40 micron deposition, with Fig. 6b the desired gradient achieved by diffusion during the deposition. Figure 6c shows a profile which sometimes occurs as a result of the "dope holdover" discussed in III.B. Several deposits, of thickness from 40 to 80 microns, were made by this approach.

4. Relative Merits of the Three Selected Approaches

Although each of these three (and other) approaches may prove feasible for building-in a drift field, certain approaches are to be favored on economic and practical bases. At the beginning of the contract, when it appeared desirable to maximize the number of orders of magnitude difference in dopant concentration from substrate to near the surface, the second approach above (two layers and diffusion) seemed attractive for the reasons cited. For thicker deposits, e.g. above 40 microns, approach three (programed doped) seemd to be favored on the basis of reduced diffusion times. However, since the optimum drift field (see II and Appendix I, section V) is probably no wider than 25 microns and consists of an

Fig. 6 - Dope Programing During Deposition

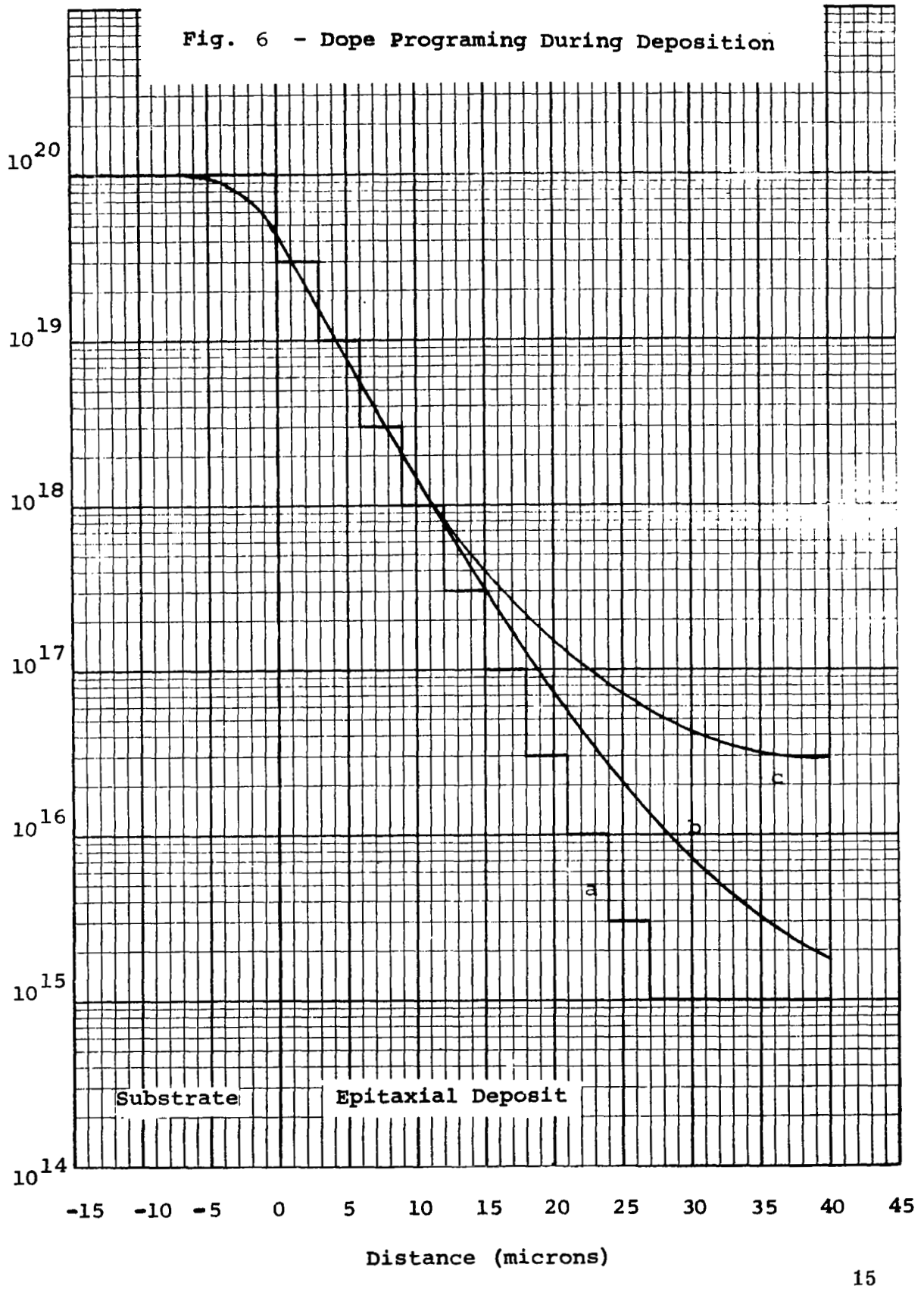

impurity ratio of no more than three orders of magnitude, the attractiveness of approaches two and three are reduced relative to the principal advantages of approach one.

To maintain satisfactory quality control (reproducibility) from one epitaxial run to the next when using approaches two and three would require extensive measurement time for representative samples extracted from the various runs. Although the method developed for determining the concentration profile (IV.B.) would provide the necessary information, the method is not a short, routine measurement.

An additional comment relative to the programed dope approach is in order. Experiments made (outside the realm of this contract) with a motor-driven valving system for regulation of dope gas suggest that while the shape of the dopant profile and the ratio of the impurity concentration at the end points may be easily reproduced, the absolute value of the impurity concentrations at the end points may be displaced either both higher or both lower from one run relative to another. For example, in attempting to repeat the profile shown in Fig. 7a, the lack of absolute resetability of the valve may bring about a profile represented by either curve b or c. There remains the possibility of obtaining a profile curvature as shown in Fig. 6c at the low dopant concentrations. The use of a programed dope arrangement is advocated only for those applications for which ordinary epitaxy and diffusion cannot supply the required concentration profile.

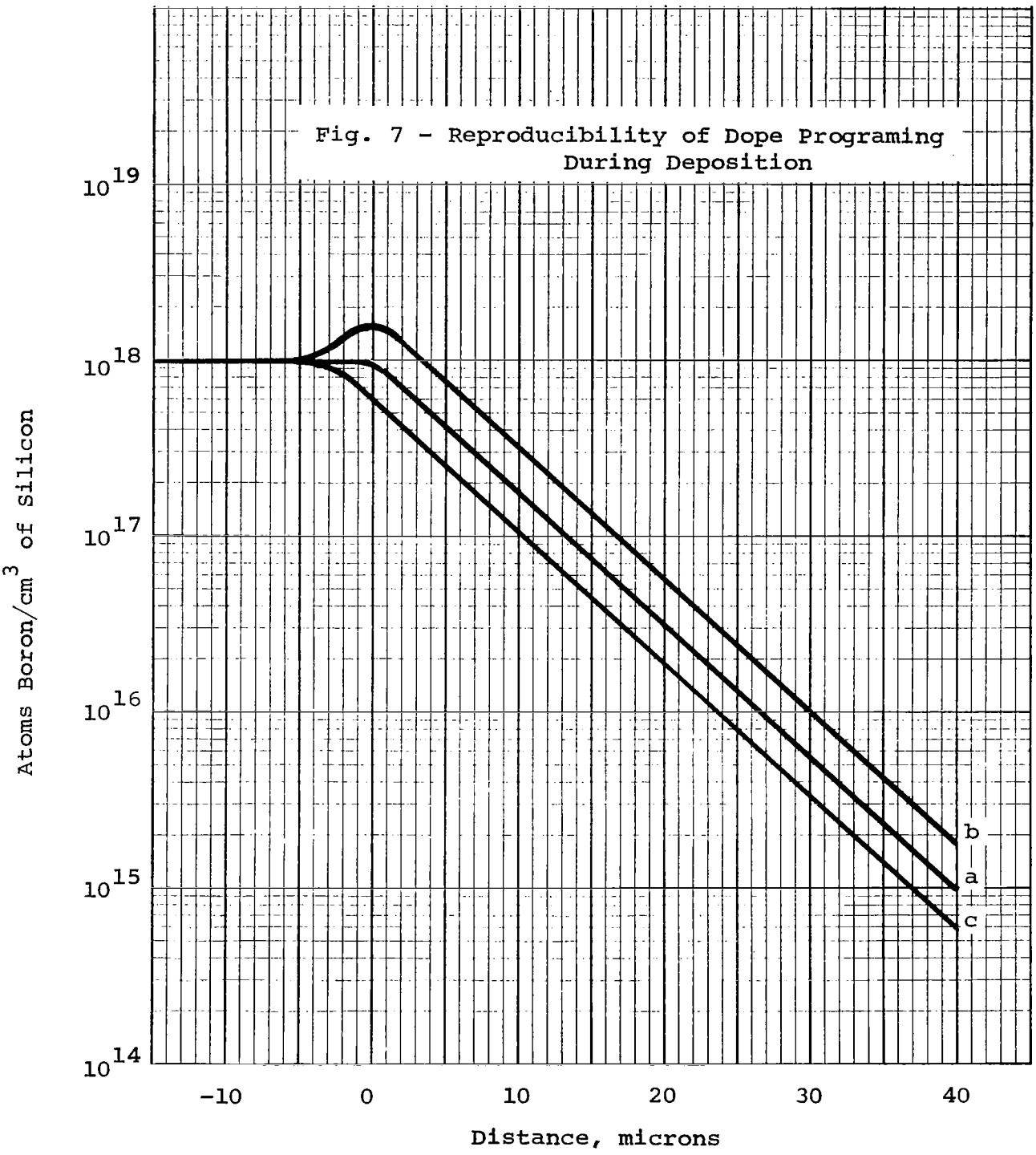
Fig. 7 - Reproducibility of Dope Programing During Deposition
Atoms Boron/cm3 of Silicon
10^19
10^18
10^17
10^16
10^15
10^14
-10
0
10
20
30
40
Distance, microns
b
a
c

For the formation of drift-field structures for solar cells, use of approach one, the single epitaxial layer followed by diffusion, is to be favored on the bases of its simplicity and its reproducibility. Should something go wrong during the deposition step, conventional measurements of epitaxial layer thickness and resistivity permit rejection of "out-of-spec" silicon slices. The two principal variables in the subsequent diffusion operation, time and temperature, are readily controlled. While the time required to diffuse the substrate impurities out to the surface is indeed long (e.g. for $N_0/N_1$ = 1000 and field width = 25 microns, time $\approx$ 28 hours at 1250°C), it is by no means economically prohibitive.

## D. Epitaxial Layer Evaluation

All epitaxial slices, prior to their introduction into any subsequent operation, were evaluated for layer thickness, layer resistivity, and surface appearance. Results of these evaluations determined the conditions necessary for diffusion and other operations.

### 1. Thickness Evaluations

Three techniques are available for layer thickness determination prior to gradient diffusion. These are the use of infrared interferometery[3,4], stacking fault size measurement[5], and bevel lap and stain. Thicknesses of all single epitaxial layers (approach one) were determined non-destructively by the infrared interferometer. Thicknesses of layers formed by the other approaches were determined by one of the other above techniques or were approximated by use of an epitaxial pilot run.

2. Resistivity Evaluation

Resistivity evaluation of the p/p+ epitaxial layer as grown is quickly made by using the three-point probe technique[6] in which the point contact diode breakdown voltage of an unknown resistivity sample is compared with that of a melt grown standard. Equipment used for the measurement is pictured in Fig. 8. The validity of this evaluation is dependent on (a) the reproducibility of a point contact diode, and (b) the assumption that the epitaxial film has a uniform impurity concentration throughout its thickness. The layer thickness of a typical sample was, e.g., 25 microns and had a resistivity of 10 Ω-cm. Although the resistivity of the layer may not have been absolutely constant throughout its total thickness, the top 15 microns were thought to be relative uniform. This thickness of uniform resistivity material is adequate to allow a dependable three-point probe measurement. (If the thickness of the epitaxial layer is decreased to a value less than the width of the space charge region at avalanche breakdown, the three-point probe is no longer usable.)

3. Surface Appearance

All epitaxial layers were subjected to a non-microscopic examination of the surface. Use of a bright light can reveal presence of a "haze" symptomatic of epitaxial system leaks. Epitaxial slices having any "haze", slip, pitting, poly-growth, "orange peel," or "tetrahedra" were generally rejected from further use. During epitaxial deposition on some of the more highly doped substrates,

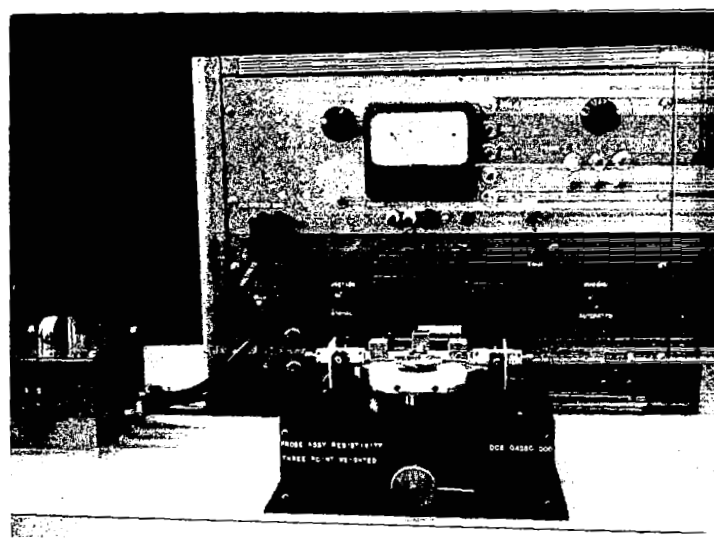

Fig. 8 - Automatic Point Contact Breakdown Equipment

numerous growths having an appearance much like tetrahedra formed on the surface. This phenomenon, which resulted in pebble-grained surfaces, generally increased in magnitude with the increasing doping level of the substrates. Figure 9 is a 1090X magnification of a "tetrahedron" on a 0.002 Ω-cm substrate. The magnitude of the phenomenon, which could not be correlated to the deposition temperature, is attributed both to dope segregation during substrate crystal growth and to subsequent substrate preparation.

## IV. DRIFT FIELD FORMATION AND MEASUREMENT

### A. Diffusion

Two of the three approaches described in III.C. required post-epitaxial diffusion to grade the substrate impurities through the epitaxial layer to the surface. Epitaxial slices were separated into groups according to the length of time required to effect the desired diffused structure. Selections of the diffusion coefficient-time products appropriate to the desired diffused structure and the diffusion temperature were facilitated by use of a master curve[7] keyed to the diffusion equation (III.C.1.). Diffusion constants of Williams[8] were used initially. Profile determinations (see next section) later suggested that constants reported by Kurtz and Yee[9] represented more accurately the diffusion of boron in silicon from a concentration step. Thus in a number of the earlier samples submitted to NASA, the thickness of uniform concentration (undiffused) material

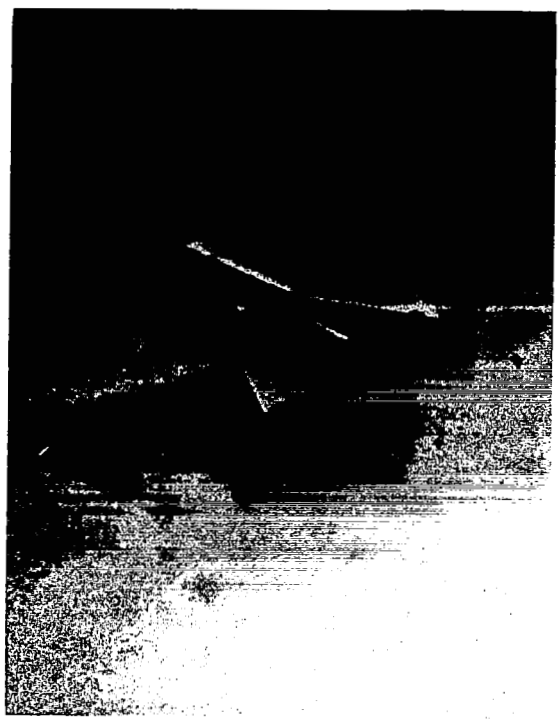

"Tetrahedral" Growth on Epitaxial Surface

Fig. 9

adjacent to the surface was greater than intended.

Diffusions were made in a globar-heated furnace. The epitaxial slices were placed in a quartz boat and inserted into the furnace heated to about 1250°C. (The exact temperature was chosen so as to make the removal time a convenient one.) A steam ambient was provided during the first twenty to thirty minutes which formed an oxide about 5,000Å thick. This prevented the silicon surface from becoming pitted by any impurities in the high-temperature nitrogen ambient subsequently provided. At the end of the selected diffusion time, the material was removed from the hot zone effecting a quench rather than a slow cool. Removal of the thermally-grown oxide with HF prepared the epitaxial material for cell fabrication.

## B. Determination of Concentration Profile

In this section is given an historical account of the developmental work on impurity concentration profile techniques. Results and evaluations of the various approaches are given throughout the account. A portion of this work, describing the technique in its final form, has been submitted for journal publication.

Two techniques are known which could possibly be adapted to the specific problem of concentration profiling. The first is the diode voltage-capacitance technique,[10] requiring the fabrication of low leakage diodes from the diffused epitaxial slices.

The calculated resistivity profile after a twenty-two hour diffusion at 1200°C for a typical sample (25 micron-thick, 10 Ω-cm layer deposited on a 0.008 Ω-cm substrate) is shown as the dotted line in Fig. 10. This

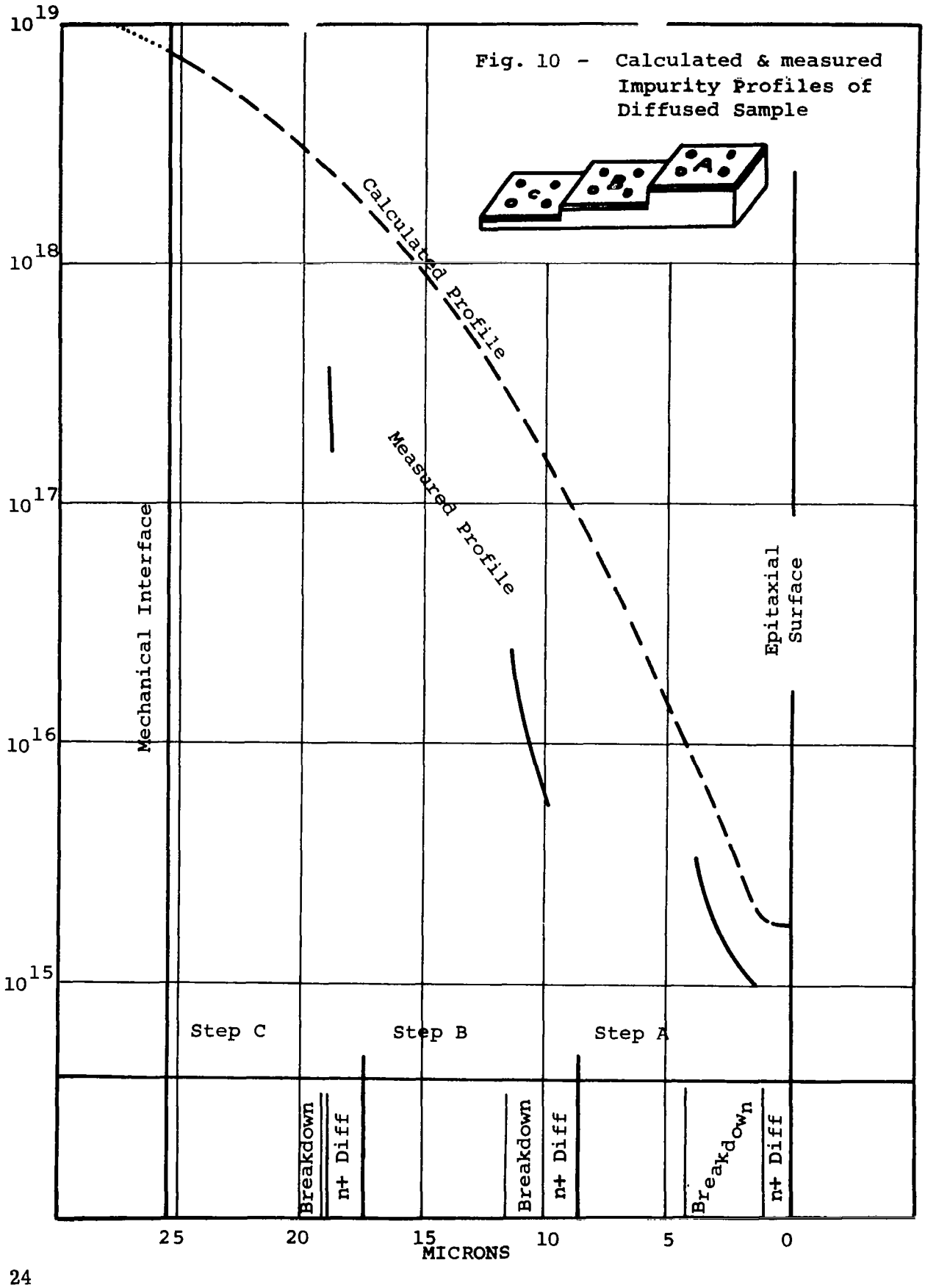


Fig. 10 - Calculated & measured Impurity Profiles of Diffused Sample

sample was evaluated by the diode voltage-capacitance technique using the equipment shown in Fig. 11. The depletion region at breakdown will not advance through the total layer; therefore, a stepped surface was chosen so that the depletion region could be moved into different representative concentrations. The surface of the sample was divided into areas which were selectively etched, after which 1.2μ n+ diffusions were made into these areas. Four small ohmic contacts were evaporated in each area using titanium and Kovar, followed by a soft solder dip (Fig. 12). Titanium, Kovar, and solder were applied to the back of the sample. Each contact was masked and the slice etched to form small diodes. The profile data obtained from diodes measured on Step A (See Fig. 10) should be reasonably accurate, as the concentration of the diffused n+ layer is very much greater than that of the epitaxial layer. The measured values are shown as the solid curve in the Step A region, and it is seen to approximate the shape of the calculated curve. Results of diodes measured in Steps B and C are progressively more in error since the junction is no longer between a heavily doped and a more lightly doped semicondutor. Special theoretical consideration must be made for such specific cases. Step A furnishes usable but limited data.

The second technique is the Incremental Sheet Resistance Technique, which involves incrementally removing material and measuring the sheet resistance of the remainder. In order to prevent reading the sheet resistance of the low resistivity substrate, lapping must proceed from the substrate

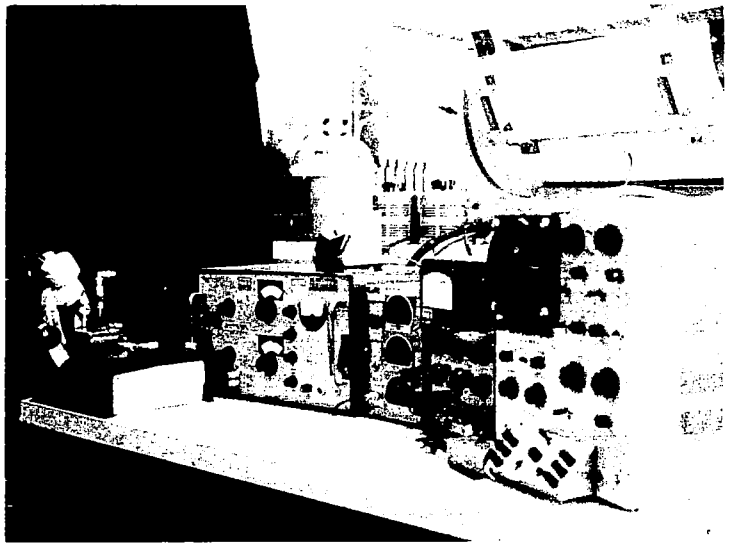

Fig. 11 - Diode Voltage-Capacitance Equipment. Included are Diode Probe, Capacitance Bridge, Voltage Source, Voltmeter, and Curve Tracer.

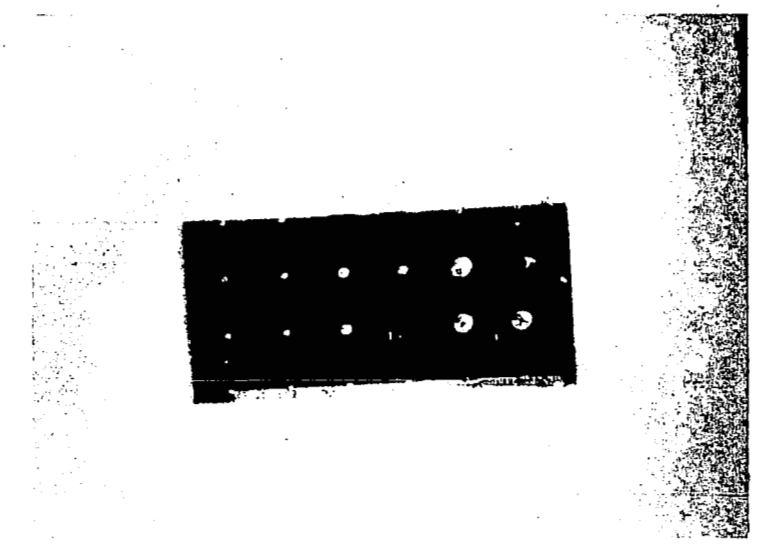

Fig. 12 - Selectively Etched Slice. The slice is shown after gradient diffusion and diode contacting.

side toward the epitaxial surface. Special techniques must be employed for this incremental removal so as not to destroy the increasingly thinner epitaxial layer by the removal technique or by the sheet resistance measurement. Laboratory experiments have shown that this can best be done by lapping.

Figure 13 shows an inline four-point probe array which is fixed to the epitaxial layer surface by the evaporation of four ohmic contacts (100 mil spacing), using titanium and Kovar followed by a soft solder dip. A wire is secured to each contact prior to epoxy potting. Values of sheet resistance readings increase very slowly until most of the substrate has been removed, then increases at a rate dependent on the concentration profile and remaining layer thickness. This technique had the inherent difficulty of not being able to remove uniform thin layers and to accurately determine the thickness of the remaining sample.

Modifying the incremental sheet resistance technique resulted in a bevel and probe procedure which gave improved accuracy. A sample is mounted with the epitaxial layer down on a precision lapping block. Lapping then proceeds through the sample at a specified angle. After each incremental lap, sheet resistance readings are made at regular intervals down the slope of the lapped surface using an ac four-point probe, see Fig. 14. Studies of this method thus far, involved principally with the mechanisms of the mounting and lapping operations, have used angles down to nine minutes ($\tan \alpha = .0026$). Resistivity values in a small interval $(X_1 - X_2) = \Delta X$ were calculated from

$$\rho = \frac{R_1 R_2}{R_2 - R_1} \Delta X$$

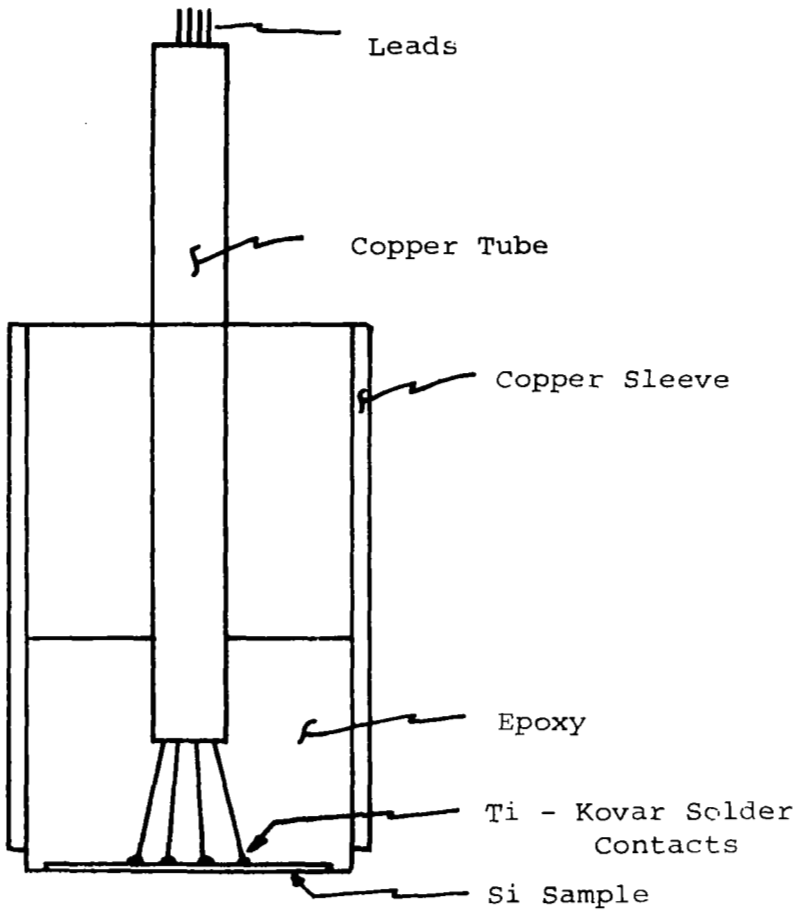


Fig. 13 - Incremental Lapping Fixture

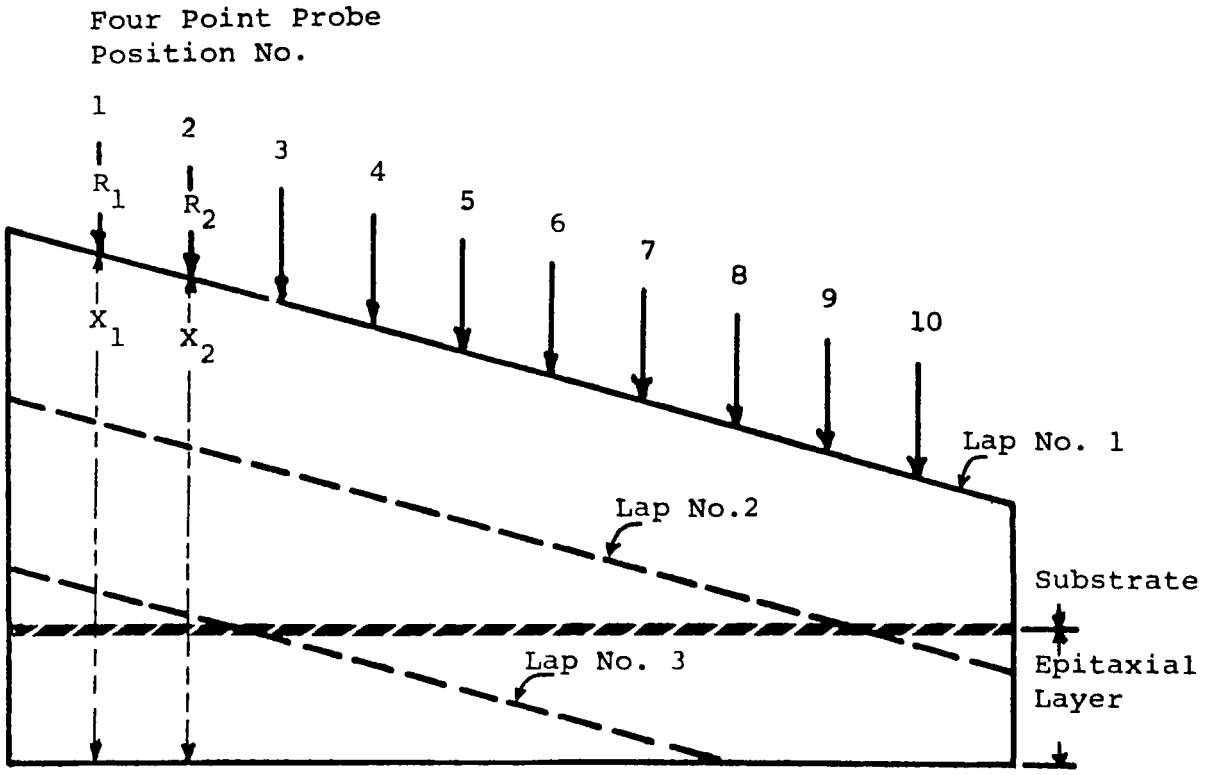


Fig. 14 - Diffusion Profile Determination By Incremental Angle Lapping

and plotted at $X_1-\Delta X/2$. $R_1$ and $R_2$ are the sheet resistances at $X_1$ and $X_2$ respectively.

In order to facilitate the perpendicular sectioning of the beveled sample, the technique was refined such that each sample is secured to a silicon blank of equal size by a thin epoxy layer. The silicon blank provides a rigid support for the sample which is lapped to zero thickness at one end. (Fig. 15) The epoxy provides a solid-subsurface to prevent the probes from damaging the sample at the thin end, and an insulating surface for the sample to rest on. Sheet resistance readings are made at ten mil increments horizontally along the two centimeter length of the sample. Figure 16 shows typical measured sheet resistance variation with thickness for an epitaxial slice which has not been subjected to a drift field diffusion. A comparison of the calculated and measured concentration profiles for a 59 micron thick, 4.4 Ω-cm epitaxial film is shown in Fig. 17. The deviation between the calculated and measured curves may have been the result of an undesired tilt (see Fig. 15) in a direction perpendicular to the intended beveling direction. Another source of error may be the improper choice of diffusion constant for this particular set of epitaxial growth conditions.

Several slices which had been given their drift field diffusion were also profiled. Figure 18 is a comparison of the calculated and measured sheet resistance versus layer thickness for a typical sample.

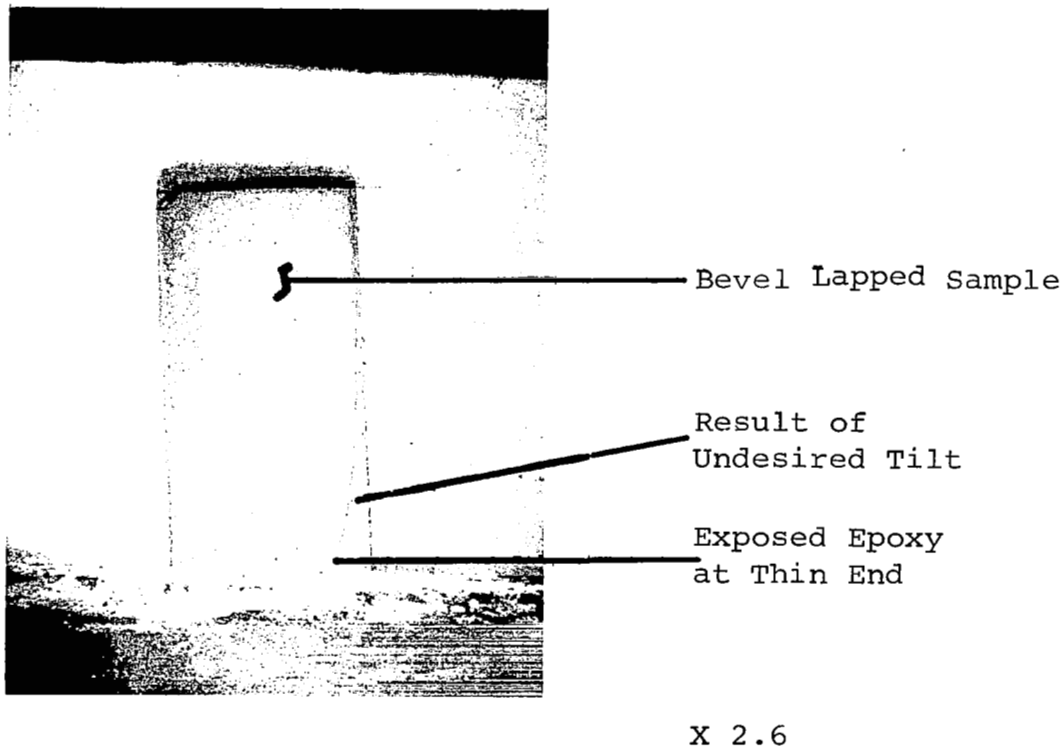


Fig. 15 - Top View of Lapped Sample
Ready for Probing

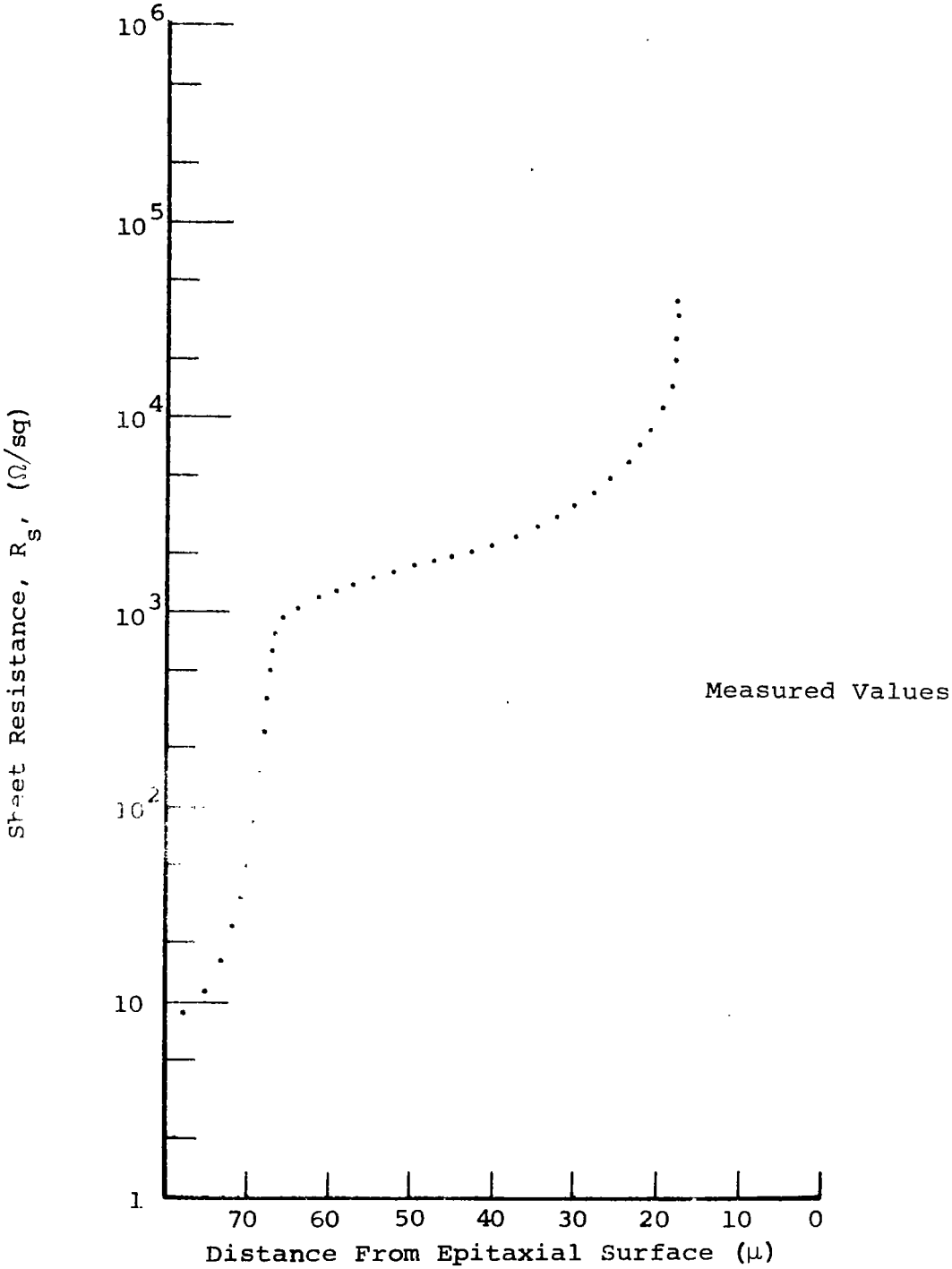


Fig. 16 - Sheet Resistance vs Depth For Epitaxial Layer Prior to Gradient Diffusion

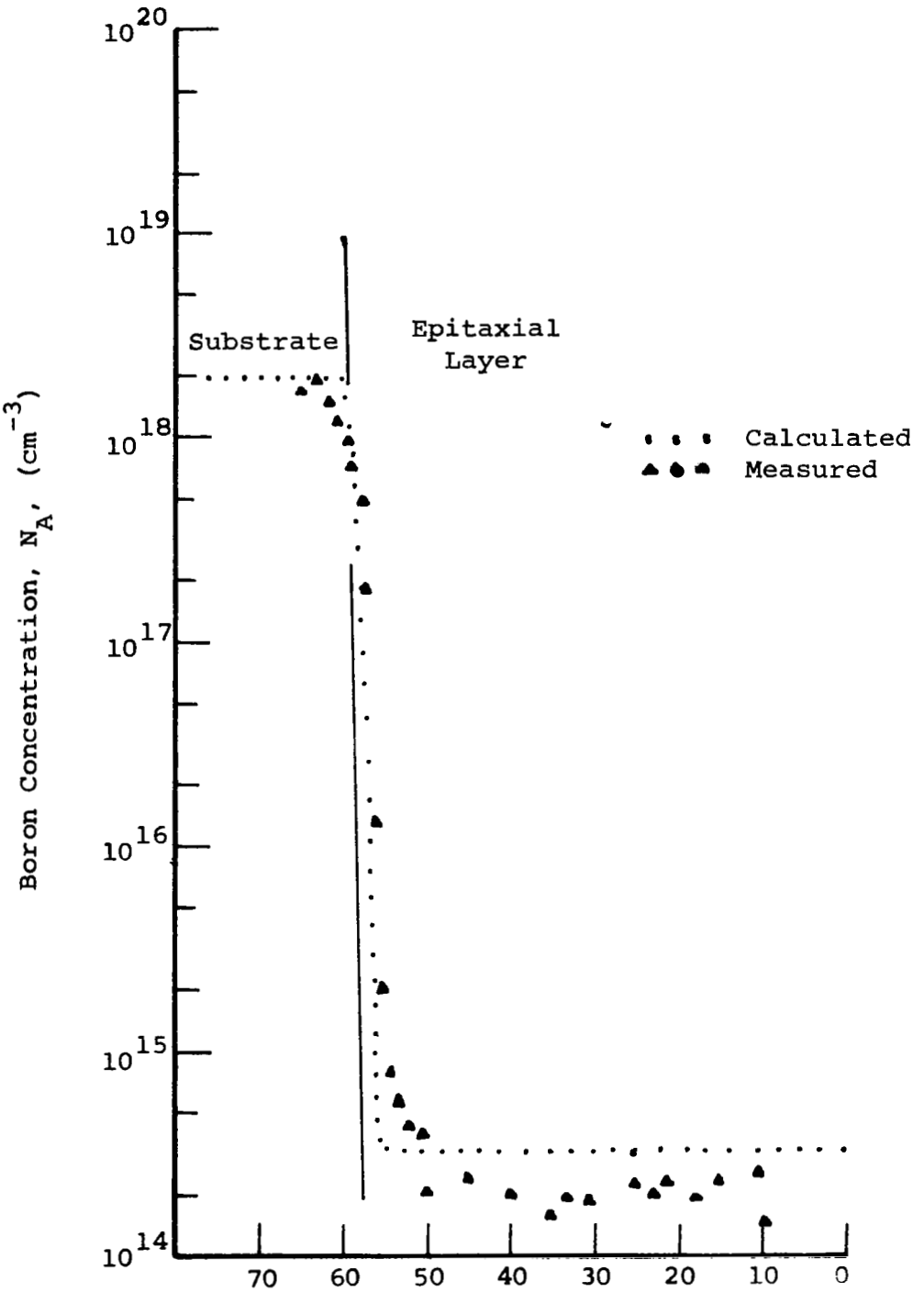


Fig. 17 - Boron Concentration vs Depth For Epitaxial Layer Prior to Gradient Diffusion

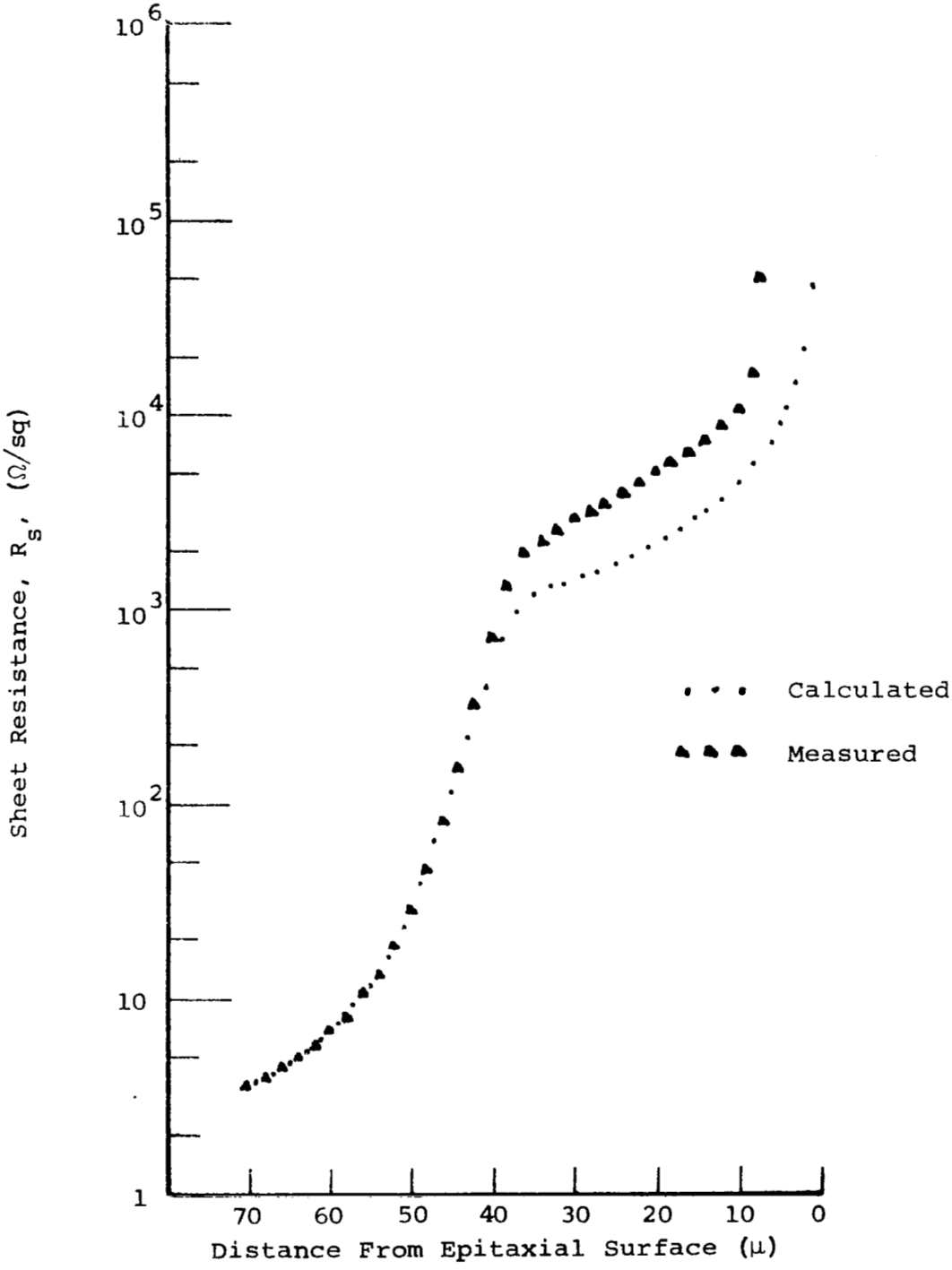


Fig. 18 - Comparison of Calculated and Measured Sheet Resistance vs Depth For a Gradient Diffused Sample

A comparison of calculated and measured concentration profiles is shown in Figs. 19, 20, and 21. Each of these measured curves was compared with calculated curves whose diffusion constant was chosen for a best fit. Figures 19 and 20 represent samples grown in one run and diffused together. The value of their optimum diffusion constant is $2.0 \times 10^{-12}$ $cm^2$ $sec^{-1}$. This value is the same as that reported by Kurtz and Yee[9]. The drift field diffusion times thus far had been calculated on the basis of $D = 5 \times 10^{-12}$ $cm^2$ $sec^{-1}$; therefore, the thickness of uniform concentration (undiffused) material was actually thicker than intended. Figure 21 represents a sample grown at a different time but diffused simultaneously with samples shown in Figs. 19 and 20. Its best fit diffusion constant is $1.0 \times 10^{-12}$ $cm^2$ $sec^{-1}$. Sheet resistances as measured on all samples increased more rapidly than expected near the thin end. This is apparently due to abrasion damage during lapping as was substantiated by preparing an additional sample in each of two concentrations and grinding an identical angle using a diamond grinding wheel (which is known to produce less damage). Surface roughness comparisons of lapping vs grinding show maximum surface excursions of 2.3μ and 0.38μ, respectively. Boron concentration profiles for each technique in each range are shown in Fig. 22. In both ranges the bevel ground samples gave accurate concentration measurements for thinner sample regions. Also, low concentration material allowed accurate measurements of thinner sample regions than high concentration material prepared by either technique. The apparent reason is the greater ease of transmitting mechanical damage (lapping or grinding) in a sample which already has its lattice distorted by a very large number of impurity atoms.

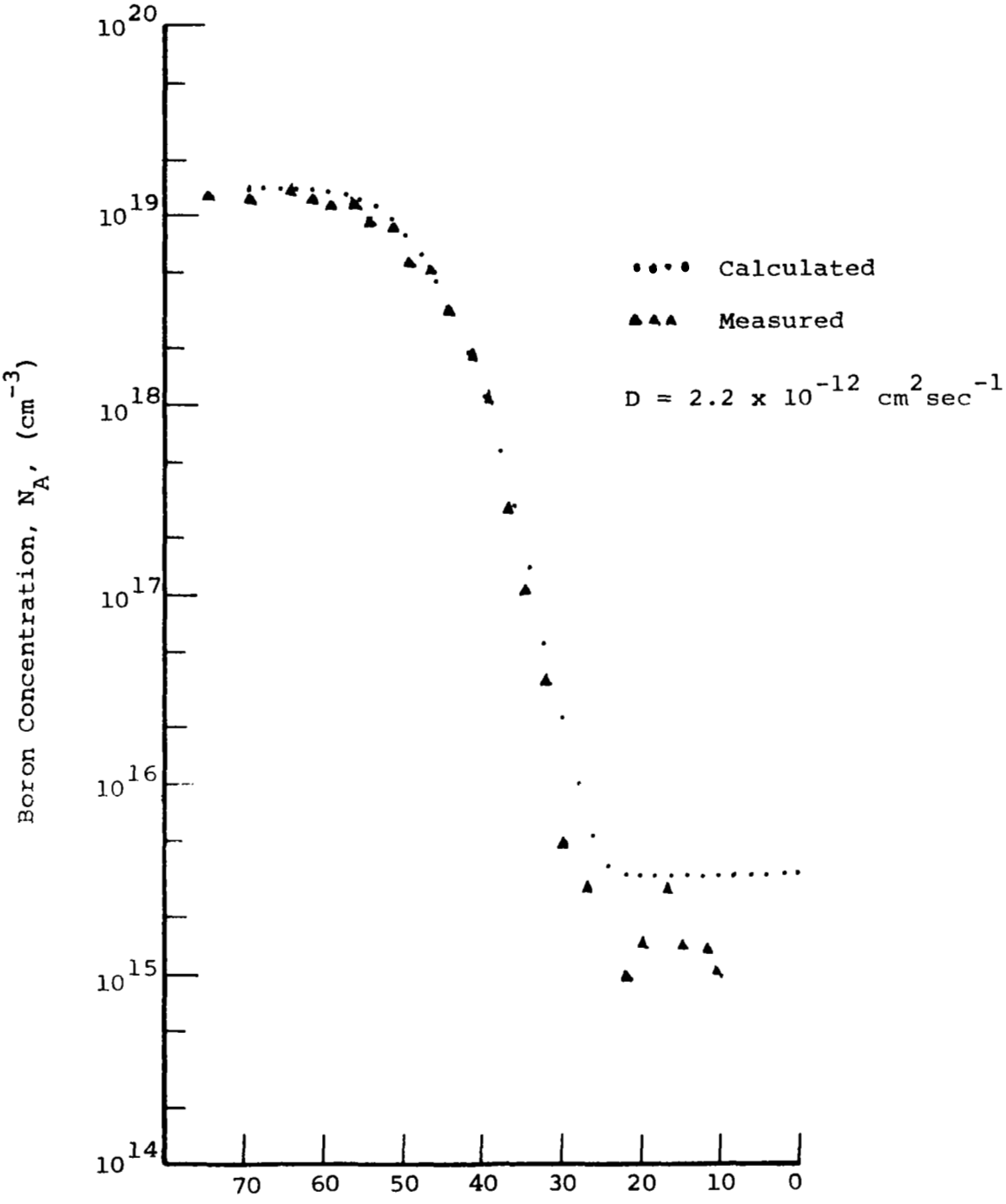


Fig. 19 - Comparison of Calculated and Measured Boron Concentration vs Depth For a Gradient Diffused Sample

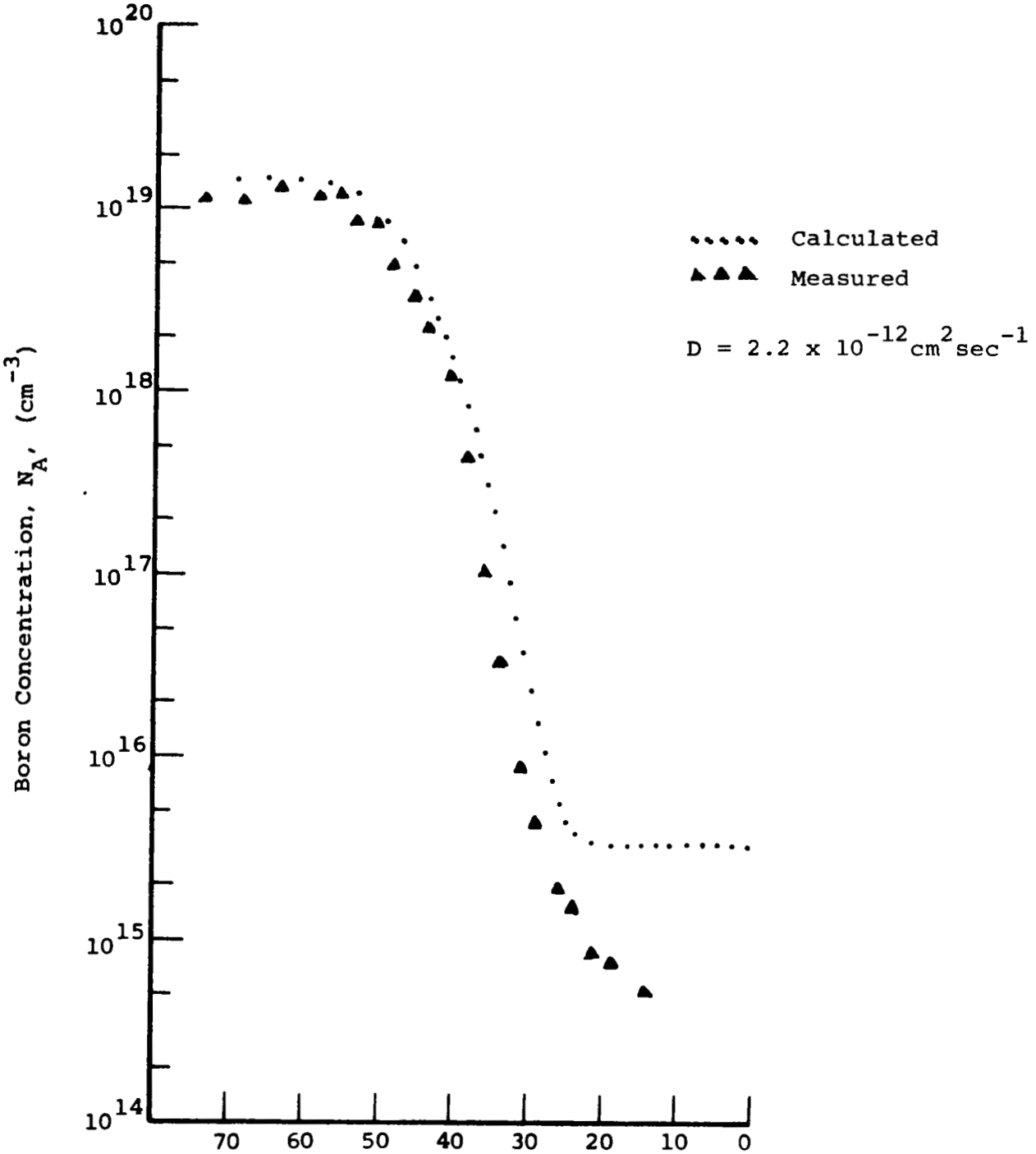


Fig. 20 - Comparison of Calculated and Measured Boron Concentration vs Depth For a Gradient Diffused Sample

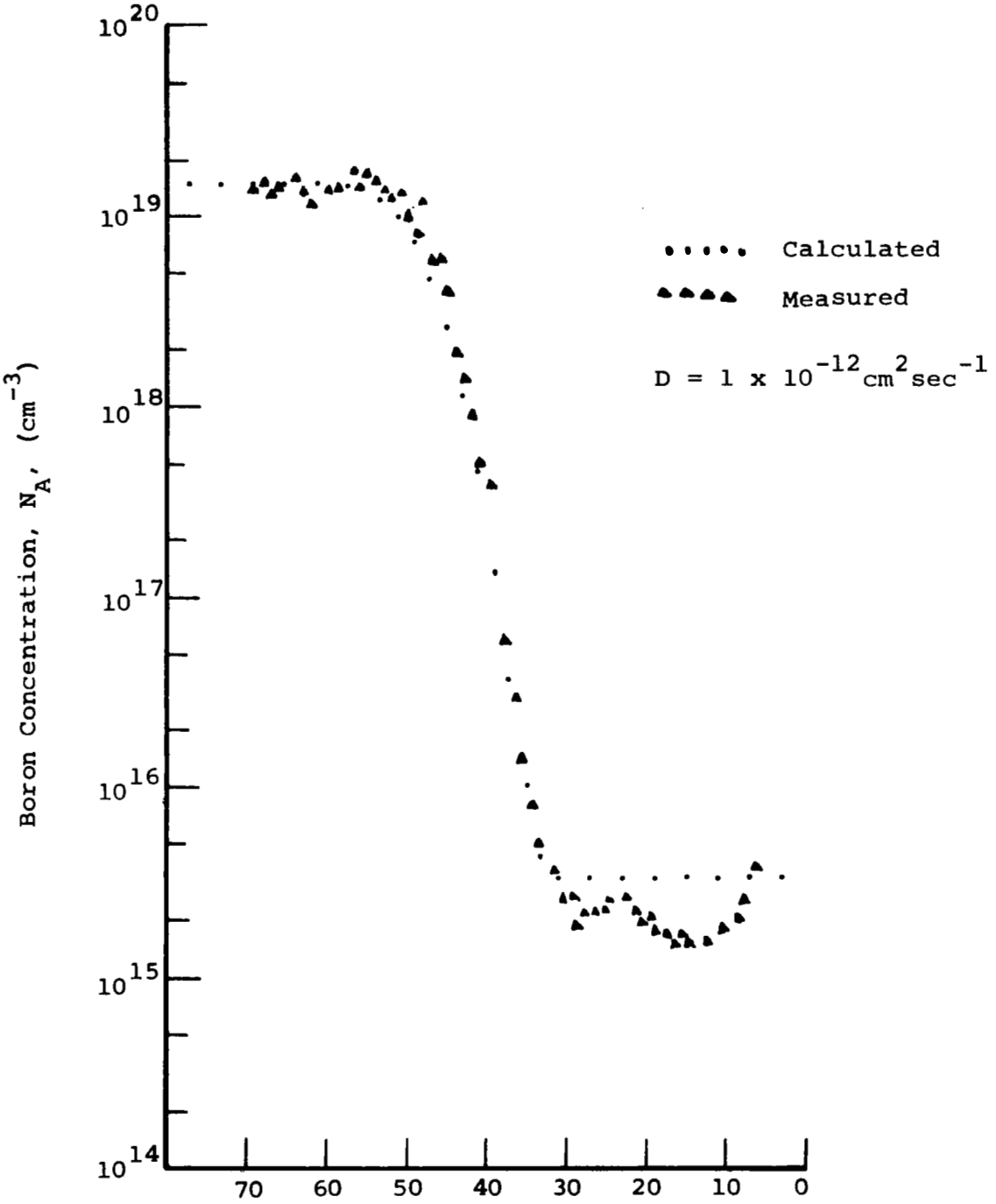


Fig. 21 - Comparison of Calculated and Measured Boron Concentration vs Depth For a Gradient Diffused Sample

COMPARISON OF MECHANICAL
BEVELING TECHNIQUES FOR CONCENTRATION
PROFILE MEASUREMENTS

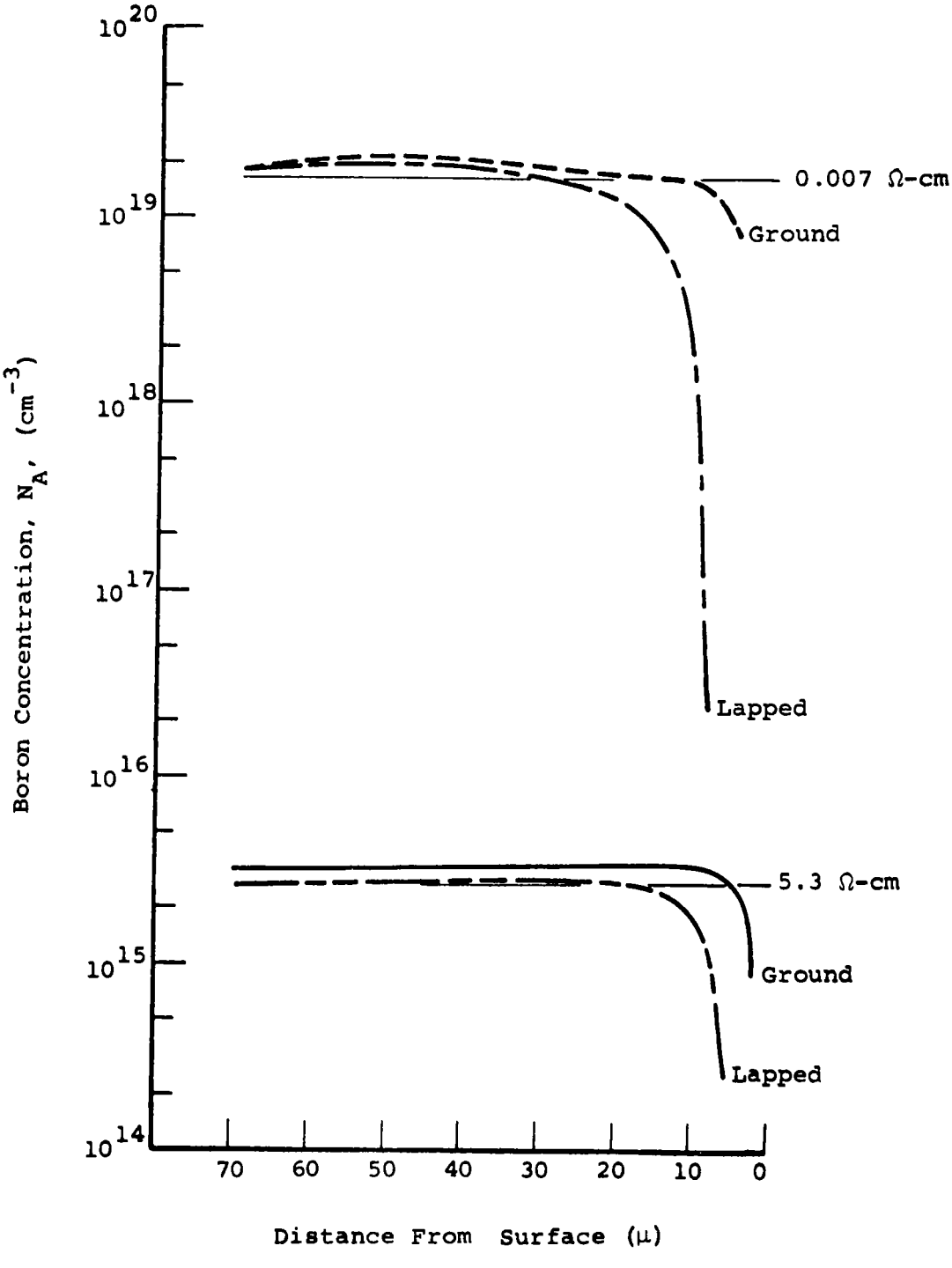


Fig. 22

This bevel grind and probe technique has the ability to measure the true concentration in these ranges to within 30% of its real value.

The problem of identifying a particular sample thickness at an exact corresponding probe position was solved by the addition of a two mil deep groove across the silicon support slice and perpendicular to the beveling direction. The sectioned sampled, shown in part in Fig. 23, permits thickness measurement positions to be referenced from this center groove even if both end reference points are damaged in sectioning. Horizontal reference positions are accurate to within 5.0 microns.

The support slice is made wider than the sample so that the reference groove can be correlated to a corresponding four-point probe position while obtaining the raw data.

A computer program was initiated which performs the necessary smoothing of raw data, makes necessary profile calculations, and graphically presents the results. Selection of the smoothing parameters is completely automatic and spurious data points are rejected. Figure 24 is a computer plotted representation of the variation of sheet conductance vs thickness for raw and smoothed data. Rejected data points are indicated by stars. Figure 25 shows the variation of boron concentration with depth. Agreement at the end points is excellent.

## V. GETTERING EXPERIMENTS

As mentioned earlier, carrier lifetime in the epitaxial material, apparently either with or without extended high-temperature diffusion, is quite low. The cause of this

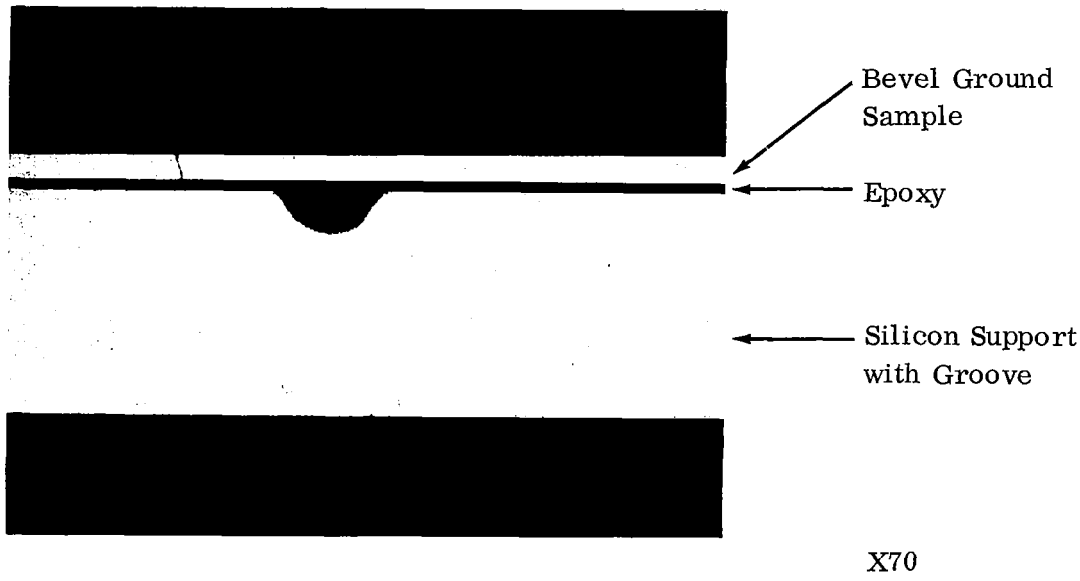


**Fig. 23 - Bevel Ground Sectioned Sample Incorporating Reference Groove**

Fig. 24 - Computer-plotted Sheet Conductance Profile

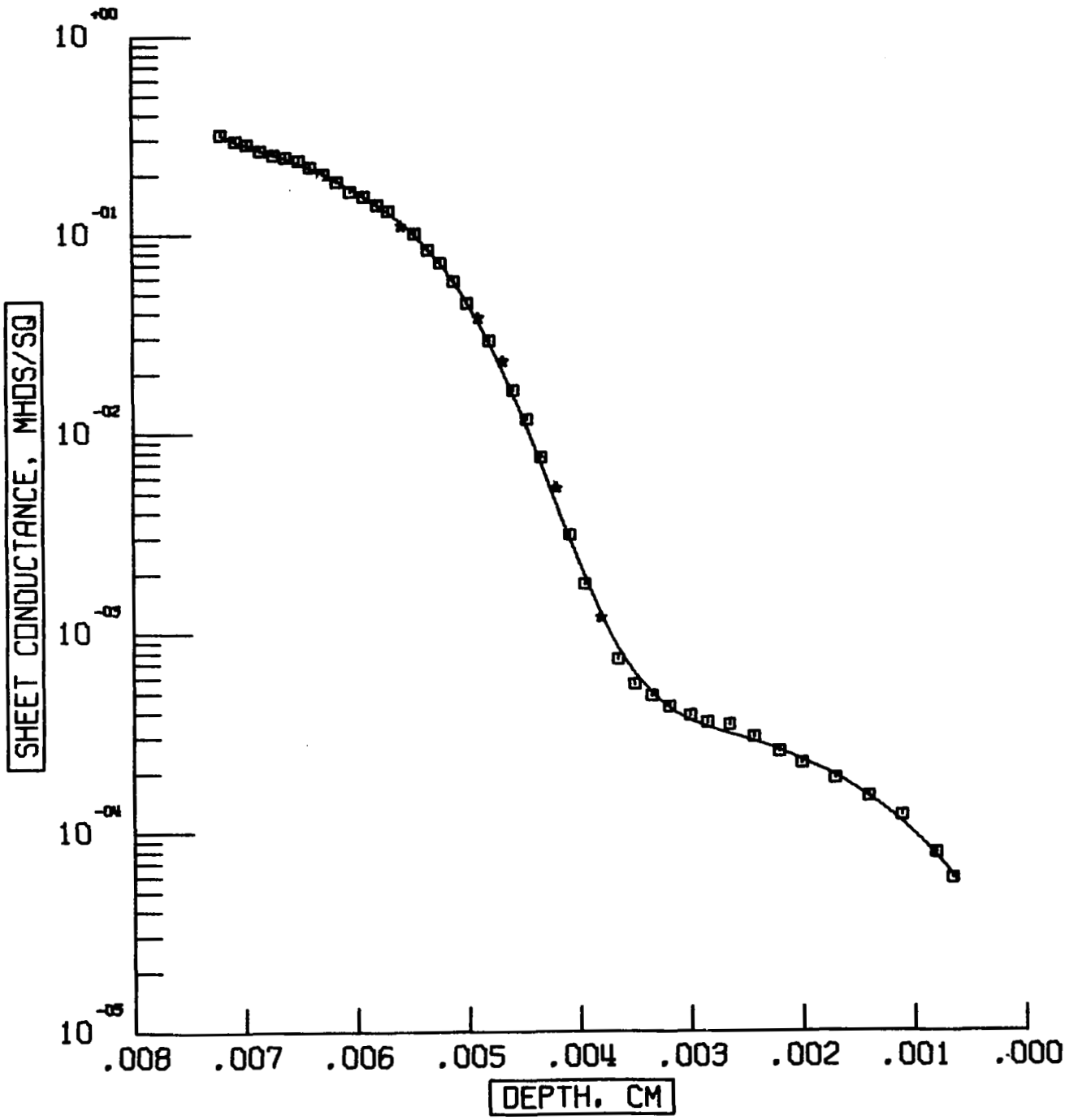

Fig. 25 - Computer-plotted Boron Concentration Profile

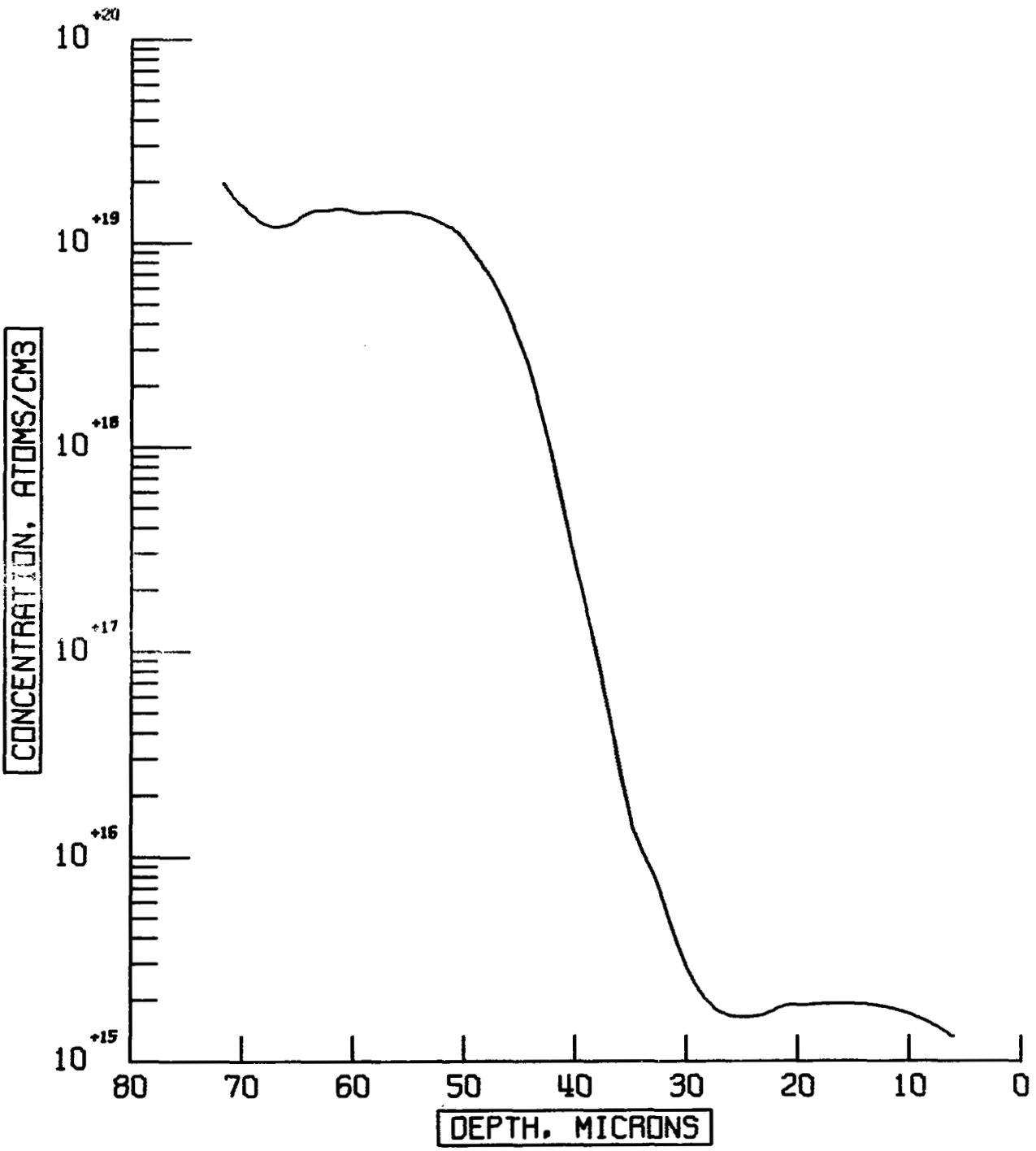

low lifetime in epitaxial material is not fully understood, but may be attributed in part to accidental transition metal doping.[11] Duffy, et al[12] suggest that these elements (metallic impurities) are initially present in the silicon substrates rather than being introduced during the epitaxial and/or diffusion processes. Thus, although there are opportunities in which transition metals may dope during the epitaxial process, the quantity of metal present may be strongly dependent on the substrate crystal growth process.

A special emphasis was placed on improving carrier lifetime by "gettering" of metallic impurities from the cell base region after other high temperature process steps. This was an attempt to enhance the cell efficiency, particularly in the long wavelength portion of the spectrum.

Several variations of a gettering technique, adapted from Ing, et al[13], were tried. A methanol solution of boric acid was painted on the low resistivity side of the epitaxial blanks (after the diffusion grading) and the blanks were inserted into a furnace tube heated in air ambient to allow a glassy layer to form. After one or two hours at the elevated temperature, the furnace was cooled to 600°C, the slices were taken from the furnace, and after the borate glaze was removed, the slices were ready for fabrication.

Removal of the gettering glaze was, in some instances, a real problem. Gettering at 1100°C supposedly is more effective than at 800°C, but the glaze formed at the higher temperature was much more difficult to remove. Concentrated

HF removed a glaze formed at 800°C, but glazes formed at temperatures of 900°, 1000°, and 1100°C were only partially removed by HF. A refluxing mixture known to attack boron (50 cc $H_2O$, 2 cc $H_2SO_4$, 10 cc $HNO_3$, 5 cc HCl) also was tried on the high temperature glazes, which remained virtually intact. Glaze removal was effected on a good portion of the cell blanks either by lapping or by concentrated HF followed by a planar type etchant.

It was anticipated that gettering action (rate, effectiveness, etc.) in lightly doped silicon, for which there are literature data, might differ substantially[14] from gettering of metal impurities from heavily doped silicon, such as in the present application. For this reason, gettering from the high resistivity epitaxial side of the slice was thought to be desirable. Removal of a glaze on this side by lapping or etching of the silicon would, obviously, remove the drift field. Failure to remove all of the glaze from the epitaxial side would alter junction diffusion conditions and result in a higher cell series resistance. Thus, an effective glaze removal technique which removes a minimum of silicon was needed. A brief steam oxidation at 850°C interposed between two treatments in concentrated HF effectively removed the borate glaze and boron "stain."

A number of epitaxial blanks were processed through a gettering operation prior to fabrication. Results of the experiments are given in VII.

## VI. SOLAR CELL FABRICATION

All cells described in this report were fabricated in Texas Instruments' solar cell developmental laboratory. Two

separate procedures were used.

Procedure I, which was used for the first seventy sample cells shipped to NASA, consisted of processing 1-cm x 2-cm rectangular epitaxial slices through the fabrication steps.

Several problems arose during fabrication as a result of the epitaxial structures not conforming to the standard production blank size. For example, the epitaxial deposition would add silicon not only to the top surface but to the edges. In addition, for thick deposits (several mils) edges became rough where the slices were separated from the epitaxial reactors' graphite susceptor after deposition. The epitaxial slices then required a rather laborious edge-lapping operation to remove the roughness and decrease the lateral dimensions. In most cases, slices subjected to this operation were undersized when ready for fabrication. Frequently, excess metal from the contact evaporation step would remain on the edges of the cells after fabrication, and thus partially short the structure. Because of these difficulties, the fabrication results were quite variable for many cells.

Procedure II, used for the last thirty sample cells, processed round epitaxial slices through contact application, trimmed the material to standard size (two 1-cm x 2-cm cells per slice), and then applied the SiO coating. Use of Procedure II, similar to that used by Smith, et al[15], effectively removed most of the difficulties associated with the first procedure.

Because of the experimental nature of these cells, they were not quality control inspected to the rigid production specifications. Thus, sample cells shipped may not necessarily have met all usual specifications such as size, coating, contact adherence, etc. All sample cells, however, were nominally the standard 1-cm x 2-cm size, mostly with a lateral 5-grid geometry and an approximately 1.8 $cm^2$ active area.

## VII. EPITAXIAL RESULTS AND CELL CHARACTERISTICS

### A. Epitaxial Structures Formed

Epitaxial depositions were made using the approaches described in III. Substrate resistivities ranged from 0.002 to 0.20 Ω-cm, but were generally from 0.006 to 0.008 Ω-cm. The silicon substrates were in every case from boron-doped, p-type crystals.

The substrates were cut from one of two kinds of silicon crystals, Czochralski and Lopex*. One of the principal differences between silicon crystals of these two preparative methods is the oxygen content. Whereas Czochralski material may have as much as $1 \times 10^{18}$ atoms of oxygen per $cm^3$ of silicon, Lopex* silicon has less than $1 \times 10^{16}$ atoms/$cm^3$. While the effects of oxygen-containing defects (arising during irradiation in silicon) on minority carrier lifetime and carrier concentration are not presently known, it seemed appropriate to examine cells made from silicon in which no

---

* Texas Instruments Incorporated Tradename

oxygen was present. It should be pointed out that epitaxially deposited silicon may have appreciable oxygen content due to oxygen's very rapid diffusion from the substrate. For example, the diffusion coefficient for oxygen in silicon is 100 times that of boron in silicon at 1250°C. Thus, to ensure no oxygen in the epitaxial film the substrate itself must also be oxygen free. Approximately one-third of the epitaxial depositions were made on Lopex* substrates.

By far the majority of epitaxial drift-field structures were made using the simple deposit and diffusion approach given in III.C.1. Epitaxial layer thicknesses ranged from as low as six microns to as much as 75 microns. Resistivities of the layers ranged from 0.4 Ω-cm to above 30 Ω-cm, but were generally between two and twenty Ω-cm. Diffusion conditions ranged from 3 to 162 hours at 1250°C.

## B. Current-voltage Characteristics

Current-voltage characteristics were measured with the solar cell developmental laboratory's standard test equipment. Three tungsten reflector-type sealed lamps (150 watt, 2800°K ± 50°K color temperature) were mounted on swivels and fed by a dc power supply. Illumination was filtered through 3 cm of recirculating deionized water on a 1/4" plate glass tray. Solar cell temperature was controlled by a water-cooled test block at 26°C ± 2°C. Intensity was set for 100 milliwatts/$cm^2$ ± 2 per cent (tungsten equivalent to sunlight). Repeatibility was within ± 2 per cent.

---

* Texas Instruments Incorporated Tradename

Short circuit current $I_{sc}$, open circuit voltage $V_{oc}$, and maximum per cent conversion efficiency (air mass one) were determined for all cells fabricated from the epitaxial material. In a few instances dark reverse currents were measured to provide a measure of cell shunt resistance.

One hundred sample solar cells containing drift fields were delivered to NASA for further evaluation. These cells were selected to provide a representative cross section of the various epitaxial, diffusion, and other conditions used throughout the contract. These conditions and current-voltage characteristics for the sample cells are enumerated in Tables I through VIII. Listed for each cell (either tabulated or in footnotes) are sample number, substrate preparation and resistivity, epitaxial layer thickness and resistivity, diffusion time and temperature, gettering conditions (if used), and values of $I_{sc}$, $V_{oc}$, and maximum per cent efficiency. With but five exceptions, the sample cells had maximum efficiencies of 7.0 per cent or better. Average maximum efficiency of cells delivered was 8.65 per cent.

In section VI was mentioned the fact that for the first seventy sample cells, fabricated by Procedure I, the fabrication step could not be considered a constant one. The problems with Procedure I were manifest in wide variations of electrical characteristics within a group of cells which hopefully had received similar pre-fabrication treatment. Lack of reproducibility from one cell to another within a common group frustrated efforts to draw conclusions in many instances. Thus, some qualitative remarks are made

TABLE I

Characteristics of Sample Cells Delivered to NASA

| Solar Cell # | Epitaxial Film Thickness (microns) | Epitaxial Film Resistivity (Ω-cm) | Diffusion | | Cell Characteristics | | |
|---|---|---|---|---|---|---|---|
| | | | Hours | Temp°C | $I_{sc}$ (ma) | $V_{oc}$ (V) | Max% efficiency |
| 1 | 28.4 | 3.2 | 25.0 | 1200 | 40.1 | .542 | 7.7 |
| 2 | 29.5 | 2.75 | 25.0 | 1200 | 41.0 | .550 | 7.9 |
| 3 | 26.8 | 2.75 | 25.0 | 1200 | 40.7 | .551 | 8.0 |
| 4* | ≈25 | 0.59 | 26.0 | 1200 | 36.3 | .556 | 7.4 |
| 5 | 25.9 | 2.4 | 16.5 | 1200 | 38.1 | .532 | 7.5 |
| 6 | 25.0 | 3.5 | 22.0 | 1200 | 39.1 | .539 | 7.6 |
| 7 | 16.2 | 8.5 | 3.1 | 1250 | 36.2 | .552 | 7.9 |
| 8 | 28.9 | 5.2 | 26.5 | 1200 | 42.9 | .533 | 7.9 |
| 9 | 25.9 | 20.5 | 16.5 | 1200 | 41.3 | .547 | 8.2 |
| 10 | 26.8 | 1.4 | 22.0 | 1200 | 37.3 | .556 | 8.2 |
| 11 | 27.3 | 3.6 | 16.5 | 1200 | 40.2 | .573 | 8.4 |
| 12 | ≈25 | 2.6 | 26.0 | 1200 | 39.1 | .542 | 8.5 |
| 13 | 26.3 | 2.5 | 16.5 | 1200 | 41.7 | .567 | 9.4 |

* Substrate resistivity was .003 - .005 Ω-cm; deposits for all other cells in Table were made on .005 - .009 Ω-cm substrates.

TABLE II

Characteristics of Sample Cells Delivered to NASA

| Solar Cell # | Epitaxial Film Thickness (Microns) | Epitaxial Film Resistivity (Ω-cm) | Diffusion Hours | Diffusion Temp°C | Cell Characteristics $I_{sc}$ (ma) | $V_{oc}$ (V) | Max% efficiency |
|---|---|---|---|---|---|---|---|
| 14 | 36.9 - | 7.0 - | 16 | 1250 | 41.2 | .539 | 8.3 |
| 15 | 36.9 - | 2.2 - | 16 | 1250 | 39.4 | .538 | 7.3 |
| 16 | ~25 + ~25 | 0.13 2.4 | 4.5 | 1250 | 41.8 | .488 | 7.0 |
| 17 | ~25 + ~25 | 0.09 3.0 | 4.5 | 1250 | 41.6 | .541 | 8.6 |
| 18 | ~25 + ~25 | 0.12 2.0 | 4.5 | 1250 | 42.0 | .525 | 7.3 |
| 19 | ~25 + ~25 | 0.13 2.5 | 4.5 | 1250 | 41.6 | .539 | 7.0 |
| 20* | ~40 | 5 step | - | - | 43.5 | .409 | 5.5 |
| 21 | ~33 | 5 step | - | - | 41.4 | .515 | 6.1 |

* Substrate resistivity was .007 - .009 Ω-cm; deposits for all other cells in Table were made on .005 - .007 Ω-cm substrates.

TABLE III

Characteristics of Sample Cells Delivered to NASA

| Solar Cell # | Substrate† Resistivity (Ω-cm) | Epitaxial Film Thickness (microns) | Epitaxial Film Resistivity (Ω-cm) | Diffusion Hours | Diffusion Temp°C | Cell Characteristics $I_{sc}$ (ma) | $V_{oc}$ (V) | Max% efficiency |
|---|---|---|---|---|---|---|---|---|
| 22 | .008 | 25.4 | 3.2 | 16 | 1200 | 40.8 | .557 | 9.8 |
| 23 | .008 | 23.1 | 7.0 | 16 | 1200 | 43.2 | .563 | 9.0 |
| 24 | .008 | 24.6 | 8.9 | 16 | 1200 | 44.5 | .570 | 9.6 |
| 25 | .008 | 26.8 | 17 | 16 | 1200 | 44.6 | .565 | 9.7 |
| 26 | .008 | 25.9 | 9.0 | 6 | 1250 | 41.3 | .546 | 8.7 |
| 27 | .008 | 23.1 | 11.0 | -- | -- | 43.1 | .566 | 9.2 |
| 28 | .008 | ~50 | ~25 | 17 | 1250 | 40.4 | .497 | 7.9 |
| 29 | .008 | ~50 | ~25 | 17 | 1250 | 40.4 | .497 | 8.1 |
| 30 | .008 | ~50 | ~25 | 17 | 1250 | 44.6 | .485 | 8.1 |
| 31 | .008 | ~50 | ~25 | 17 | 1250 | 38.9 | .480 | 7.3 |
| 32 | .008 | ~50 | ~25 | 17 | 1250 | 41.4 | .503 | 8.3 |
| 33 | .008 | ~50 | ~2.1 | 25 | 1250 | 43.7 | .552 | 9.6 |
| 34 | .008 | ~50 | ~2.1 | 25 | 1250 | 40.4 | .544 | 8.6 |
| 35 | .008 | ~50 | ~2.1 | 25 | 1250 | 36.5 | .521 | 7.3 |
| 36‡ | .008 | ~50 | ~2.1 | 25 | 1250 | 41.5 | .533 | 6.5 |
| 37 | .002 | ~50 | ~1.1 | 25 | 1250 | 35.1 | .515 | 6.5 |
| 38‡ | .002 | ~50 | ~1.1 | 25 | 1250 | 40.2 | .553 | 7.2 |
| 39‡ | .002 | ~50 | ~1.1 | 25 | 1250 | 39.3 | .539 | 6.8 |

† All substrates were cut from LOPEX* crystals. (*Texas Instruments Trade Name)

‡ Gettered two hours at 1000°C.

TABLE IV

Characteristics of Sample Cells Delivered to NASA

| Solar Cell # | Silicon Substrate Material** | Epitaxial Film Thickness (microns) | Epitaxial Film Resistivity (Ω-cm) | Diffusion Hours | Diffusion Temp°C | $I_{sc}$ (ma) | $V_{oc}$ (V) | Max % Efficiency‡ |
|---|---|---|---|---|---|---|---|---|
| 40† | Lopex* | 52.7 | 1.9 | 25 | 1250 | 45.0 | .551 | 8.9 |
| 41† | " | 46.1 | 2.3 | 25 | 1250 | 44.2 | .514 | 7.0 |
| 42†† | " | 54.6 | 1.9 | 30 | 1250 | 39.8 | .530 | 7.2 |
| 43‡ | " | 27.3 | 2.2 | 6 | 1250 | 45.1 | .559 | 8.7 |
| 44‡ | " | 24.2 | 7.6 | 6 | 1250 | 40.7 | .550 | 7.5 |
| 45‡ | Czochralski | 50.9 | 6.0 | 19.5 | 1250 | 46.2 | .533 | 8.5 |
| 46 | " | 44.7 | 9.8 | 19.5 | 1250 | 44.1 | .564 | 9.9 |
| 47 | " | 56.7 | 15.0 | 19.5 | 1250 | 44.7 | .566 | 9.7 |
| 48‡ | " | 41.0 | 18.5 | 19.5 | 1250 | 40.9 | .510 | 7.0 |
| 49 | " | 59.0 | 38 | 19.5 | 1250 | 46.9 | .556 | 10.1 |
| 50 | Lopex* | 47.6 | 12.5 | 19.5 | 1250 | 44.7 | .531 | 8.7 |
| 51 | " | 52.7 | 4.3 | 47.0 | 1250 | 42.2 | .532 | 8.0 |
| 52 | " | 50.9 | 5.0 | 47.0 | 1250 | 44.4 | .553 | 9.5 |
| 53 | " | 47.6 | 5.6 | 47.0 | 1250 | 40.8 | .537 | 8.7 |
| 54 | " | 52.7 | 4.4 | 47.0 | 1250 | 45.6 | .540 | 9.0 |

All cells 1 cm x 2cm; cells 40-44 are 3-grid, cells 45-54 are 5-grid geometry.

* Texas Instruments Incorporated Tradename

** All substrates were 0.008 Ω-cm except 40 and 41, which were 0.002 Ω-cm.

† Gettered one hour at 900°C

†† Gettered two hours at 800°C

‡ Gettered two hours at 1000°C

TABLE V

Characteristics of Sample Cells Delivered to NASA

| Solar Cell # | Silicon Substrate Material** | Epitaxial Film Thickness (microns) | Epitaxial Film Resistivity (Ω-cm) | Diffusion Hours | Diffusion Temp°C | $I_{sc}$ (ma) | $V_{oc}$ (V) | Max % Efficiency ‡ |
|---|---|---|---|---|---|---|---|---|
| 55† | Czochralski | 39.9 | 1.7 | 17 | 1250 | 37.4 | 0.532 | 8.8 |
| 56† | " | 39.9 | 2.6 | 24 | 1250 | 38.8 | 0.477 | 7.7 |
| 57 | " | 41.0 | 5.1 | 24 | 1250 | 37.5 | 0.525 | 8.7 |
| 58 | " | 50.9 | 25.5 | 17 | 1250 | 41.6 | 0.499 | 9.2 |
| 59 | " | 49.2 | 27.0 | 17 | 1250 | 42.6 | 0.505 | 9.4 |
| 60† | Lopex* | 49.2 | 3.7 | 24 | 1250 | 38.5 | 0.459 | 7.9 |
| 61 | " | 73.2 | 10.0 | 144 | 1250 | 39.2 | 0.508 | 7.7 |
| 62 | " | 75.7 | 10.0 | 100 | 1250 | 41.7 | 0.503 | 8.9 |
| 63 | " | 66.7 | 12.0 | 144 | 1250 | 41.0 | 0.500 | 7.9 |
| 64 | " | 69.7 | 16.5 | 66 | 1250 | 41.2 | 0.513 | 8.6 |

* Texas Instruments Incorporated Trademark

** Substrates were 0.005 Ω-cm for 55 to 60 and 0.008 Ω-cm for 61 to 64

† Gettered two hours at 900°C

‡ Based on 1.6 $cm^2$ active area

TABLE VI

Characteristics of Sample Cells Delivered to NASA

| Solar Cell # | Silicon Substrate Material† | Epitaxial Film Thickness (microns) | Epitaxial Film Resistivity (Ω-cm) | Diffusion Hours | Diffusion Temp°C | $I_{sc}$ (ma) | $V_{oc}$ (V) | Max % Efficiency‡ |
|---|---|---|---|---|---|---|---|---|
| 65 | Lopex* | 55.8 | 22 | 63 | 1250 | 37.9 | 0.550 | 8.3 |
| 66 | " | 51.8 | 17 | 120 | 1220 | 38.3 | 0.545 | 8.0 |
| 67 | " | 53.8 | 18 | 120 | 1220 | 43.0 | 0.567 | 8.4 |
| 68 | " | 49.3 | 17 | 120 | 1220 | 40.8 | 0.577 | 8.7 |
| 69 | " | 52.6 | 18 | 120 | 1220 | 42.0 | 0.574 | 10.4 |
| 70 | " | 73.7 | 12 | 120 | 1220 | 45.2 | 0.550 | 10.3 |

* Texas Instruments Incorporated Trademark

† Substrates were 0.007 Ω-cm.

‡ Based on 1.6 $cm^2$ active area

TABLE VII

Characteristics of Sample Cells Delivered to NASA

| Solar Cell # | Silicon Substrate Resistivity (Ω-cm)* | Epitaxial Film Thickness (microns) | Epitaxial Film Resistivity (Ω-cm) | Diffusion Hours | Diffusion Temp°C | $I_{sc}$ (ma) | $V_{oc}$ (V) | Max% Efficiency |
|---|---|---|---|---|---|---|---|---|
| 71 | 0.008 | 49.3 | 19 | 76.5 | 1250 | 43.3 | 0.562 | 9.3 |
| 72 | 0.008 | 50.7 | 13 | 76.5 | 1250 | 45.1 | 0.563 | 8.8 |
| 73 | 0.008 | 50.7 | 15 | 76.5 | 1250 | 43.8 | 0.561 | 8.2 |
| 74 | 0.008 | 23.1 | 12 | 18.5 | 1250 | 38.9 | 0.562 | 7.9 |
| 75 | 0.008 | 23.1 | 12 | 18.5 | 1250 | 39.1 | 0.562 | 7.4 |
| 76 | 0.008 | 13.7 | 7 | 5.8 | 1250 | 32.7 | 0.562 | 7.4 |
| 77 | 0.008 | 13.7 | 7 | 5.8 | 1250 | 33.6 | 0.562 | 7.5 |
| 78 | 0.20 | 27.4 | 11 | 51 | 1250 | 51.9 | 0.561 | 11.7 |
| 79 | 0.20 | 27.4 | 11 | 51 | 1250 | 53.0 | 0.561 | 12.3 |
| 80 | 0.20 | 27.4 | 12 | 51 | 1250 | 51.2 | 0.562 | 11.2 |
| 81 | 0.20 | 27.4 | 12 | 51 | 1250 | 53.6 | 0.562 | 12.7 |
| 82 | 0.20 | 25.9 | 14 | 51 | 1250 | 50.6 | 0.562 | 12.0 |
| 83 | 0.20 | 25.9 | 14 | 51 | 1250 | 51.0 | 0.562 | 11.6 |
| 84 | 0.20 | 27.4 | 11 | 51 | 1250 | 52.7 | 0.563 | 12.0 |
| 85 | 0.20 | 25.9 | 12 | 51 | 1250 | 53.2 | 0.562 | 12.7 |

* Substrates are Czochralski pulled.

TABLE VIII

Characteristics of Sample Cells Delivered to NASA

| Solar Cell # | Silicon Substrate Resistivity (Ω-cm)* | Epitaxial Film Thickness (microns) | Epitaxial Film Resistivity (Ω-cm) | Diffusion Hours | Diffusion Temp°C | $I_{sc}$ (ma) | $V_{oc}$ (V) | Max % Efficiency |
|---|---|---|---|---|---|---|---|---|
| 86 | 0.20 | 50.8 | 12 | 162 | 1265 | 50.0 | 0.557 | 9.5 |
| 87 | 0.20 | 14.0 | 9 | 12 | 1265 | 47.4 | 0.575 | 10.8 |
| 88 | 0.20 | 13.7 | 9 | 12 | 1265 | 44.2 | 0.572 | 9.5 |
| 89 | 0.20 | 13.7 | 9 | 12 | 1265 | 46.0 | 0.569 | 9.8 |
| 90 | 0.20 | 13.7 | 9 | 12 | 1265 | 43.1 | 0.567 | 9.5 |
| 91 | 0.20 | 13.7 | 9 | 12 | 1265 | 43.9 | 0.570 | 9.7 |
| 92 | 0.20 | 13.7 | 9 | 12 | 1265 | 48.0 | 0.579 | 10.9 |
| 93 | 0.20 | 13.7 | 9 | 12 | 1265 | 44.8 | 0.578 | 10.3 |
| 94 | 0.20 | 5.9 | 3 | 3.25 | 1265 | 41.0 | 0.565 | 7.9 |
| 95 | 0.20 | 5.9 | 3 | 3.25 | 1265 | 40.5 | 0.566 | 8.3 |
| 96 | 0.20 | 5.9 | 3 | 3.25 | 1265 | 40.7 | 0.567 | 8.5 |
| 97 | 0.20 | 5.9 | 3 | 3.25 | 1265 | 43.0 | 0.563 | 8.2 |
| 98 | 0.20 | 5.9 | 3 | 3.25 | 1265 | 42.1 | 0.564 | 8.1 |
| 99 | 0.20 | 5.9 | 3 | 3.25 | 1265 | 39.3 | 0.560 | 7.8 |
| 100 | 0.20 | 5.9 | 3 | 3.25 | 1265 | 41.5 | 0.547 | 7.2 |

* Substrates are Czochralski pulled.

regarding sample cells one through seventy, but more quantitative statements are given regarding cells 71 through 100, which were fabricated by Procedure II (See VI).

A number of cells were prepared by approaches 2 and 3 described in III.C. Only six cells, however, were considered worthy of shipment as sample cells. Characteristics of these cells, numbers 16 through 21, are shown in Table II. As a result of a decision to emphasize attempts to improve carrier lifetime, the relatively poor resistance to radiation (see VIII), and the relative difficulty of preparing cells by these two approaches, approach one (single deposit and diffusion) was utilized for all the other sample cells.

Cells 28 through 36 (Table III) were fabricated from 50-micron thick epitaxial deposits on 0.008 Ω-cm Lopex* substrates. Layer resistivities for cells 28-32 were about 25 Ω-cm and for cells 33-36, about 2 Ω-cm. Whereas values of $I_{sc}$ and the maximum efficiencies do not indicate any significant difference between the two groups, the values of $V_{oc}$ for cells 28-32 are almost 0.05 volt lower than those for cells 33-36. This was expected due to the higher base resistivity.[15]

Ten cells were subjected to a gettering treatment. On the basis of data from these cells and a number of others not included as sample cells, it appears that use of the

---

* Texas Instruments Incorporated Tradename

gettering step (front or backside) did not improve current-voltage characteristics of cells fabricated from deposits either on Lopex* or on Czochralski silicon. In fact, the average maximum efficiency of a group of four gettered cells was less than seven per cent compared with an average efficiency above nine per cent for five ungettered but otherwise comparable cells.

With respect to $I_{sc}$, $V_{oc}$, and maximum conversion efficiency, no significant differences could be found between unirradiated cells fabricated from Lopex* and from Czochralski silicon material.

As mentioned in IV.A, for sample cells 1 through 50 the thickness of uniform concentration material adjacent to the surface was greater than intended. Sample cells 51 through 100 utilized longer diffusion times and the concentration gradient thus extends more closely to the surface. (In the optimum cell, as pointed out in Appendix I, the drift field should begin as near to the junction as possible.) Sample cells 45-50 and 51-54 constitute two groups in which the principal difference is the diffusion time. Using the diffusion constant of Williams[8] suggested a requirement of 19.5 hours at 1250°C. The diffusion constant of Kurtz and Yee[9] required 47.0 hours at 1250°C to diffuse the impurities out to the surface. There appear to be no significant differences in the values of $I_{sc}$, $V_{oc}$, and maximum conversion efficiency between the two groups.

In terms of $I_{sc}$, $V_{oc}$, and maximum conversion efficiency for sample cells fabricated by Procedure I, the variation of epitaxial layer thickness from 16 microns to 76 microns had no visible effect.

---

* Texas Instruments Incorporated Tradename

For cells fabricated by Procedure II (See VI.) the variation of epitaxial layer thickness had a marked effect on the electrical characteristics (unirradiated cells). Cells fabricated by this procedure (this includes sample cells 71 through 100) were divided into seven groups depending on substrate and epitaxial values and time required to diffuse the impurities to the surface. Preparation conditions for the groups are shown in Table IX. Examination of Tables VII and VIII show that whereas values of $V_{oc}$ are for all seven groups consistently high, some significant differences occur in values of $I_{sc}$ and the maximum efficiency. Significance of these variations is easily seen in Fig. 26, which shows the distributions of the short circuit current values for cells in the seven groups. For cells made on 0.008 Ω-cm substrates (groups I, II, and III), values of $I_{sc}$ decrease with decreasing width of the drift field. Particularly low are the current values for cells in Group III. In this group, by far the majority of carriers were generated in a region in which the mobility was quite low. For cells made on 0.20 Ω-cm substrates (groups IV, V, VI, and VII), however, a maximum in value of $I_{sc}$ is observed as the drift-field width decreases. Highest values of $I_{sc}$ occur for cells in Group V. Of the seven groups, V is closest in drift-field characteristics to the "optimum" structure (see Appendix I) for an irradiated cell.

Although there is some variation in values of the epitaxial film resistivity among the seven groups, effect of this variation on $I_{sc}$ is not considered significant except perhaps for Group VII, for which the resistivity values are somewhat lower than intended.

Table IX

Preparation Conditions for Cells Fabricated by Procedure II

| Group Number | Number of Cells in Group Evaluated | Silicon Substrate Resistivity (Ω-cm)* | Nominal Epitaxial Film Thickness (microns) | Nominal Epitaxial Film Resistivity (Ω-cm) | Diffusion Hours | Diffusion Temp°C |
|---|---|---|---|---|---|---|
| I | 26 | 0.008 | 50 | 17 | 76.5 | 1250 |
| II | 20 | 0.008 | 25 | 14 | 18.5 | 1250 |
| III | 16 | 0.008 | 13 | 9 | 5.8 | 1250 |
| IV | 15 | 0.20 | 50 | 12 | 162 | 1265 |
| V | 16 | 0.20 | 25 | 13 | 51 | 1250 |
| VI | 14 | 0.20 | 13 | 9 | 12 | 1265 |
| VII | 21 | 0.20 | 6 | 3 | 3.25 | 1265 |

* Substrates were Czochralski pulled.

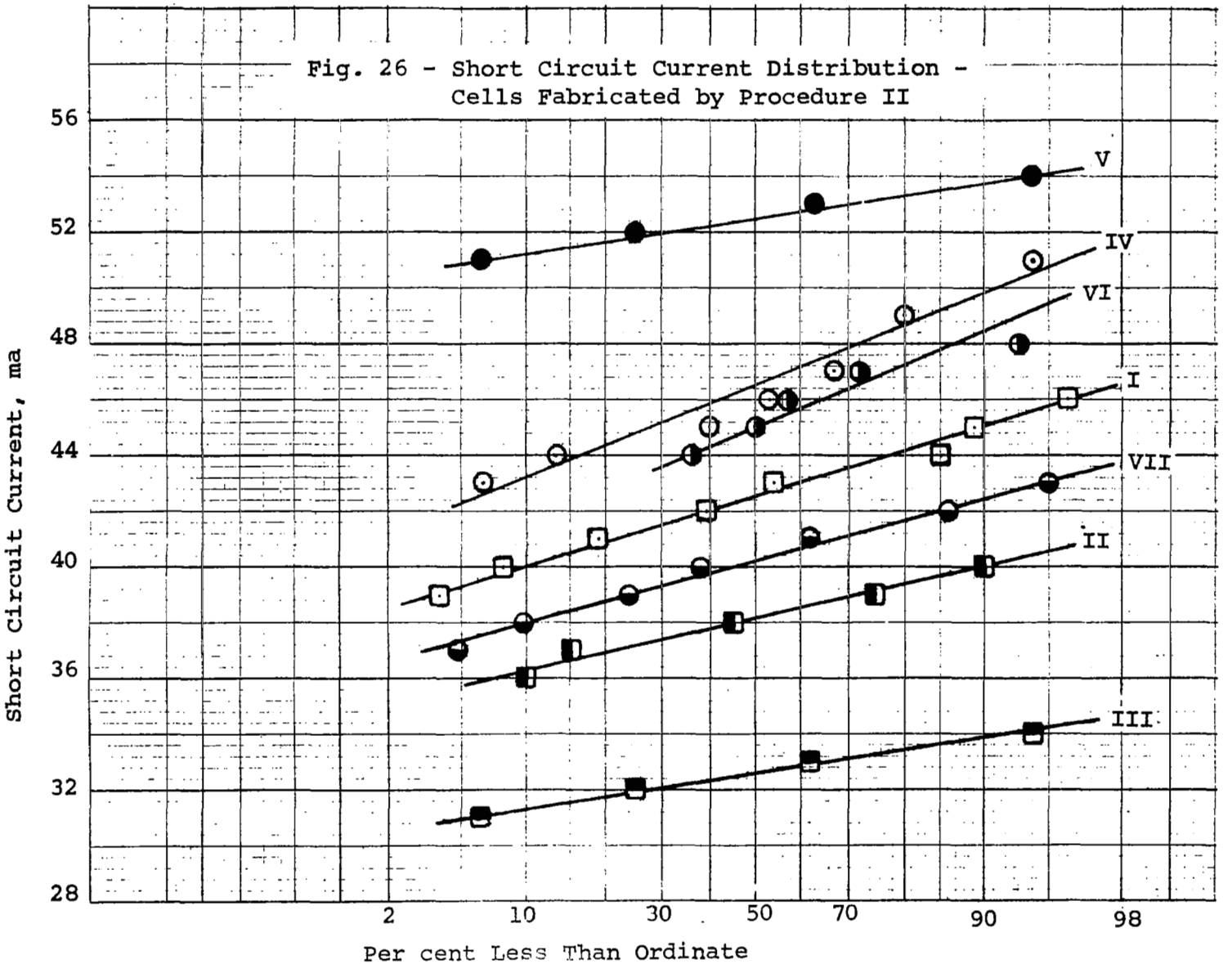
Fig. 26 - Short Circuit Current Distribution -
Cells Fabricated by Procedure II
Short Circuit Current, ma
56
52
48
44
40
36
32
28
2
10
30
50
70
90
98
Per cent Less Than Ordinate
V
IV
VI
I
VII
II
III

C. Spectral Response

In this section data are given regarding relative collection efficiency versus wavelength for various cells. Absolute efficiency data are not available for these cells, and thus the relative comparison of the ordinate does not extend from cell to cell. The ordinate, in every case, is the relative response per photon.

Figure 27 gives spectral response data for three cells. Curve A represents the relative response per photon of a normal n-p, non-epitaxial solar cell manufactured by Texas Instruments Incorporated. This cell had a maximum efficiency of 12.5 per cent. Curves B and C represent relative photon efficiencies of cells fabricated (by Procedure I) from epitaxial material. Both had 38-micron thick, 2 Ω-cm deposits. Cell B received a diffusion of 16 hours at 1250°C; Cell C was not diffused before fabrication. Carrier lifetime in Cells B and C are substantially lower than the lifetime in Cell A. These shortened lifetimes result in reduced efficiencies at the longer wavelengths.[16] Because Cell C received no drift diffusion after epitaxy, the concentration profile in the base region is similar to that in Fig. 4a. of III.C.1. Thus, the field to accelerate the electrons to the collector junction does not coincide with the region in which the majority of the photons are absorbed. In Cell B, the drift field extends closer to the junction, but does not reach the surface.

Employment of a gettering treatment apparently broadened the relative collection efficiency for cells made

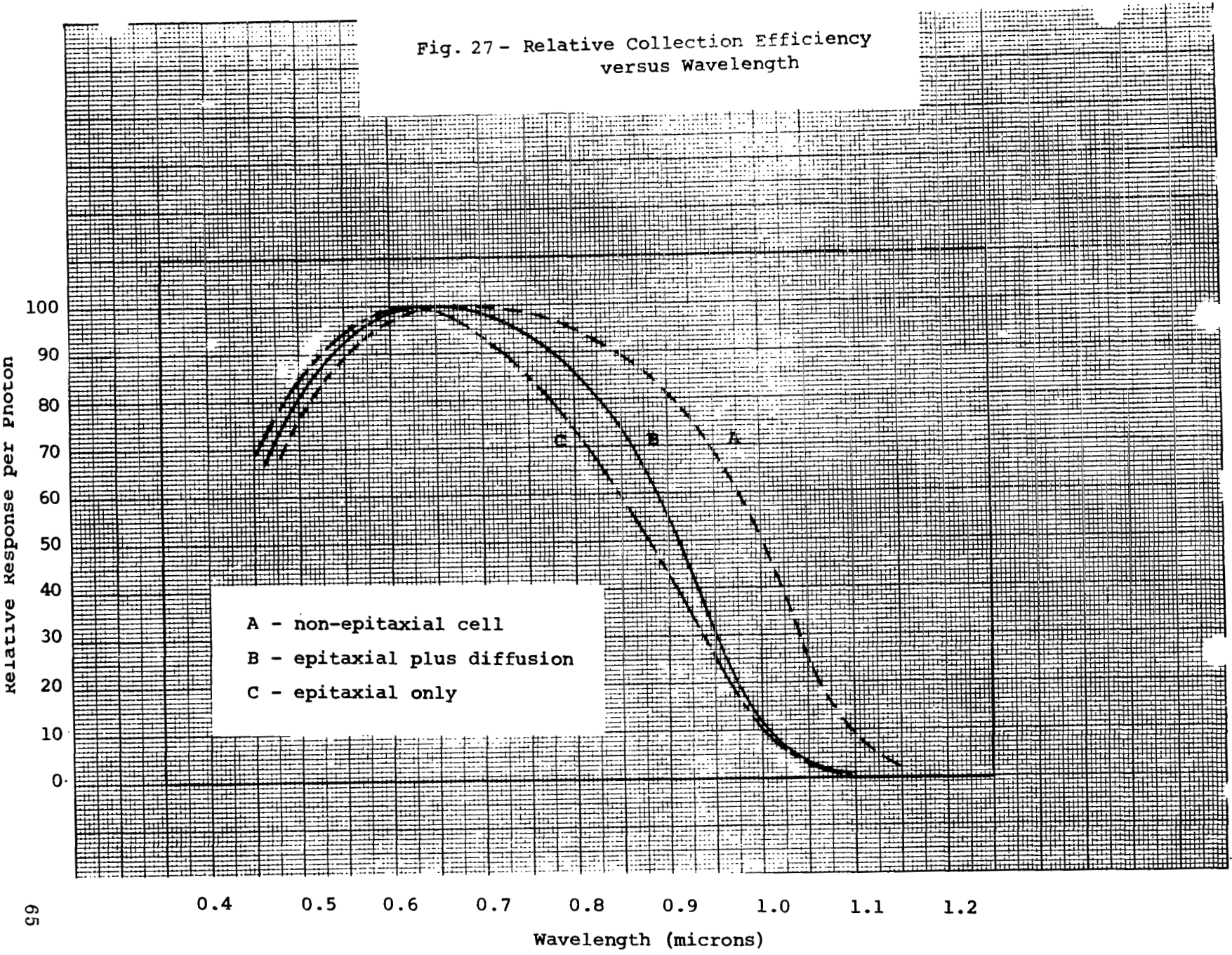


Fig. 27 - Relative Collection Efficiency versus Wavelength

on 0.002 Ω-cm Lopex* and 0.008 Ω-cm Czochralski substrates with about 50-micron thick deposits. Curves D and E of Fig. 28 represent, respectively, relative response of cells 37 and 38. Cell 38, which was gettered, shows a broadened response. The curves in Fig. 29 show similar broadening by gettering for cell 45 relative to Cell 47.

Curves B and C of Fig. 30 provide a comparison of the response of Cells 25 and 32, respectively. These cells had similar epitaxial layer resistivities, but the Cell 32 layer is twice as thick as the Cell 25 layer. For Cell 32, in which the impurity gradient extends over about 50 microns, the peak response is broader than for Cell 25, but neither are as flat as the response for a normal n-p cell represented by curve A.

The cells represented in Figs. 28 and 30 have peak responses in the 0.70 to 0.78 micron region. Cells made from epitaxial deposits on Czochralski silicon substrates showed less sensitivity in the red region, peaking at 0.65 micron or less. These and other observations suggest that the cells fabricated from deposits on Lopex* crystals exhibit higher lifetime than those which were made from deposits on Czochralski crystals. (This assumes constant fabrication conditions, which for cells fabricated by Procedure I probably is not a good assumption.)

Cells fabricated by Procedure II afforded a good opportunity for examination of relative spectral response as a function of epitaxial layer thickness and substrate resistivity.

---

* Texas Instruments Incorporated Tradename.

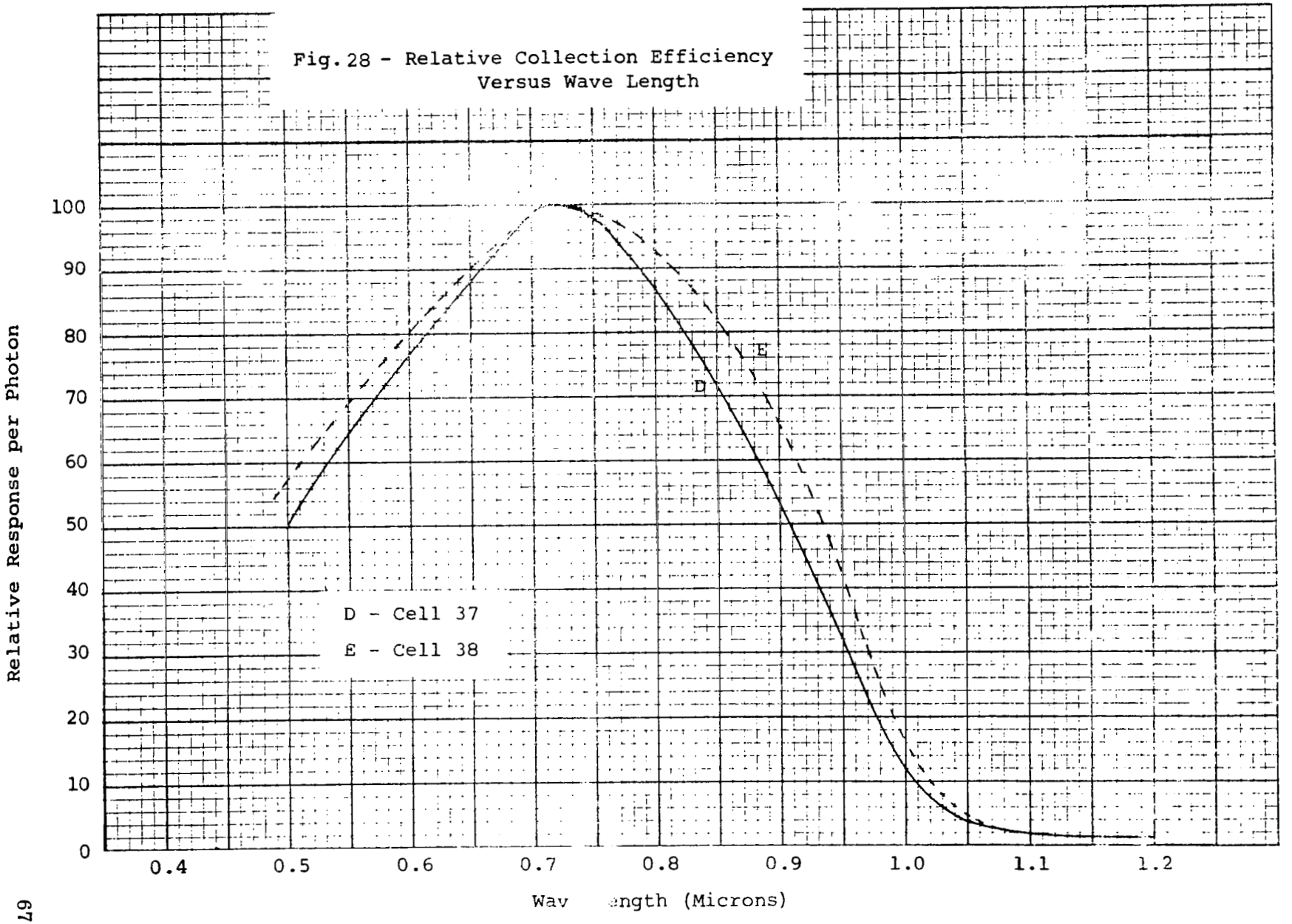
Fig. 28 - Relative Collection Efficiency
Versus Wave Length
Relative Response per Photon
100
90
80
70
60
50
40
30
20
10
0
0.4
0.5
0.6
0.7
0.8
0.9
1.0
1.1
1.2
Wav ength (Microns)
D - Cell 37
E - Cell 38
D
E

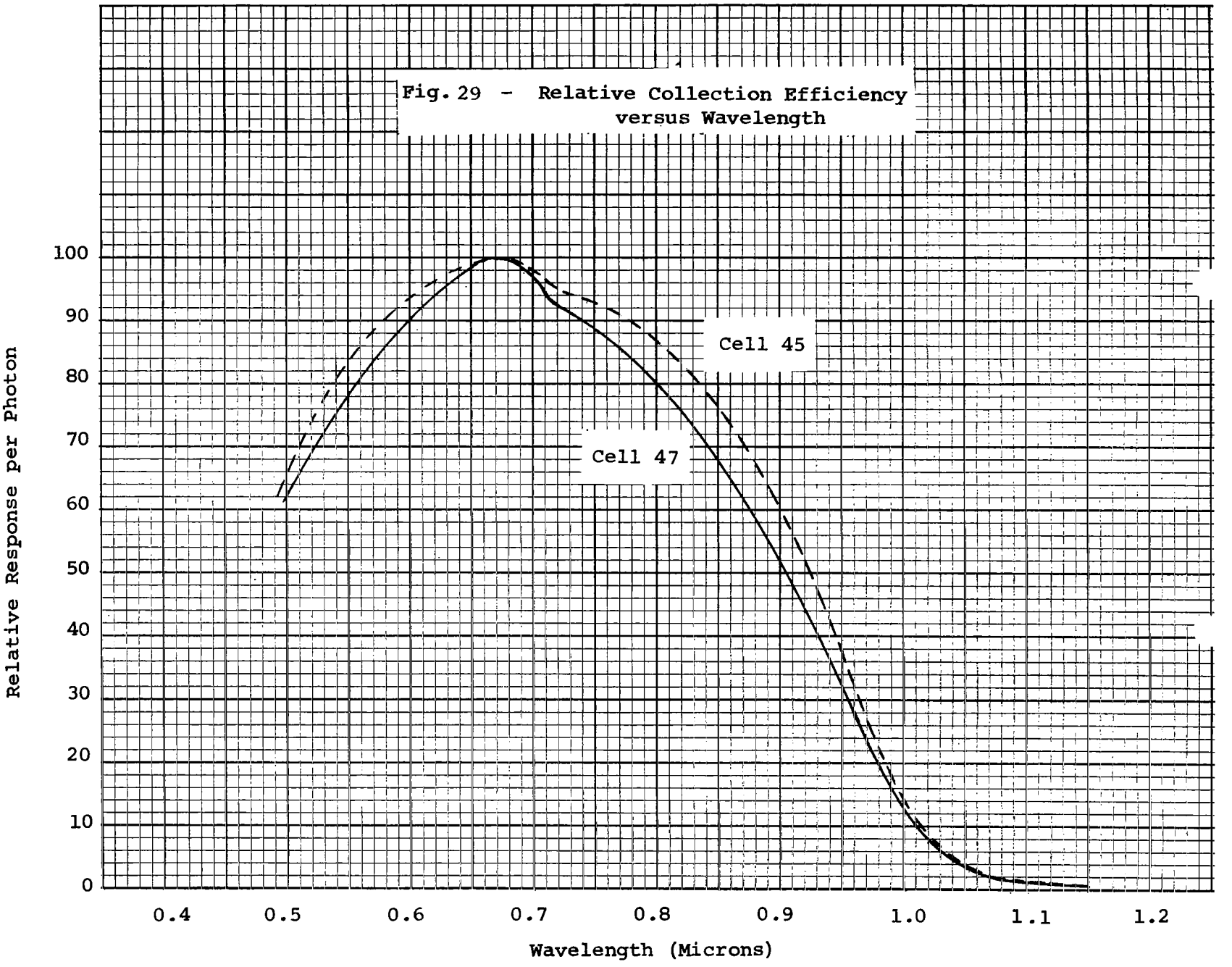
Fig. 29 - Relative Collection Efficiency versus Wavelength
Cell 45
Cell 47
Relative Response per Photon
100
90
80
70
60
50
40
30
20
10
0
0.4
0.5
0.6
0.7
0.8
0.9
1.0
1.1
1.2
Wavelength (Microns)

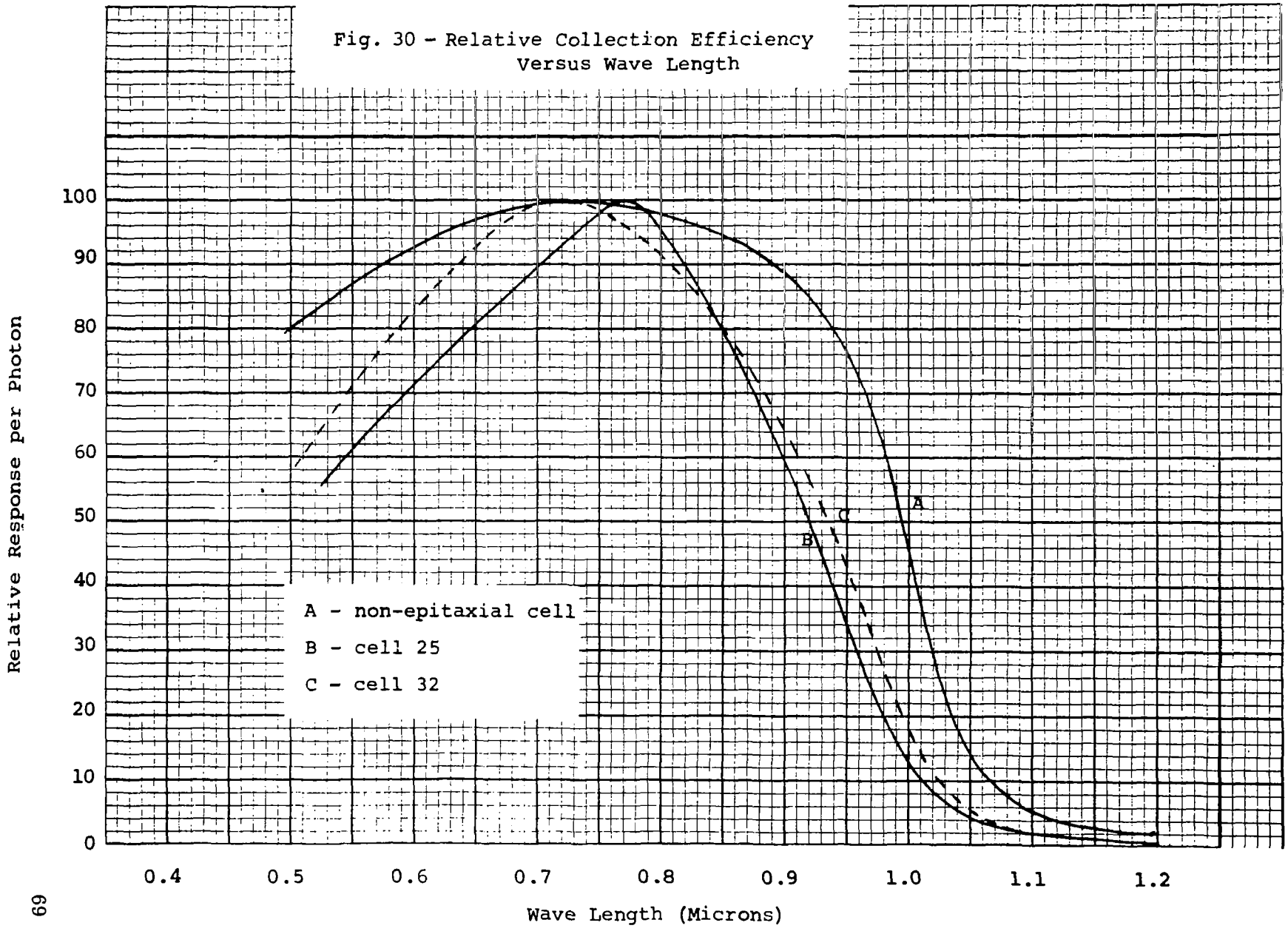
Fig. 30 - Relative Collection Efficiency
Versus Wave Length
Relative Response per Photon
100
90
80
70
60
50
40
30
20
10
0
0.4
0.5
0.6
0.7
0.8
0.9
1.0
1.1
1.2
Wave Length (Microns)
A - non-epitaxial cell
B - cell 25
C - cell 32
A
B
C

Relative collection efficiency was determined for a representative cell from each of the seven groups listed in Table IX. The curves in Fig. 31 show the spectral response for cells from Groups I, II and III. The relative response is broader and slightly more sensitive in the red region for the thicker drift-field. Figure 32 shows the curves for cells from Groups IV, V, VI, and VII. The same relation of increasing sensitivity to red with increasing drift-field thickness holds, except for the cell from Group IV.

## VIII. RADIATION RESULTS

Radiation experiments were conducted by NASA on cells selected from the first seventy sample cells. Since the last two sample lots (cells 71 through 100) were transmitted only recently, irradiation data have not yet been received for them. Therefore, the data presented in this section does not include irradiation results for what is now thought to be the optimum drift-field structure.

Previous sections of this report have mentioned the lack of reproducibility of cell characteristics from one cell to another among cells in a common grouping. This lack of reproducibility, ascribed to the partial shorting of cells fabricated by Procedure I, also is evident in widespread variation in the radiation experiments. Presented in Figs. 33, 34, and 35 are curves which show the degradation of short circuit current as a function of 1 MeV electron flux for 32 cells. Current-voltage values were obtained for 100 $mW/cm^2$ xenon light illumination. The current values are normalized to their pre-bombardment values. Sample cell numbers correspond to those in Tables I-VI.

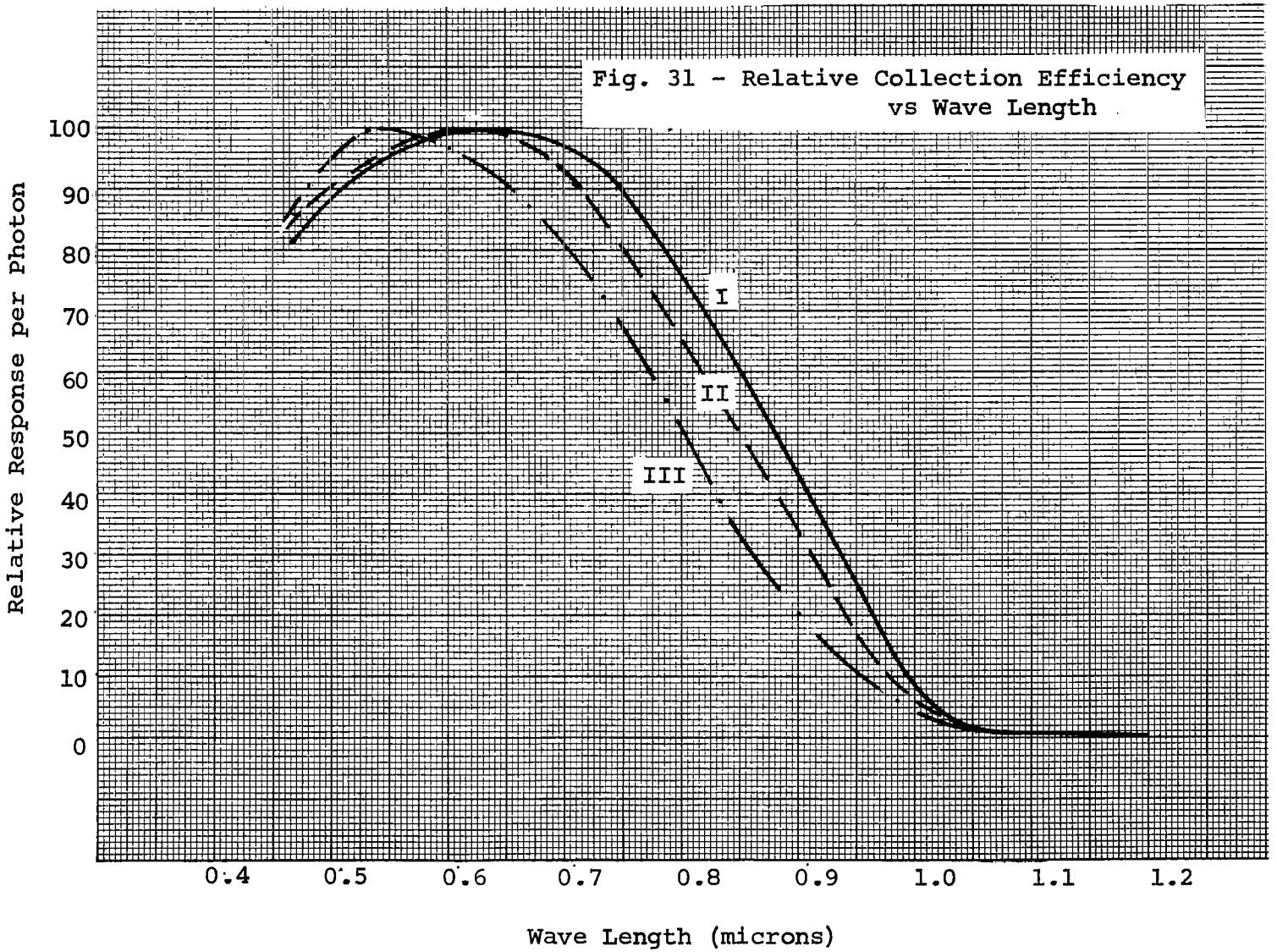
Fig. 31 - Relative Collection Efficiency vs Wave Length
Relative Response per Photon
100
90
80
70
60
50
40
30
20
10
0
I
II
III
0.4
0.5
0.6
0.7
0.8
0.9
1.0
1.1
1.2
Wave Length (microns)

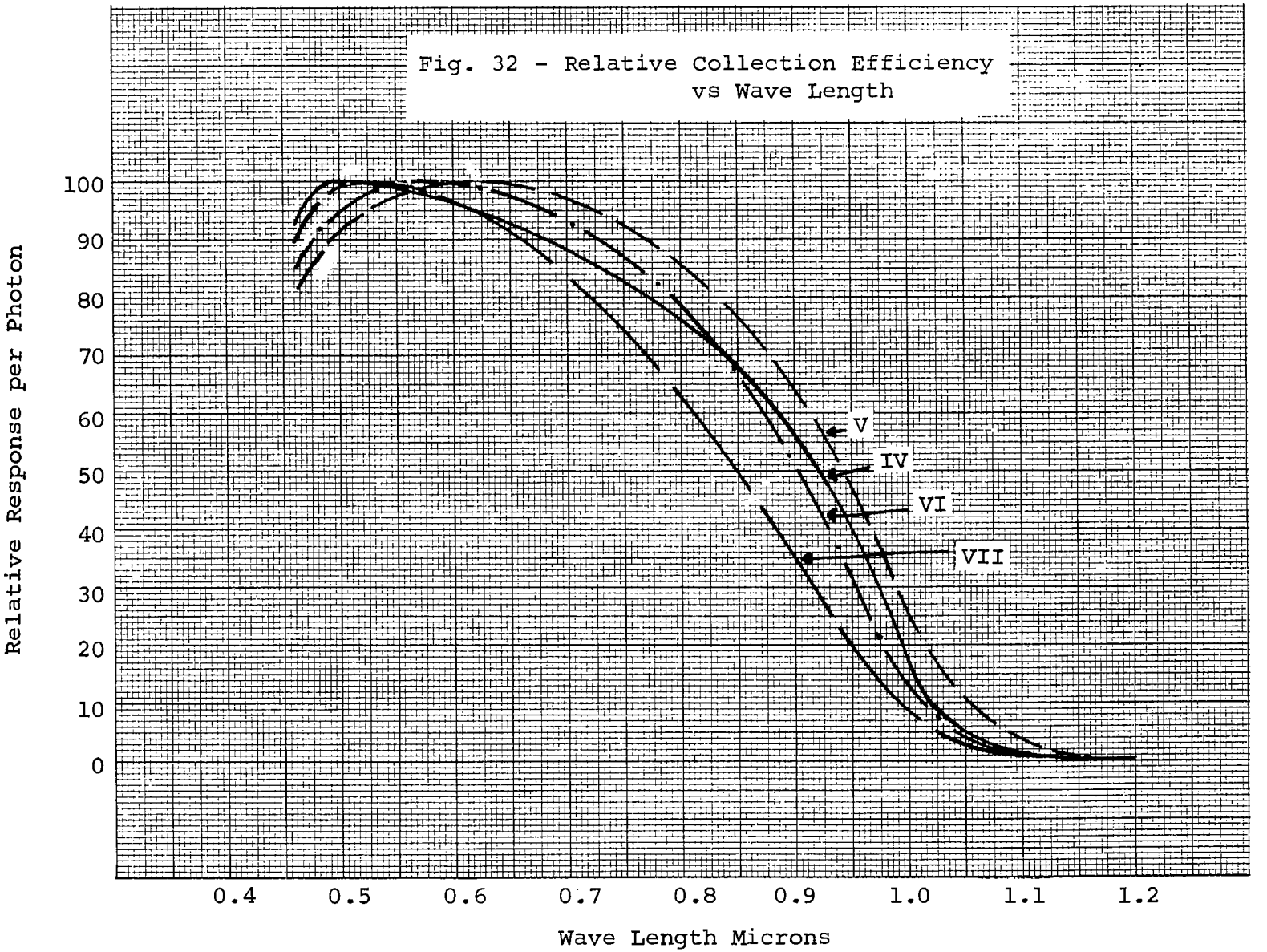
Fig. 32 - Relative Collection Efficiency
vs Wave Length
Relative Response per Photon
100
90
80
70
60
50
40
30
20
10
0
V
IV
VI
VII
0.4
0.5
0.6
0.7
0.8
0.9
1.0
1.1
1.2
Wave Length Microns

Fig. 33 - Normalized Short Circuit Current Degradation vs Electron Flux

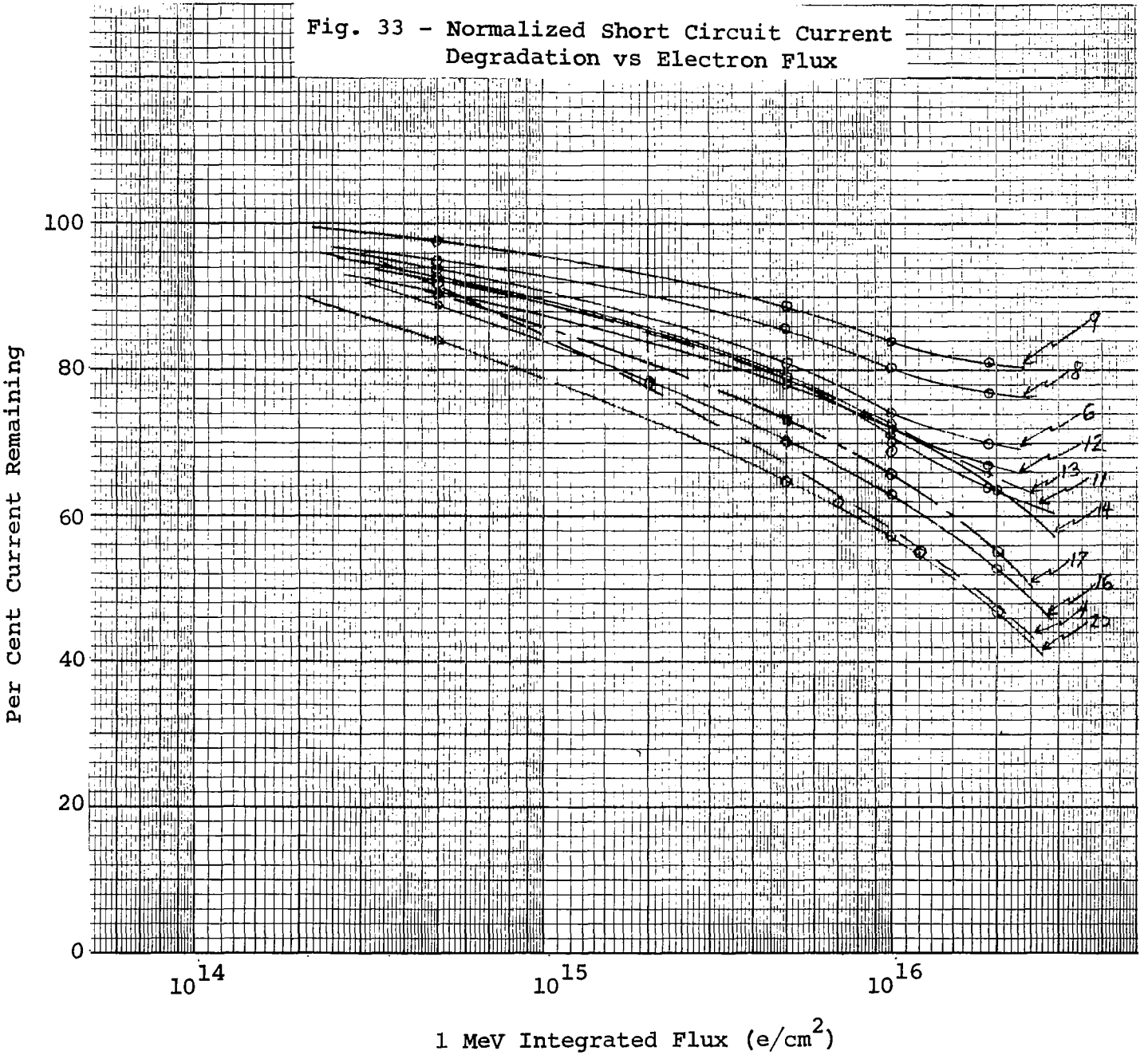

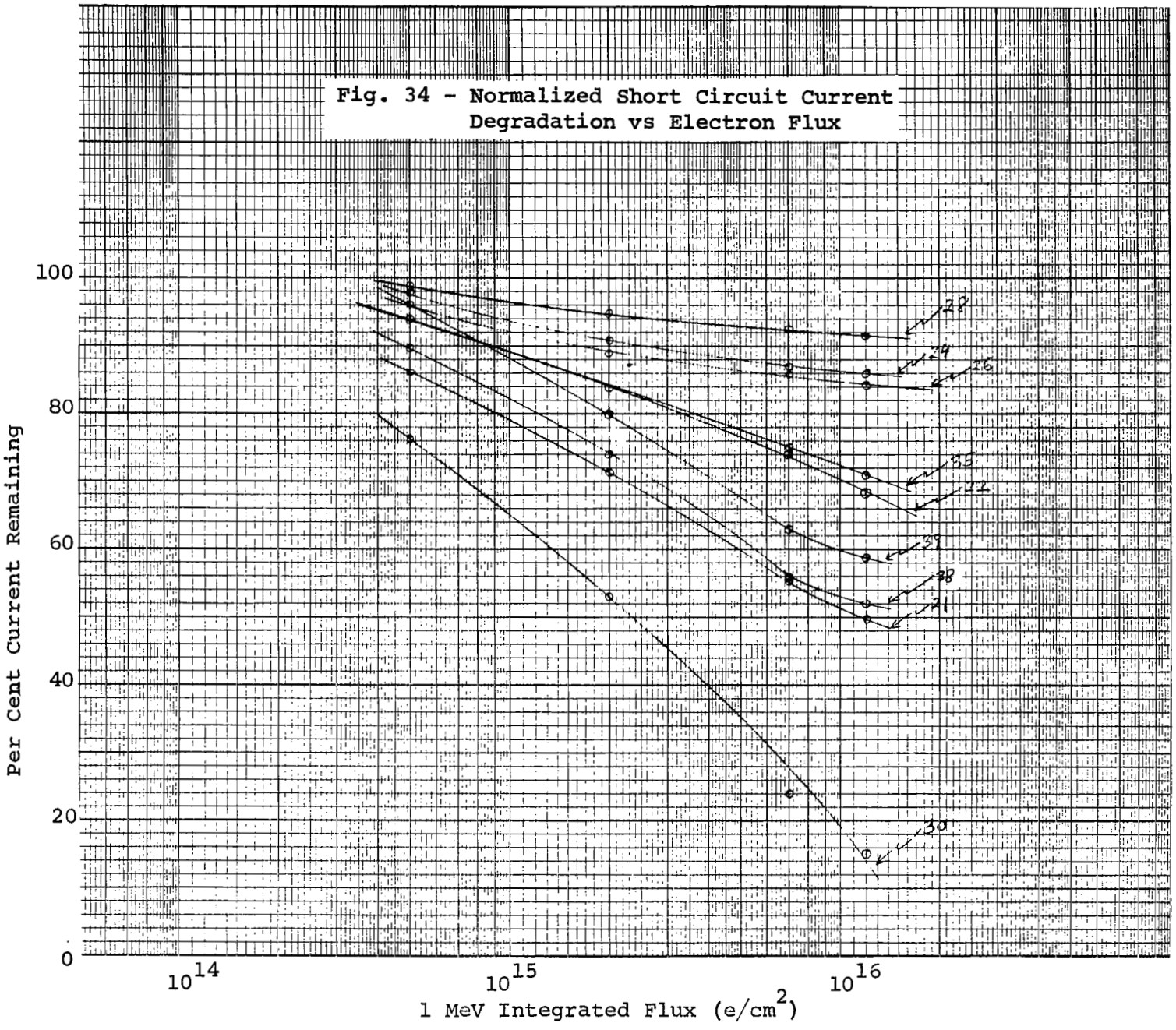


Fig. 34 - Normalized Short Circuit Current Degradation vs Electron Flux

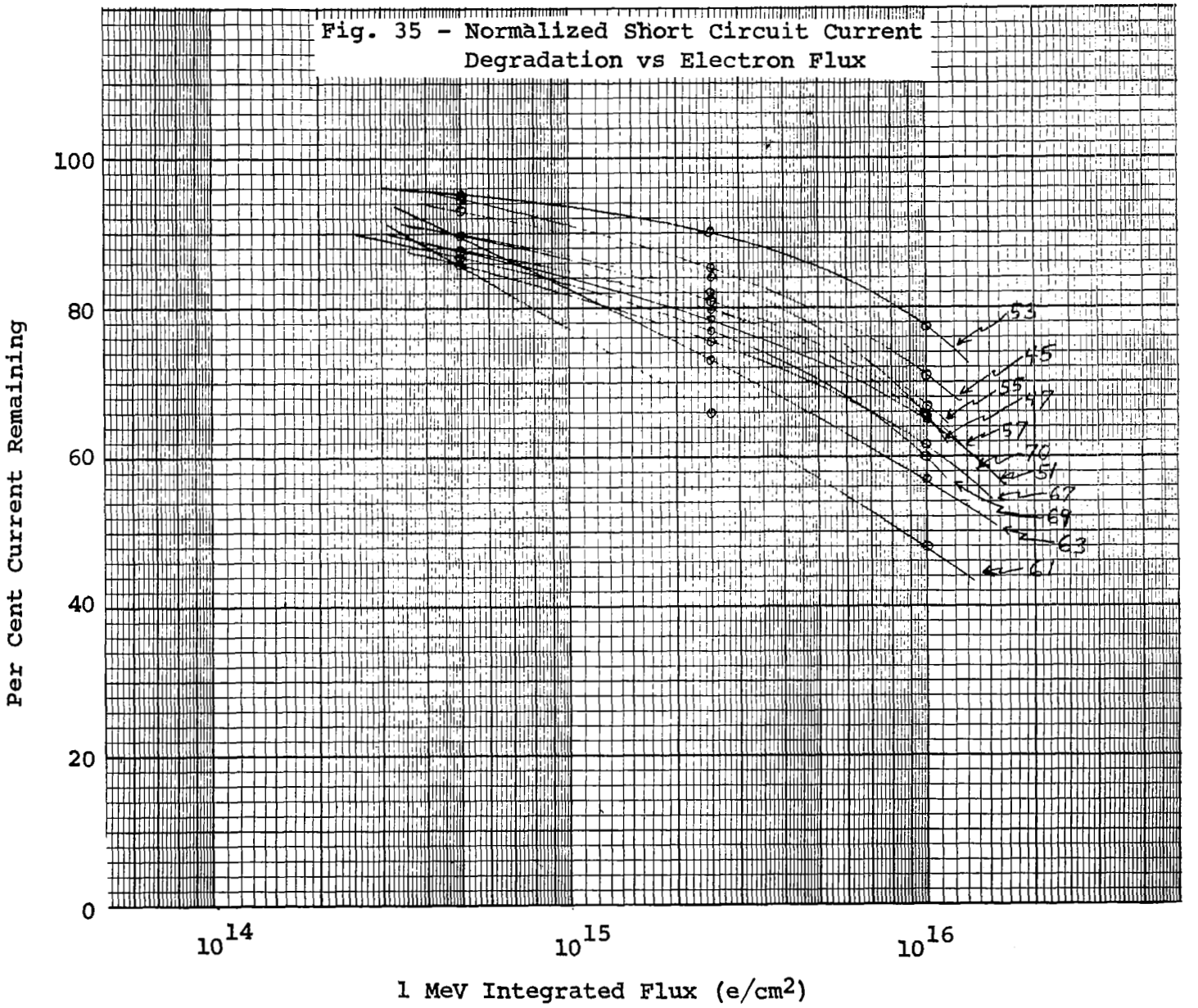
Fig. 35 - Normalized Short Circuit Current Degradation vs Electron Flux
Per Cent Current Remaining
100
80
60
40
20
0
$10^{14}$
$10^{15}$
$10^{16}$
1 MeV Integrated Flux ($e/cm^2$)
53
45
55
47
57
70
51
67
69
63
61

For cells fabricated with a high-resistivity epitaxial layer, other conditions being equal, the short circuit current decreases less rapidly and the open circuit voltage decreases more rapidly with one MeV electron radiation than for cells fabricated with a lower resistivity epitaxial layer. Over-all degradation is less, however, for the former than for the latter, in agreement with a similar base resistivity-radiation resistance dependency observed for field free cells.[17] Figure 36 shows the increased resistance to degradation with decreasing impurity atoms in the base (increasing resistivity) for a group of eleven cells, each having an epitaxial layer about 25 microns thick. Data correspond to a cumulative flux of $1 \times 10^{16}$ electrons per $cm^2$. Numbers adjacent to the data points correspond to sample cell numbers in Tables I-III. Magnitude of the decrease in the open circuit voltage with radiation as a function of doping level is less marked and is not shown.

Best of the sample cells tested in terms of per cent current remaining after irradiation was cell 28 which had lost only eight per cent of its $I_{sc}$ value at a cumulative one MeV electron flux of $1.2 \times 10^{16}$. For this cell, however, the reduction in the $V_{oc}$ value at the same flux level was nineteen per cent. Best of the cells tested in terms of absolute maximum efficiency in a 100 $mW/cm^2$ xenon light source was cell 24, which still had 5.4 per cent efficiency after $1.2 \times 10^{16}$ one MeV electrons.

On the basis of radiation experiments with sample cells fabricated by Procedure I, no improvement (at a level of statistical significance) in radiation resistance can be ascribed

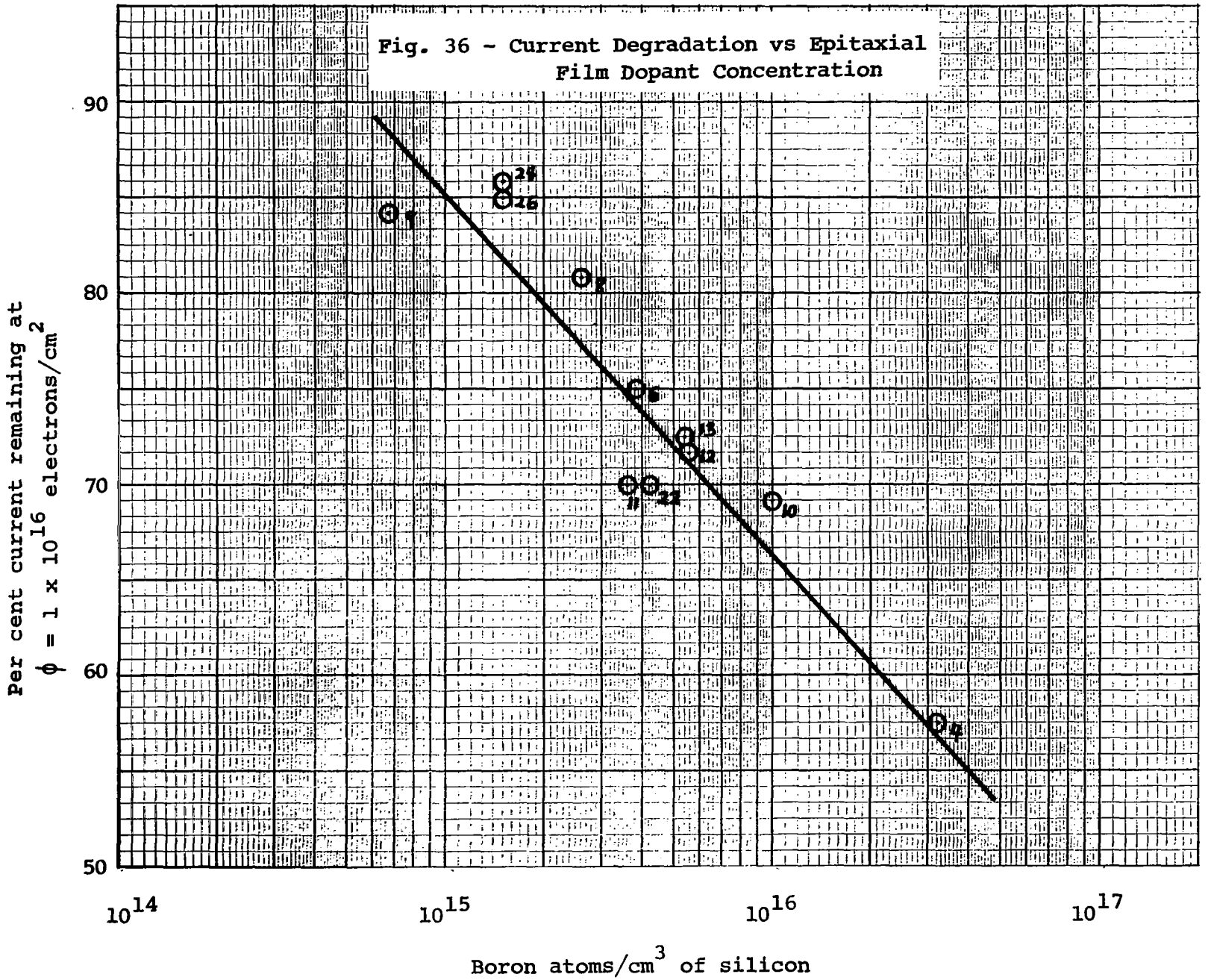
Fig. 36 - Current Degradation vs Epitaxial Film Dopant Concentration
Per cent current remaining at $\phi = 1 \times 10^{16}$ electrons/cm$^2$
90
80
70
60
50
$10^{14}$
$10^{15}$
$10^{16}$
$10^{17}$
Boron atoms/cm$^3$ of silicon

either to the use of a gettering operation (front or backside) or to the use of Lopex* silicon.

The calculations in Appendix I were made on the basis of optimizing the short-circuit electron current from the p-region of the cell. They were not concerned with the effects of degradation of the open circuit voltage. It seems quite possible, in view of the experimental evidence cited above, that the optimization of $I_{sc}$ may be at the expense of $V_{oc}$. Thus, to secure maximum usable power may involve some "trade-off" between the respective parameters. The sample cells closest in drift-field structure to the optimum suggested in Appendix I are cells 78-85 and 87-93 (see Table VII and VIII). Data from radiation experiments with these cells should be helpful in showing the relative degradations of $V_{oc}$ and $I_{sc}$ for a structure near optimum for $I_{sc}$.

## IX. CONCLUSIONS AND RECOMMENDATIONS FOR FUTURE WORK

Experimental silicon drift-field solar cells were produced by means of advanced epitaxial and diffusion technology. A variety of drift-field structures were made, some of which produced cells more resistant to bombardment by one MeV electrons than are ordinary n-p solar cells. A number of sample cells, fabricated near the end of the contract period from near-optimum drift-field structures, exhibited high current values in the unirradiated state. On the basis of the theoretical analysis of drift fields which was made, these sample cells when irradiated should show superior radiation resistance.

---

* Texas Instruments Incorporated Tradename.

Drift-field structures built by the single epitaxial deposit and drift diffusion technique (section III.C.1) and fabricated into cells by Procedure II (section VI) represent the best combination of methods by which a drift-field solar cell may be produced. Excellent reproducibility of electrical characteristics from one cell to another within a common group of those cells was noted. Over-all high yields (electrical and mechanical) obtained with this procedure were almost as high as for production of a standard n-p solar cell, establishing the production feasibility of this procedure to build drift-field solar cells. This process promises to be much less expensive than one which involves a precision lapping operation after the epitaxial deposition due to the low yields inherent in that process.

Good reproducibility was not found for cells fabricated by Procedure I and production yields were low because of the reasons cited in section VI.

The theoretical analysis of drift-fields (Appendix I), which takes into account the variation of mobility with concentration, suggests that the ratio of the impurity concentrations in the gradient making up the drift field should not exceed three orders of magnitude. Also, the width of the drift field probably should not exceed 25 microns. Low carrier lifetime prevents the improvement of over-all collection efficiency by use of significantly thicker deposited layers.

Though the longer wavelength response was improved in some instances by wider drift fields and/or by higher initial

lifetime (e.g. by use of Lopex* silicon or gettering), the maximum conversion efficiency after irradiation apparently was not improved. On the basis of radiation experiments with sample cells fabricated by Procedure I, no improvement in radiation resistance could be ascribed to the use of a gettering operation or to the use of Lopex* silicon.

The method developed for determining the concentration profile (IV.B.) represents an important advance in cell evaluation. In future work, it is recommended that cells which show particularly good (or poor) resistance to radiation be subjected to a profile measurement to determine the exact drift-field structure.

The calculations in Appendix I were made on the basis of optimizing the collection efficiency and short-circuit current. They were not concerned with the effects of degradation of the open circuit voltage. The radiation data show that to secure maximum usable power may involve some "trade-off" between the current and the voltage. Thus, it is recommended that subsequent work include a study of the degradation of the open circuit voltage and its effect on available power output from the cell.

## X. NEW TECHNOLOGY

During the course of the contract, a method was developed for the determination of a concentration gradient profile in silicon structures. Description and uses of the method, which is a substantial improvement over any method previously used, are given in section IV.B.

---

* Texas Instruments Incorporated Tradename

## XI. REFERENCES


1. Kenneth Bean and Paul Gleim, "Vapor Etching Prior to Epitaxial Deposition of Silicon," presented at the Fall Meeting of the Electrochemical Society Meeting, New York, Sept. 1963.

2. F. M. Smits, "Diffusion in Covalent Semiconductors," Ergeb. Exakt. Naturw. 31, 167 (1959).

3. W. G. Spitzer and M. Tanenbaum,"Interference Method for Measuring the Thickness of Epitaxially Grown Films," J. Appl. Phys. 32 744 (1961).

4. M. P. Albert and J. F. Combs, "Thickness Measurement of Epitaxial Films by the Infrared Interference Methods," J. Electrochemical Society 109, 710 (1962).

5. T. B. Light, "Imperfections in Germanium and Silicon Epitaxial Films," Metallurgy of Semiconductor Materials, John B. Schroeder, Editor, Interscience Publishers, N. Y. (1962), p 137.

6. John Brownson, "A Three-point Probe Method for Electrical Characterization of Epitaxial Silicon Films," presented at the Electrochemical Society Meeting, Los Angeles, May, 1962.

7. W. R. Runyan, Silicon Semiconductor Technology, McGraw-Hill, N. Y. (1965), p 138.

8. E. L. Williams, "Boron Diffusion in Silicon," J. Electrochemical Society 108, 795 (1961).

9. A. D. Kurtz and R. Yee, "Diffusion of Boron into Silicon," J. Appl. Phys. 31, 303 (1960).

10. J. Hiligrand, and R. D. Gold, "Determination of the Impurity Distribution in Junction Diodes From Capacitance-voltage Measurements," R.C.A. Review 21, 245, (1960).

11. G. Bemski, "Recombination Properties of Gold in Silicon," Phys. Rev. III, 1515 (1958).

12. M. C. Duffy, W. J. Armstrong, and M. S. Hess, "Detection of Low Concentration Impurities in Silicon," presented at the Electrochemical Society Meeting, Toronto, May, 1964.

13. S. W. Ing, Jr., R. E. Morrison, L. L. Alt, and R. W. Aldrich, "Gettering of Metallic Impurities from Planar Silicon Diodes," J. Electrochemical Society 110, 533 (1963).

14. R. N. Hall and J. H. Racette, "Diffusion and Solubility of Copper in Extrinsic and Intrinsic Germanium, Silicon, and Gallium Arsenide," J. Appl. Phys. 35, 379 (1964).

15. K. D. Smith, H. K. Gummel, J. D. Bode, D. B. Cuttriss, R. J. Nielsen, and W. Rosenzweig, "The Solar Cells and Their Mounting," Bell System Tech. Journal 42, 1765 (1963).

16. B. Dale and F. P. Smith, "Spectral Response of Solar Cells," J. Appl. Phys. 32, 1377 (1961).

17. R. Babcock, et al, "Radiation Resistance of Webbed Dendritc Solar Cells," presented at the Fourth Photovoltaic Specialists Conference, Cleveland, June, 1964; and others.

# APPENDIX I

## "INFLUENCE OF MOBILITY VARIATIONS ON DRIFT FIELD ENHANCEMENT IN SILICON JUNCTION DEVICES"

# APPENDIX I

## INFLUENCE OF MOBILITY VARIATIONS ON DRIFT FIELD ENHANCEMENT IN SILICON JUNCTION DEVICES

W. Murray Bullis and W. R. Runyan

Texas Instruments Incorporated, Dallas, Texas

ABSTRACT

An analysis of drift fields formed by an impurity gradient is carried out allowing for mobility variations with impurity concentration. It is shown that in the case of a transistor base of specified width there is a minimum time for transport of carriers across the base which occurs at some optimum value of the ratio of impurity concentrations at the two edges of the base region. In the case of photovoltaic solar cells, a field width of about twice the diffusion length of the minority carriers maximizes the collection efficiency. For lifetimes longer than one microsecond the optimum field width is about 25 microns, a value governed by the absorption characteristics rather than the diffusion length. In most cases, increasing the concentration ratio above 3 orders of magnitude is of little or no assistance in improving the collection efficiency.

## I. INTRODUCTION

Internal electric fields resulting from a density gradient of majority impurities may be used to enhance the motion of minority carriers in appropriate regions of a device structure. In particular, such aiding drift fields have been suggested for increasing the high frequency response of transistors with specified base width[1-3] and for enhancement of the current collected in a photovoltaic solar cell[4-7]. However, the necessity for varying the impurity density to produce the drift field will also change other characteristics. For example, Varnerin[8] has shown that if the total number of majority impurities in the base region of a high frequency transistor is held constant, the highest frequency devices result from the incorporation of retarding rather than aiding drift fields.

With the exception of this last paper and some correspondence concerning it[9], all previous analyses have neglected the variation of mobility and lifetime with impurity concentration. Since the mobility of carriers drops sharply as the impurity concentration

is increased, it can be naively assumed that at some point, increasing the drift field would not result in further enhancement of the desired effects and that, at least in some cases, optimum configurations might exist. It is the purpose of this paper to examine certain aspects of transistor and solar cell behavior from this more general point of view.

## II. TRANSIT TIME IN A TRANSISTOR BASE WITHOUT RECOMBINATION

The simplest situation to consider is the base region of a transistor. In this case, minority carriers are injected at one side and collected at the other. In general, the width of the base can be made small enough that losses due to recombination in the base region can be neglected, so that the current is constant. Following Varnerin,[8] we define the base transit time t as the ratio of stored charge $Q_s$ to the emitter current $I_e$:

$$t = Q_s/I_e. \tag{2-1}$$

If a one-dimensional structure is considered, this relation may be expressed more generally as

$$t = -q \int_o^W \frac{n\, dx}{J}, \tag{2-2}$$

where q is the electronic charge, w is the base width, and J is the emitter current density. If we consider the case where electrons are injected into a p-type base, the current density is given by

$$J_n = q \mu_n n E + q D_n \frac{dn}{dx} , \qquad (2-3)$$

where $D_n$ is the electron diffusion coefficient, $\mu_n$ is the electron mobility, and E is the electric field seen by the electrons. The mobility and diffusion coefficient are related by the Einstein equation:

$$D_n = \mu_n \frac{kT}{q} , \qquad (2-4)$$

and the electric field is given by

$$E = - \frac{d\Psi}{dx} = \frac{kT}{q} \frac{d \ \ln N_A}{dx} \qquad (2-5)$$

when the majority carrier (hole) density can be obtained from the Boltzmann distribution and when there is no applied external field in the region of interest.

If Eqs. (2-4) and (2-5) are substituted in Eq. (2-3), a linear differential equation of the first order is obtained. By the use of an integrating factor, it can be solved in a convential way even when $D_n$ is a function of the distance.[10] If it is assumed that all minority carriers are collected at the base-collector junction (x=w) this solution is

$$n(x) = \frac{J_n}{q\, N_A(x)} \int_x^w \frac{N_A(\xi)}{D_n(\xi)}\, d\xi . \tag{2-6}$$

Substitution of Eq. (2-6) into Eq. (2-2) yields for the transit time

$$t = \int_o^w \frac{1}{N_A(x)} \int_x^w \frac{N_A(\xi)}{D_n(\xi)}\, d\xi dx. \tag{2-7}$$

This double integral can be evaluated numerically for any arbitrary dependence of $N_A$ and $D_n$ on the distance. The diffusion coefficient is computed using the resistivity versus impurity concentration given by Irvin [11] for silicon. In applying these approximate relations to obtain the diffusion coefficient two assumptions are necessary. First, all the shallow impurity centers are assumed to be ionized at room temperature. Second, it is assumed that the mobility of electrons is the same in both n- and p-type silicon if the ionized impurity densities are equal.

At electric fields over $10^3$ V/cm, the current becomes non-ohmic and a further reduction of mobility occurs.[12] Since the fields encountered in the base region of a transistor are the order of $2x10^3/w$, where w is the base width in microns, this effect can be significant in very narrow base transistors. Calculation of the effect in the presence of both drift and diffusion components of electric current is extremely complex,[13] but qualitatively a further increase in transit time would be expected to result from this effect at very large electric fields. In the solar cell case, which was of primary interest in the present study, this effect will not be significant and so it was not considered explicitly in the calculations.

An exponential distribution results in a constant field throughout the base region and the shortest transit time for a given ratio of impurity densities at the edges of the base region in the case where the width of the base region is fixed. If this transit time is computed in the usual manner (constant mobility), the curves 1 and 2 of Fig. 1 result. The lower concentration limit in general will be $10^{14}$ or $10^{15}$ $cm^{-3}$ because the edge of the junction transition region will have moved to about that point. It follows then that the upper concentration limit will be in a region where the mobility is reduced.

The remaining curves of Fig. 1 show transit times calculated from Eq. (2-7) with the assumption of a variable mobility. It is apparent that there is indeed an optimum field and that it is produced by only two or three orders of magnitude change in doping level.

Although the exponential distribution is most desirable, it is normally not obtained in practice. Impurity gradients are usually obtained by diffusing into a region which already has a certain background impurity concentration. In the transistor case, the impurity is often that of the collector and is therefore the opposite type to the base. If this impurity has a diffusion coefficient which is significantly lower than that of the impurity forming the drift field, the background impurity can be assumed to be constant. If the diffusion profile is exponential, the final net impurity distribution is non-exponential and is given by

$$N = N_0 \exp \frac{x \ln (N_1/N_0)}{w} + N_C, \qquad (2-8)$$

where $N_0$ is the concentration of diffusant at the emitter junction, $N_1$ is the concentration at the collector junction,

and $N_C$ the background concentration of the starting material (and is negative). Because the field is enhanced near the collector junction, transit times somewhat shorter than those obtained for a constant field with the same $N_0$ and $N_1$ are obtained in this case as can be seen in Table I. Two points should be noted in this connection. First, a true exponential with the end points $N_0$ and $N_1-N_C$ would give the minimum value of transit time for these end points. Examples of this are also given in Table I. Second, as was mentioned earlier, the minimum value of impurity concentration on the base side of the base collector junction is controlled by space charge considerations at the junction and cannot drop below $10^{14}$ $cm^{-3}$ for reasonable geometries.

If the impurities in both regions are the same type (not likely in transistors, but applicable to the solar cell case to be considered next), Eq. (2-8) can be used with $N_C$ positive. Examples of this case are also given in Table I. It can be seen that for the cases shown, the effect of the background impurity is almost negligible. As $N_1$ approaches $N_C$, the effect increases somewhat.

The distribution of diffused impurities turns out more often to be a complementary error function (erfc) than an exponential. In Fig. 2, transit times for several cases of interest for both exponential and erfc distributions in the absence of a background impurity are compared. That the exponential distribution always yields the shorter transit time may be qualitatively understood by referring to Figs. 3 and 4. From Fig. 3, it can be seen that the erfc concentration is greater at each point in the base region. Further, where the concentration is greatest, it is most slowly varying. Hence the aiding field is lowest as is shown in Fig. 4. When the concentration is sufficiently large, the mobility is significantly reduced over a large portion of the base and the transit time increases sharply.

In the presence of a background impurity with a low diffusion coefficient, the distribution is given by:

$$N_A = N_0 \text{ erfc } \left(\frac{x}{w}\right) \cdot R + N_C \qquad (2\text{-}9)$$

where erfc $R = \frac{N_1}{N_0}$. Examples of transit times for $N_C$ both positive and negative are also given in Table I. As before, the effects of a background concentration are not large.

## III. COLLECTION EFFICIENCY IN A SOLAR CELL

In a solar cell the conditions are somewhat more complex than those considered in the previous section. If the base region of an n-on-p cell is considered, the electron current is again given by Eq. (2-3) where the junction is in the y-z plane. It is necessary to include both generation and recombination in the present case. In the steady state, for the p-type base region, the continuity equation becomes

$$\frac{1}{q}\frac{dJ}{dx} - \frac{n}{\tau} + G = 0, \tag{3-1}$$

where it is assumed that the electron density n resulting from the illumination is much greater than the equilibrium minority carrier concentration. The generation term is given by

$$G(x) = \int_0^{\lambda_g} \alpha(\lambda)\ \phi(\lambda)\ e^{-\alpha(\lambda)x}\ d\lambda, \tag{3-2}$$

where $\alpha(\lambda)$ is the absorption coefficient at a wavelength $\lambda$, $\phi(\lambda)$ is the absorbed photon density at a wavelength $\lambda$, and $\lambda_g$ is the wavelength corresponding to the band gap of the solar cell material. Kleinman[6] has developed a very powerful method for obtaining collection efficiency from Eq. (3-1) for the case of constant coefficients E, D, and $\tau$. This method involves the use of photodensity functions which are related to G(x). In applying these functions numerical integration techniques are required. Kleinman[6] gives the numerical values which are necessary for the case of silicon solar cells in outer space which will be considered here.

In the present analysis, the cell is divided into 4 regions as shown in Fig. 5. In the field-free regions of the p-type base, Kleinman's solutions[6] are employed using the boundary conditions $n = 0$ at $x = x_j$ (junction) and $n = 0$ at $x = x_t$ (ohmic contact on back of cell). The first of these conditions refers to the short circuit case but the results can be easily extended to arbitrary currents.[6]

These conditions leave an undetermined constant for each region. In region III, Kleinman's solutions[6] can be employed only in the case of constant coefficients. When the coefficients are not constant, approximate methods must be employed. In both cases, however, values for both n and J are matched at the boundaries $x_1$ and $x_2$ resulting in a set of simultaneous equations. This system can be readily solved using a high-speed digital computer. The electron current at the junction is then computed from

$$J_n(x_j) = q\, D_n \left.\frac{dn}{dx}\right|_{x = x_j} . \tag{3-3}$$

In many cases of interest, $x_1 = x_j$, and there is no field-free region next to the junction. In such cases, n and J are matched at the boundary $x_2$, and one obtains a set of simultaneous equations which may be readily solved as before. Even when the field is not zero at $x = x_j$, Eq. (3-3) may still be used to compute the current at the junction since $n(x_j) = 0$.

A. Necessary Parameters

When variations of the electric field and diffusion coefficient are included, the continuity equation in the steady state may be written

$$\frac{d^2n}{dx^2} + \frac{dn}{dx}\left[\frac{1}{N_A}\left(\frac{dN_A}{dx}\right) + \frac{1}{D_n}\left(\frac{dD_n}{dx}\right)\right] + n\left[\frac{1}{N_A}\left(\frac{d^2N_A}{dx^2}\right) - \frac{1}{N_A^2}\left(\frac{dN_A}{dx}\right)^2 + \frac{1}{N_A}\left(\frac{dN_A}{dx}\right)\frac{1}{D_n}\left(\frac{dD_n}{dx}\right) - \frac{1}{D_n\tau_n}\right] + \frac{G}{D_n} = 0. \tag{3-4}$$

Since the derivative of $D_n$ is required, the function based on Irvin's approximation[11] for the conductivity which was used in Section II will no longer be adequate since its derivative is not continuous. Therefore, a curve was fitted to experimental values of mobility vs impurity concentration using smooth and spline subroutines developed for another application.[14] From these subroutines, a third-order expression relating $D_n$ to log $N_A$ is obtained from which the value and derivative of the diffusion coefficient may be easily computed at any point. As in the previous section, it is assumed that donor and acceptor impurities scatter electrons

equally efficiently so that the electron mobility in n-type silicon can be used as a basis for the calculation. However, the assumption that all impurities are ionized is no longer necessary. The mobility curve used in the calculations is shown in Fig. 6 together with the experimental data[15-21] from which it was derived.

The minority carrier lifetime in silicon is a slowly varying function of the impurity concentration. To obtain an estimate of the effect of this variation a simple relationship was assumed:

$$\log \tau = 1 - \frac{2}{5} \log N_A, \qquad (3\text{-}5)$$

for $10^{15}$ cm$^{-3} \leq N_A \leq 10^{20}$ cm$^{-3}$. A plot of Eq. (3-5) is shown in Fig. 7 together with measured values of the lifetime reported by Ross and Madigan.[22] Since the relationship is intended only to be qualitative, the agreement is not unreasonable, particularly at the lower concentrations.

The generation of electron hole pairs is a function of the spectral composition of the source, the absorption of silicon, position within the solar cell, and the characteristics of the surface of the cell. In applying Eq. (3-2) to the case of silicon solar cells, it is assumed that the source is the sun outside the earth's atmosphere, that absorption of radiation is the same in n- and p-type silicon and is independent of impurity density for the spectral region of interest, that any reflection which occurs at the surface does not alter the spectral composition of the radiation, and that the quantum efficiency is constant over the region of interest. With these assumptions, the numerical values given by Kleinman[6] are appropriate. Over most of the cell, the ten-point Gaussian quadrature between 0.42 and 1.08 microns described by Kleinman[6] is adequate. However, near the front surface where both the junction and the drift fields are located it is necessary to include the contributions from wavelengths as short as 0.22 microns. The correction may be included by the use of the trapezoid

rule for numerical integration and Kleinman[6] gives the necessary numerical quantities. The resulting generation function is plotted in Fig. 8 as cumulative percentage of photons absorbed at a distance equal to or less than the abscissa. It can be seen that nearly 18% of the photons are absorbed in the thin n-layer at the front surface if the junction is 0.3 microns deep. Nearly two thirds of the remaining photons are absorbed in the first 10 microns of the cell; over three fourths, in the first 25 microns. In the second 25 microns, (25-50μ), only about 7% of the photons are absorbed and in the second 50 microns (50-100μ) only about 5%. It is thus quite clear that variations designed to be improved in the collection efficiency from the p-type base region must occur in the first 25 microns of the cell in order to have a significant effect.

B. Constant Coefficient Calculations

Kleinman[6] has given the general solution to Eq. (3-4) when E, D and $\tau$ are constants. His result is

expressed in terms of the reduced variables $y = nL/\Phi\tau$ and $\zeta = x/L$ where $L^2 = D\tau$ and $\Phi$ is the total photon flux density absorbed in the cell. For the case of a p-type base region with a field E, the solution is

$$y = A_1 e^{\sigma\zeta} + A_2 e^{-\rho\zeta} + F(\zeta, L, \mathcal{E}) \qquad (3\text{-}6)$$

where

$$\sigma = \sqrt{\mathcal{E}^2 + 1} - \mathcal{E}$$

$$\rho = \sqrt{\mathcal{E}^2 + 1} + \mathcal{E}$$

$$\mathcal{E} = -E\mu L/2D = -qEL/2DkT,$$

$$E = \frac{kT}{q} \frac{d \ln N_A}{dx},$$

$$F(\zeta, L, \mathcal{E}) = \int_0^{\lambda_g} \nu(\lambda) \frac{\beta(\lambda)}{1 + \rho\beta(\lambda)} \frac{e^{-\beta\zeta} - e^{-\rho\zeta}}{1 - \sigma\beta(\lambda)} d\lambda,$$

$$\beta(\lambda) = \alpha(\lambda) L,$$

$$\nu(\lambda) = \phi(\lambda)/\Phi .$$

In this case, the impurity distribution must be exponential

in order that the field E be constant. Therefore, in Region III,

$$E = \frac{kT}{q} \frac{1}{w} \ln \frac{N_2}{N_1}, \tag{3-7}$$

where $N_2$ and $N_1$ are the acceptor concentrations at $x_2$ and $x_1$ respectively and $w = x_2 - x_1$ (see Fig. 5). Since $N_2 > N_1$, the field E is positive. (It should be noted that Kleinman[6] writes the solution of Eq. (3-4) for the case of $E \neq 0$ explicitly only for n-type material. Formally the results are the same, but in this case $\sigma$ and $\rho$ are interchanged and $\xi$ does not contain a minus sign.) If E = 0, (as in Regions II and IV) the solution simplifies to

$$y = B_1 e^{\zeta} + B_2 e^{-\zeta} + F(\zeta, L), \tag{3-8}$$

where

$$F(\zeta, L) = \int_0^{\lambda g} \nu(\lambda) \frac{\beta(\lambda)}{1-\beta^2(\lambda)} (e^{-\beta\zeta} - e^{-\zeta}) \, d\lambda$$

since, in this case, $\rho = \sigma = 1$. The solution is obtained

simply by applying the boundary conditions discussed above in order to obtain a set of simultaneous equations for the constants.

The results of these calculations are similar to those of Wolf[7] and indicate that optimum collection occurs when the field-free region next to the junction vanishes. Consequently, only this case was considered in setting up the solution to the more general case.

## C. Exponential Distribution with Variable Diffusion Coefficient and Lifetime

When the coefficients of Eq. (3-4) are not constant, it is not possible to obtain an analytic solution. In this case it is necessary to replace the differential equation by a difference equation in the region with varying impurity density. Using central differences and N + 1 pivotal points, linear algebraic equations are obtained in the form

$$A_{n-1,n}n_{n-1} + A_{n,n}n_n + A_{n+1,n}n_{n+1} = B_n \qquad (3\text{-}9)$$

for each of the points $x_n$ in this region. The interval between the pivotal points $x_n$ is $h = \frac{w}{N}$. The interior N-2 of these equations have exactly the same form and may be written down directly. If the point $x_0$ is taken at the junction, $n_0 = 0$, and the first of the set of equations is

$$A_{1,1}n_1 + A_{2,1}n_2 = B_1 \tag{3-10}$$

At $x = x_N$, two additional equations are formed from the continuity of n and J across the boundary. The two additional unknowns are $n_N$ and the undetermined constant in the analytic solution for the electron in the field-free region (IV). (Once again, the condition $n = 0$ at $x = x_t$ is used to determine one of the constants in the solution.) Solution of the equation therefore is reduced to the solution of N + 1 simultaneous equations for N + 1 unknowns. This solution is carried out on a high-speed digital computer using a subroutine which employs the Gauss-Jordan reduction for solving the set. Once the values for n are found at the N pivotal points, a forward

difference approximation for $\frac{dn}{dx}$ is used to evaluate the electron current at the junction:

$$J(0) = qD \left.\frac{dn}{dx}\right|_{x = x_j} \approx qD \left[\frac{n_1}{h} - \frac{1}{2h}(n_2 - 2n_1) + \frac{1}{3h}(n_3 - 3n_2 + 3n_1) + \frac{1}{4h}(n_4 - 4n_3 + 6n_2 - 4n_1) + \ldots\right]. \quad (3\text{-}11)$$

Although values of N as high as 45 have been employed, sufficient accuracy is usually obtained with considerably smaller values.

Results of these calculations for several cases of practical interest are shown in Fig. 9 plotted as short circuit electron current density vs field width. In all these cases the acceptor concentration at the junction was taken as $10^{15}$ $cm^{-3}$. Various values for the lifetime and substrate concentration were assumed as noted. In addition the value of short circuit current computed with no drift field is also shown in Fig. 9 for acceptor concentrations of $10^{14}$ and $10^{16}$ $cm^{-3}$ and various values of lifetime. All numerical values of current are based on

a total photon flux density[6] of $3.3 \times 10^{17}$ $cm^{-2}$ $sec^{-1}$ so that the maximum electron current would be about $40ma/cm^2$ if all electrons which are generated in the 330 micron thick base region were collected.

It can be seen immediately from these results that there is an optimum field width which turns out to be roughly twice the diffusion length for the shorter lifetimes. The magnitude of the field width is in all cases as significant and in some cases much more important than the magnitude of the aiding drift field once a certain minimum field has been reached. The field generated by three-order change in impurity concentration across the width w is sufficient to optimize the collection efficiency if the proper field width is employed.

While this result has been obtained by mathematical analysis, it seems instructive to take the results of Section II and qualitatively deduce a similar conclusion.

Let it be assumed that all carriers that are generated closer to the junction than the diffusion length, L, will be collected, while any carriers formed further away than L will recombine before reaching the junction. If a field is now superimposed between $x_1$ and $x_2$ (see Fig. 5), no improvement in collection efficiency will be observed for $x_1 > L + x_j$ since all of those carriers originating beyond L will still recombine before arriving at the junction. If $x_1$ and $x_2$ are both less than L, then some improvement will be observed, but even if the transit time across the distance $x_1$ and $x_2$ were zero and if $x_1 = x_j$ and $x_2 = L + x_j$, the maximum amount of carriers collected would be those generated between 0 and 2L from the junction.

From Fig. 1 it can be seen that a drift field can reduce the transit time by a factor of about 2.5 in the case where $N_1 = 10^{15}$ cm$^{-3}$. Therefore, in this case, if $x_1$ is at the junction, then $x_2$ can be moved out for a distance of 2.5 L and provide enough velocity enhancement

to collect everything generated within 2.5 L of the junction. If the same spacing of 2.5 L is maintained and both $x_1$ and $x_2$ are moved a small distance $\Delta L$, any carriers originating between 2.5 L and 2.5 L + $\Delta L$ would have to travel in excess of 2.5 L to reach the junction, and with a portion of that distance without benefit of the built-in electric field. Since we have already said that the greatest distance any carrier could go even with the field is 2.5 L, it follows that repositioning the field to start between 0 and 2.5 L will only reduce the number of carriers collected. Thus, the maximum effectiveness of the field occurs when it starts at the junction and ends (for the specific case being considered) 2.5 L away. This result agrees well with that deduced originally despite the drastic simplifying assumptions made.

As was indicated in subsection III-B, a field width of about 25 microns results in optimum collection efficiencies at longer lifetimes ($L > 25\mu$) because of the form of the generation term in Eq. (3-1).

## D. Complementary Error Function Impurity Distribution With Variable Diffusion Coefficient and Lifetime

In fabricating drift field solar cells, the most convenient method is to begin with a p-type substrate with acceptor concentration $N_2$, epitaxially deposit a thin p-type layer with acceptor concentration $N_1 \ll N_2$ on one side, diffuse the impurity across the concentration step thus formed in order to make the drift field and then to form the p-n junction by diffusing a donor a shallow distance in from the front surface. In diffusing across a concentration step with the same impurity on both sides the resulting distribution is not exponential. Rather, it is given by the relation:[23]

$$N(y,t) = \frac{N_2-N_1}{2} \operatorname{erfc}(y \cdot R) + N_1, \qquad (3\text{-}12)$$

where R is $1/2\sqrt{Dt}$, D is the diffusion coefficient of the impurity being used at the diffusion temperature, and t is the time of diffusion. The origin of the y

coordinate is taken at the step and y is positive in the direction of the smaller concentration. Therefore, referring to Fig. 5, $y = x_2 - x$. In solving Eq. (3-4) for this case, R was first defined by the condition that the acceptor concentration at the junction is given by $N_0$ (greater than $N_1$ but much less than $N_2$):

$$\text{erfc } (x_2 - x_j) \cdot R = \frac{2(N_0 - N_1)}{N_2 - N_1} . \tag{3-13}$$

Then a width w is defined as the distance between the junction $x_j$ and the point where $N = a N_2$, a being nearly unity:

$$\text{erfc } (w + x_j - x_2) \cdot R = \frac{2N_2(1-a)}{N_2 - N_1} . \tag{3-14}$$

The solution proceeds in the same manner as in the preceding subsection but now it is necessary to compute the value of the field at each point and to include the terms involving $\frac{dE}{dx}$. For several reasons, the approximation is

not as accurate in this case as it is in the case of constant field. However, values of current accurate to several per cent can be obtained in most cases.

The results of these calculations show that there is only a slight reduction in going from the ideal, exponential case to the real, erfc case. That this is not unexpected can be seen from Figs. 10 and 11. Figure 10 shows that the impurity concentrations in the two cases are not markedly different from each other in the epitaxial layer. Further, although the field varies considerably in the erfc case as shown in Fig. 11, it is no longer weakest in the region where the concentration differences are most detremental as it was in the transistor case of Section II.

## IV. USE OF DRIFT FIELDS TO ENHANCE RADIATION TOLERANCE

If one assumes that irradiation by electrons degrades the lifetime of the solar cell material without affecting

any other parameter, then the lifetime $\tau$ may be related to the integrated electron flux density $\Theta$ by the following relation:[7]

$$\frac{1}{\tau} = \frac{1}{\tau_0} + K\Theta \qquad (4\text{-}1)$$

where $\tau_0$ is the initial lifetime in the material. Wolf[7] gives a value $K = 3.2 \times 10^{-9}$ cm$^2$/sec for 1 Mev electrons. Using this value and $\tau_0 = 10^{-5}$ sec, J(0) can be plotted against $\Theta$ as is done in Fig. 12. From this figure it follows that the field width must be chosen so as to obtain the desired operating condition at the design value of integrated flux density. For example, if the maximum current is desired at integrated flux density of $3 \times 10^{16}$ electrons per cm$^2$ a field width of about 12 microns would be best. If it is desired to maximize total integrated power output during irradiation, the shape of the curves suggests that maximization of the current at the design value of $\Theta$ will accomplish this in most cases, if a linear irradiation

rate is assumed, except in those regions very near to the cross-over of the applicable curves.

This analysis has been concerned with collection efficiency and short circuit current. There is evidence that the open circuit voltage is also degraded under electron irradiation.[24] The reasons for this degradation and its effect on available power output from the cell are not known at this time.

Only the current from the p-type base region of the solar cell has been considered. Since nearly 18 per cent of the photons are absorbed in the 0.3 micron thick n-type diffused region at the front surface of the cell, the hole current from this region makes an appreciable contribution to the total current. Computed curves of hole current vs integrated flux density are given in Fig. 13 for two limiting cases of the surface recombination velocity.

## V. Conclusions

From the analysis above it is possible to calculate the expected short circuit current for various values of drift field strength, drift field width, and electron lifetime. From these calculations it is possible to conclude that when the variations of mobility and material lifetime are considered the inclusion of a drift field will increase the collection efficiency of a silicon n-on-p solar cell under certain specified conditions. In order to maximize the increase it is necessary that:

1. The drift field should be as near to the junction as possible.
2. The width of the drift field should be approximately twice the value of electron diffusion length at the design value of lifetime (or integrated flux density) or

about 25 microns whichever is the shorter.

The following points also should be noted. First, increasing the ratio of impurity concentration at the edges of the drift field region above 1000 does not significantly improve the collection efficiency for most of the cases considered. This is in contrast to the conclusion reached from a consideration of the constant mobility approximation in which the highest ratios yield the greatest collection efficiencies. Second, the case of an erfc distribution resulting from diffusion across an impurity step at the interface of an epitaxial layer and substrate can be approximated quite accurately in the cases of interest by an exponential distribution across a width equal to the thickness of the epitaxial layer.

In the case of the transistor base, it can be concluded that an opimium field configuration exists which results in a minimum base transit time for injected minority carriers in the case where the base width is assumed to be fixed and the field is generated by a

gradient of the majority impurity density in the base region. The impurity densities required to generate fields higher than the optimum are sufficiently large that the carrier mobility is significantly reduced over a region of the base and the drift contribution to the current actually becomes smaller with increasing field. It should be emphasized that the highest frequency response of a transistor will not necessarily result from the use of the optimum field configuration for two reasons. First, the assumption of a fixed base width is not necessarily the appropriate one in the design of high frequency devices. Second, effects other than the base transit time may be more significant in determining frequency response.

## VI. ACKNOWLEDGMENTS

The authors would like to thank Mr. Ronald Wachwitz for the use of his spline and smoothing subroutines, Mr. B. M. Thompson for the use of his simultaneous equation subroutine, and the Technical Computing Center staff for their invaluable assistance in running the various parts of the programs.

## REFERENCES

* This work was supported by the National Aeronautics and Space Administration, Goddard Space Flight Center, Greenbelt, Maryland under contract No. NAS 5-3559.

1. H. Kroemer, "Der Drifttransistor," Naturwiss, 40, 578-579 (1953), see also Transistors I (RCA Laboratories, Princeton, N. J., 1956), p 202.

2. J. L. Moll and I. M. Ross, "The Dependence of Transistor Parameters on the Distribution of Base Layer Resistivity," Proc. IRE 44, 72-78 (1956).

3. M. B. Das and A. R. Boothroyd, "Impurity-Density Distribution in the Base Region of Drift Transistors," IRE Trans. on Electron Devices ED-8, 475-481 (1961).

4. A. G. Jordan and A. G. Milnes, "Photoeffect on Diffused p-n Junctions with Integral Field Gradients," IRE Trans. on Electron Devices ED-7, 242-251 (1960).

5. B. Dale and F. P. Smith, "Spectral Response of Solar Cells," J. Appl. Phys. 32, 1377-1381 (1961).

6. D. A. Kleinman, "Considerations on the Solar Cell," Bell System Tech. J. 40, 85-115 (1961).

7. M. Wolf, "Drift Fields in Photovoltaic Solar Energy Converter Cells," Proc. IEEE 51, 674-693 (1963).

8. L. J. Varnerin, "Stored Charge Method of Transistor Base Transit Analysis," Proc. IRE 47, 523-527 (1959).

9. J. A. R. Beale, "The Calculation of Transit Times in Junction Transistors When the Mobilities are not Constant," Proc. IRE 48, 1341 (1960); L. J. Varnerin, Proc. IRE 48, 1341-1342 (1960).

10. See any elementary differential equation textbook: e.g., L. M. Kells, Elementary Differential Equations (McGraw-Hill Book Co., Inc., New York, 1947) p. 52.

11. J. C. Irvin, "Resistivity of Bulk Silicon and of Diffused Layers in Silicon," Bell System Tech. J. 41, 387-410 (1962).

12. E. A. Davies and D. S. Gosling, "Non-ohmic Behaviour in Silicon," J. Phys. Chem. Solids 23, 413-416 (1962).

13. R. Stratton, personal communication.

14. S. B. Watelski, W. R. Runyan and R. C. Wackwitz, "A Concentration Gradient Profiling Method," to be published.

15. K. B. Wolfstirn, "Hole and Electron Mobilities in Doped Silicon from Radiochemical and Conductivity Measurements," J. Phys. Chem. Solids 16, 279-284 (1960).

16. P. W. Chapman, O. N. Tufte, J. D. Zook and D. Long, "Electrical Properties of Heavily Doped Silicon," J. Appl. Phys. 34, 3291-3295 (1963).

17. F. J. Morin and J. P. Maita, "Electrical Properties of Silicon Containing Arsenic and Boron," Phys. Rev. 96, 28-35 (1955).

18. P. P. Debye and T. Kohane, "Hall Mobility of Electrons and Holes in Silicon," Phys. Rev. 94, 724-725 (1954).

19. D. C. Cronemeyer, "Hall and Drift Mobility in High Resistivity Single Crystal Silicon," Phys. Rev. 105, 522-523 (1957).

20. E. M. Conwell, "Properties of Silicon and Germanium II," Proc. IRE 46, 1281-1300 (1958).

21. G. W. Ludwig and R. L. Watters, "Drift and Conductivity Mobility in Silicon," Phys. Rev. 101, 1699-1701 (1956).

22. B. Ross and J. R. Madigan, "Thermal Generation of Recombination Centers in Silicon," Phys. Rev. 108, 1428-1433 (1957).

23. W. Jost, "Diffusion in Solids, Liquids and Gases," (Academic Press, Inc., N. Y. 1962).

24. W. Luft, "Effects of Electron Irradiation on n-on-p Silicon Solar Cells," IEEE Trans. Aerospace 2, 747-758 (1964).

Table I. Effect of background impurity on transit time in a p-type silicon transistor base.

| $N_1 (cm^{-3})$ | $N_0 (cm^{-3})$ | $N_C (cm^{-3})$ | Distribution | t(nanosec) |
|---|---|---|---|---|
| $10^{17}$ | $10^{15}$ | 0 | exp | 38.1 |
| $10^{17}$ | $10^{15}$ | $10^{14}$ | exp | 38.5 |
| $10^{17}$ | $10^{15}$ | $-10^{14}$ | exp | 37.7 |
| $10^{17}$ | $9 \times 10^{14}$ | 0 | exp | 37.3 |
| $10^{18}$ | $10^{15}$ | 0 | exp | 37.3 |
| $10^{18}$ | $10^{15}$ | $10^{14}$ | exp | 37.5 |
| $10^{18}$ | $10^{15}$ | $-10^{14}$ | exp | 37.1 |
| $10^{18}$ | $9 \times 10^{14}$ | 0 | exp | 36.6 |
| $10^{17}$ | $10^{15}$ | 0 | erfc | 42.9 |
| $10^{17}$ | $10^{15}$ | $10^{14}$ | erfc | 43.2 |
| $10^{17}$ | $10^{15}$ | $-10^{14}$ | erfc | 42.5 |
| $10^{18}$ | $10^{15}$ | 0 | erfc | 53.8 |
| $10^{18}$ | $10^{15}$ | $10^{14}$ | erfc | 54.0 |
| $10^{18}$ | $10^{15}$ | $-10^{14}$ | erfc | 53.7 |

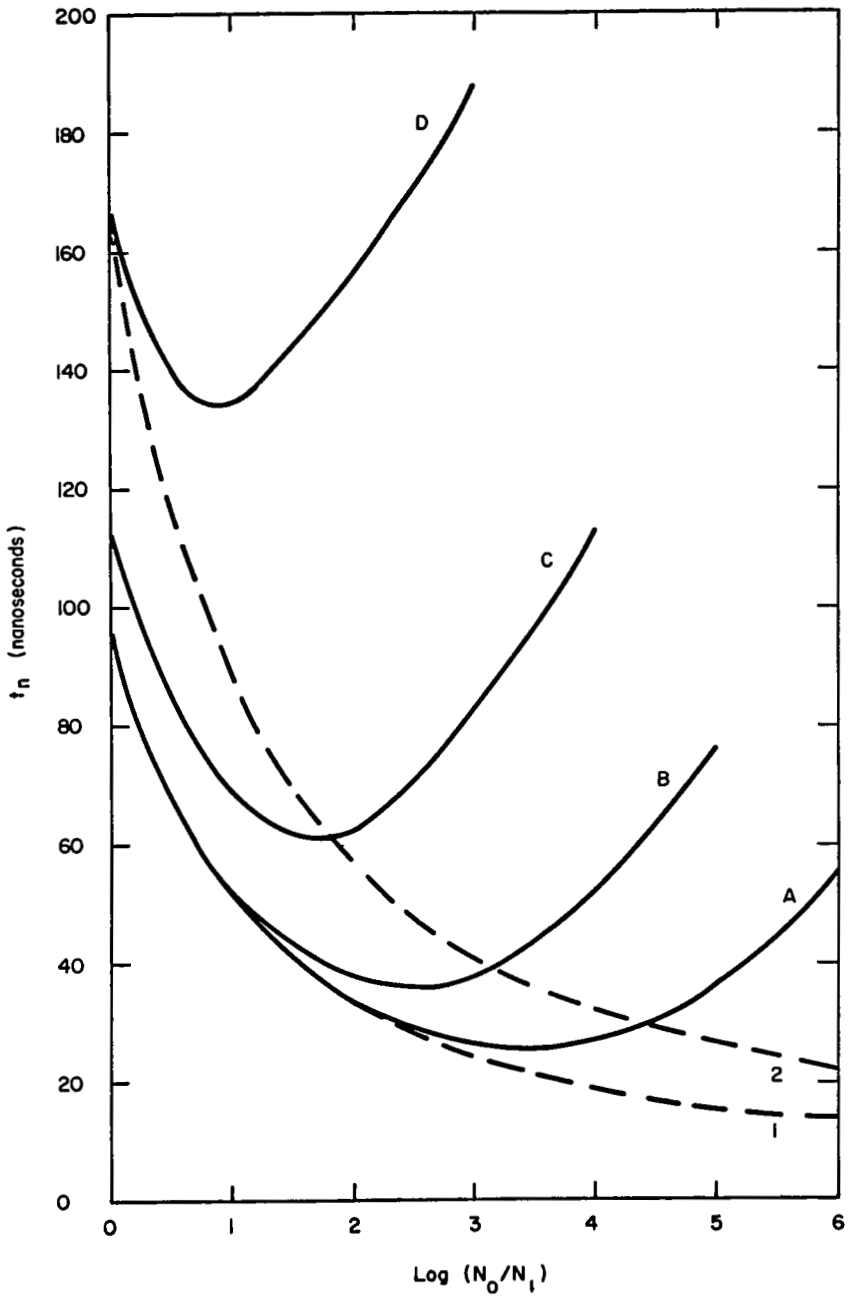


Figure 1. Computed transit time of electrons in a p-type silicon base region 25 microns wide assuming no recombination at 300°K. The impurity concentration varies exponentially as given in Eq. (2-8) with $N_C$=0. Solid Curves: electron mobility determined from impurity contration at each point (A, $N_1$ - $10^{14}$ $cm^{-3}$, B, $N_1$ - $10^{15}$ $cm^{-3}$, c, $N_1$ = $10^{16}$ $cm^{-3}$, D, $N_1$ - $10^{17}$ $cm^{-3}$). Dashed curves: electron mobility assumed to be independent of impurity concentration (1, $\mu_n$ = 1250 $cm^2$ $volt^{-1}$ $sec^{-1}$, 2, $\mu_n$ = 740 $cm^2$ $volt^{-1}$ $sec^{-1}$.)

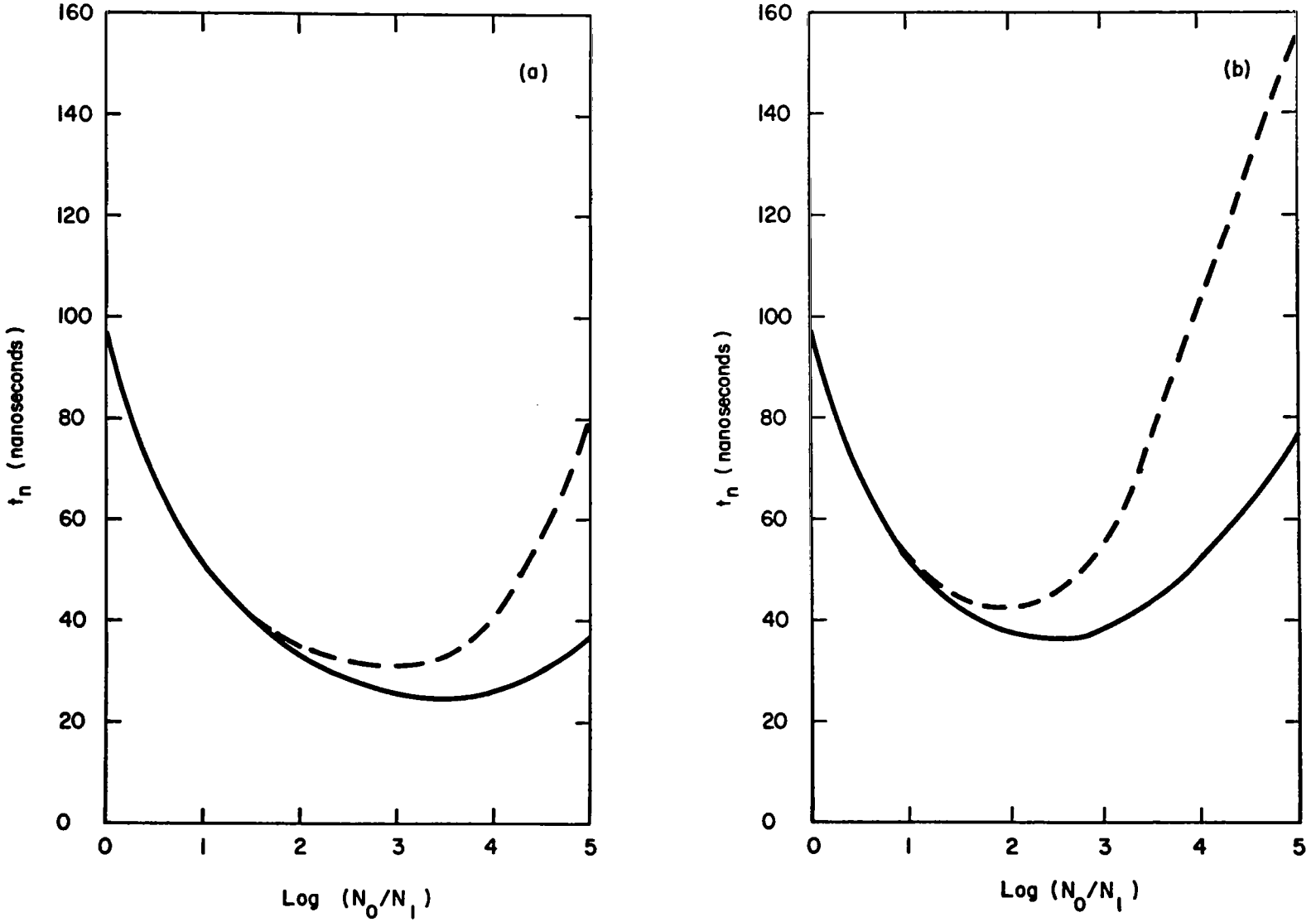


Figure 2. Computed transit time of electrons in a p-type silicon base region 25 microns wide assuming no recombination at 300°K. Comparison of exponential and complementary error function distribution. (a) $N_1 = 10^{14}$ cm$^{-3}$, (b) $N_1 - 10^{15}$ cm$^{-3}$.

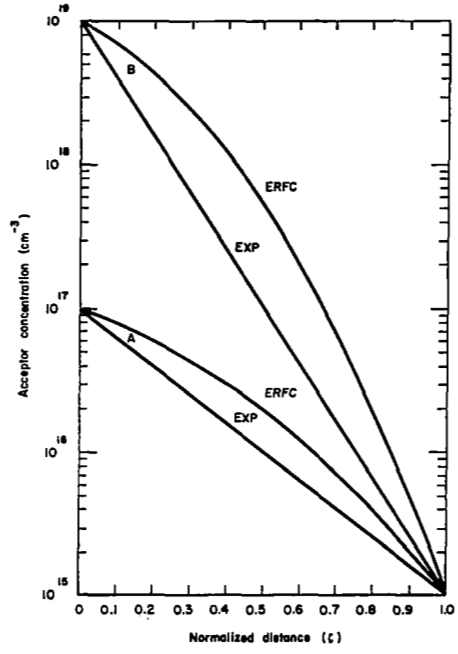


Figure 3. Impurity concentration in a base region for exponential and complementary error function distributions having the same end points. The distance is normalized to the base width. The background impurity is assumed to be very small.

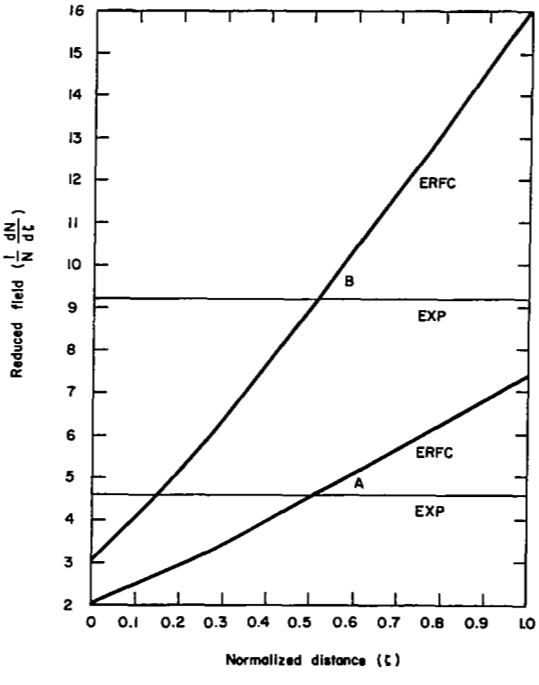


Figure 4. Electric field (in dimensionless units) for the distributions of Figure 3.

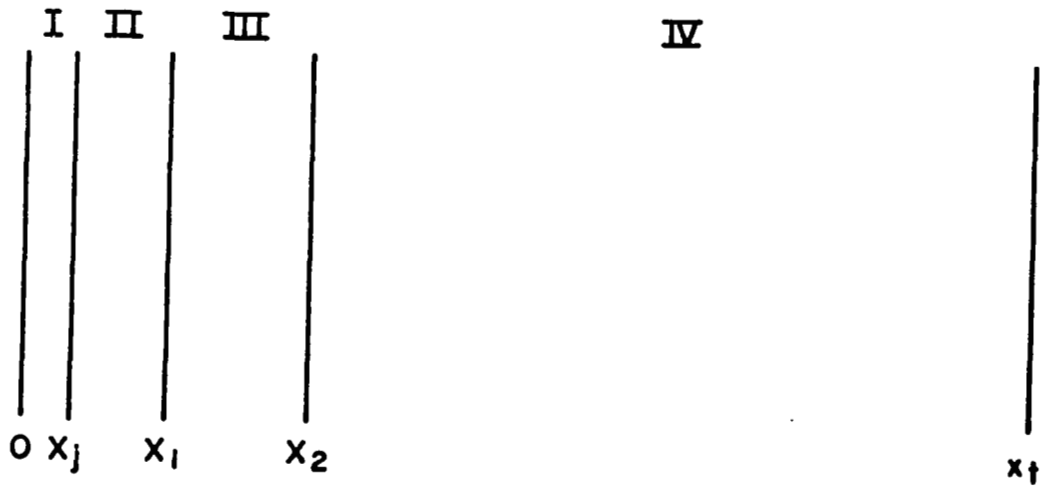


Figure 5. Schematic view of solar cell configuration. Front surface at x = 0. Region I ($0 \leq x < x_j$) n-type diffused region. Region II ($x_j \leq x < x_1$) p-type epitaxial region, no drift field, $N_A = N_1$. Region III, ($x_1 \leq x \leq x_2$) p-type diffused region, $N_1 < N_A < N_2$. Region IV ($x_2 < x \leq x_t$) p-type substrate, no drift field, $N_A = N_2$. In the usual configuration $x_j$ - 0.3 microns and $x_t$ = 330 microns. In many cases of interest, $x_1 = x_j$ and region II vanishes.

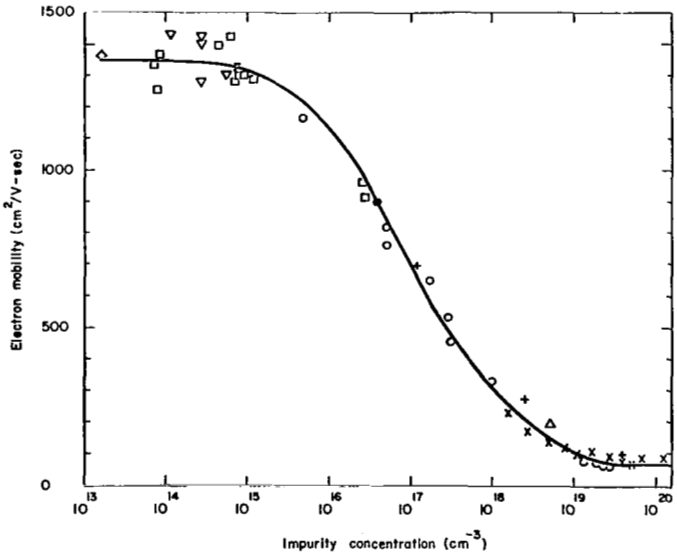


Figure 6. Electron mobility as a function of impurity concentration. It is assumed that the impurities may be either donors or acceptors. The solid line is computed from smoothed values of mobility. Data points represent experimental results for electrons in n-type silicon [based on conductivity mobility: o Wolfstirn (Ref. 12); based on Hall mobility: x Chapman, et al (Ref. 13), + Morin and Maita (Ref. 14), Δ Debye and Kohane (Ref. 15) and p-type silicon based on drift mobility: □ Cronemeyer (Ref. 16), ◇ Conwell (Ref. 17), ▽ Ludwig and Watters (Ref. 18)].

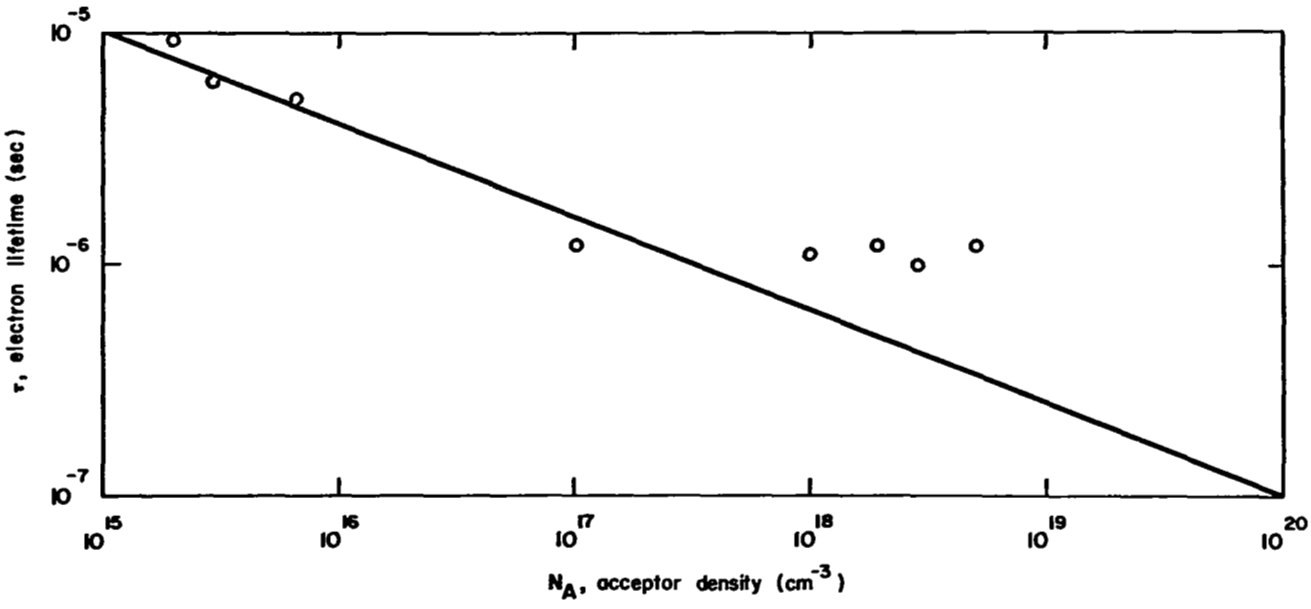


Figure 7. Electron lifetime in p-type silicon. The solid line is computed for Eq. (3-5). The points are taken from the data of Ross and Madigan (Ref. 19).

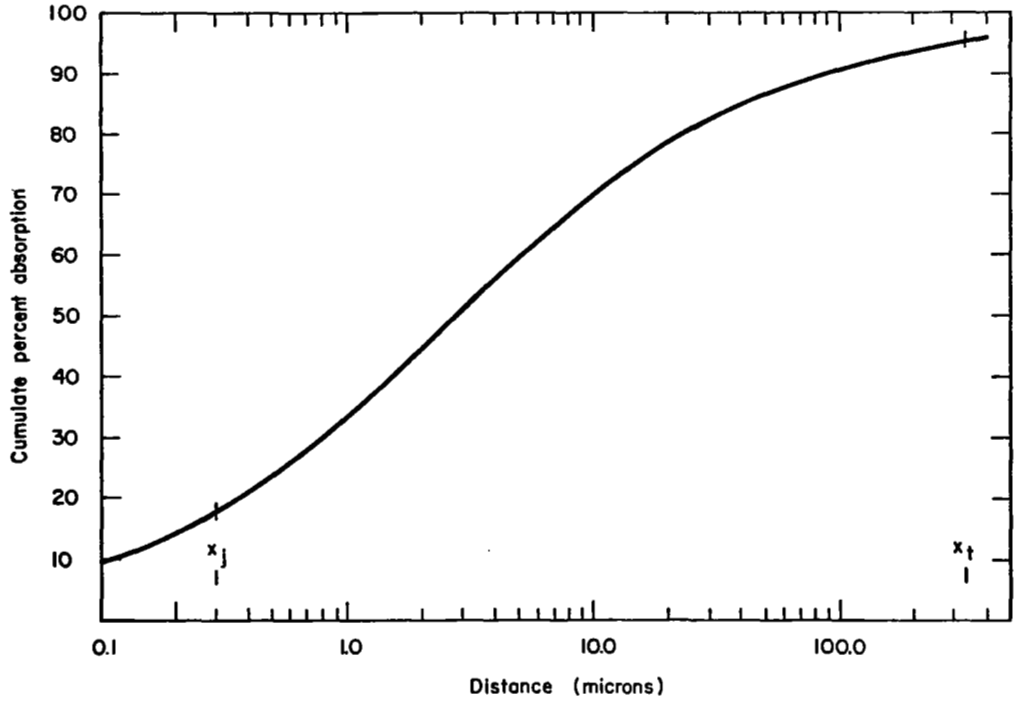


Figure 8. Cumulative per cent absorption in silicon computed from Eq. (3-2) using the method and numerical values of Kleinman (Ref. 6). The values $x_j$ and $x_t$ represent customary values of junction depth and cell thickness respectively.

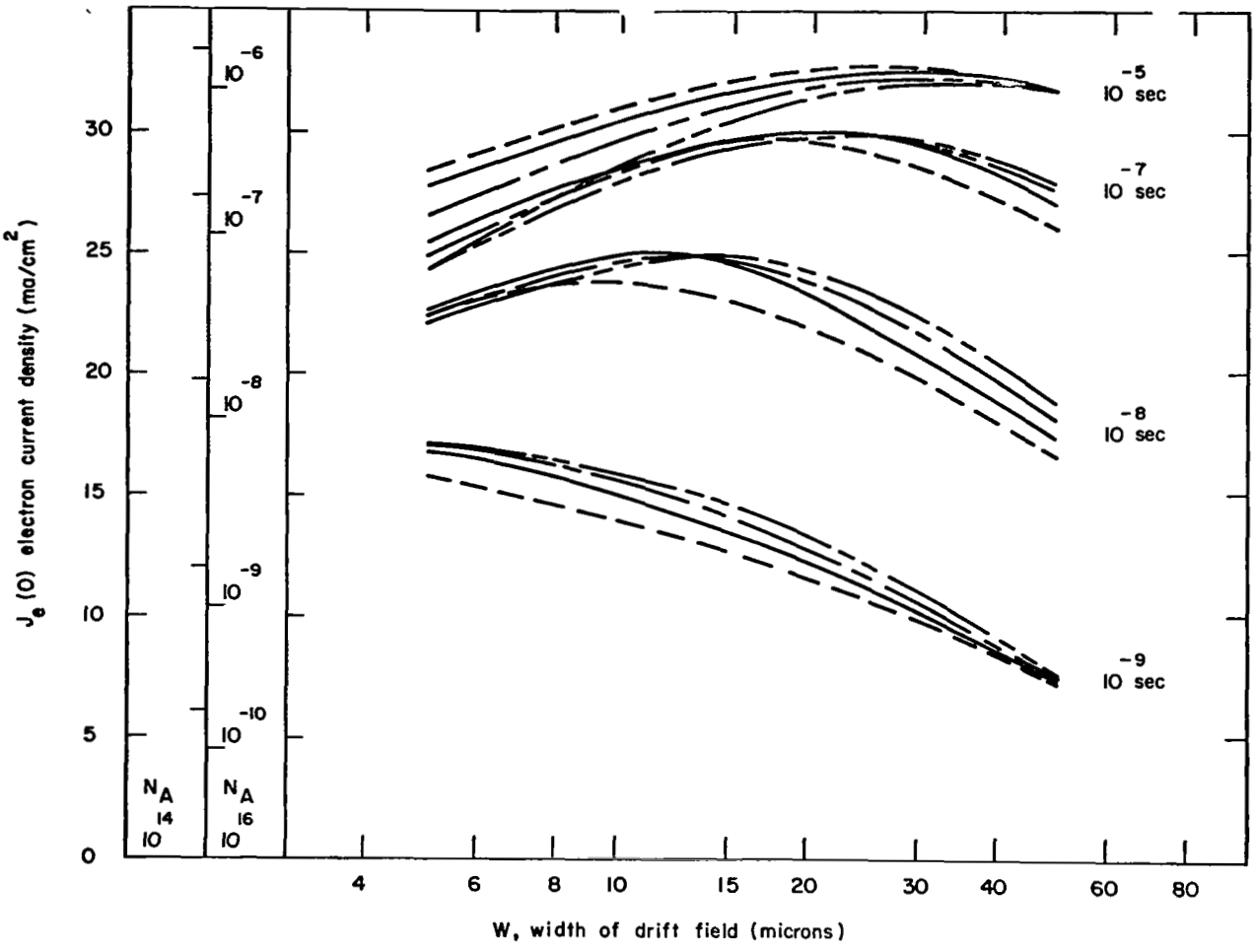


Figure 9. Electron current density computed from Eq. (3-4) assuming an exponential distribution of impurities in the drift field region, electron mobility as given in Figure 6 and various values of lifetime. The value of computed from Eq. (3-5) is used at those points where it is smaller than the value specified. In all cases the drift field extends to the junction and the acceptor concentration in Region IV is $10^{17}$ cm$^{-3}$ (----), $10^{18}$ cm$^{-3}$ (———), $10^{19}$ cm$^{-3}$ (——— – ———), and $10^{20}$ cm$^{-3}$ (——— – – ———). Values of electron current density for cells with $N_A = 10^{14}$ cm$^{-3}$ and $10^{16}$ cm$^{-3}$ are given at the left side for various lifetimes in the case where there is no drift field.

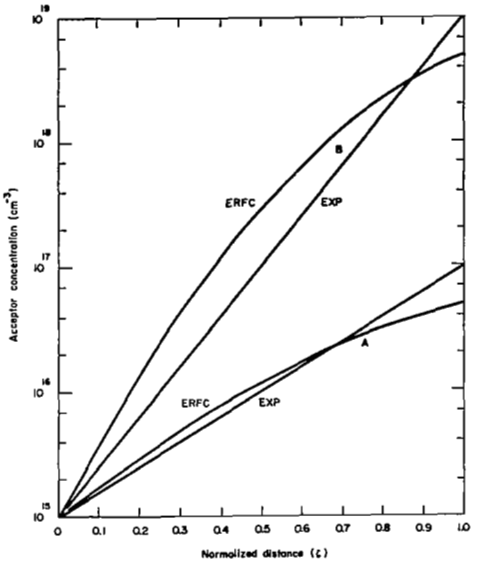


Figure 10. Impurity concentration in the expitaxial layer of a solar cell. The distance is normalized to the thickness of the layer. The junction is at $\zeta = 0$. The distribution (erfc) obtained by diffusion across a step at $\zeta = 1$ into an epitaxial layer with initial impurity concentration $10^{14}$ cm$^{-1}$ is compared with an exponential distribution (exp).

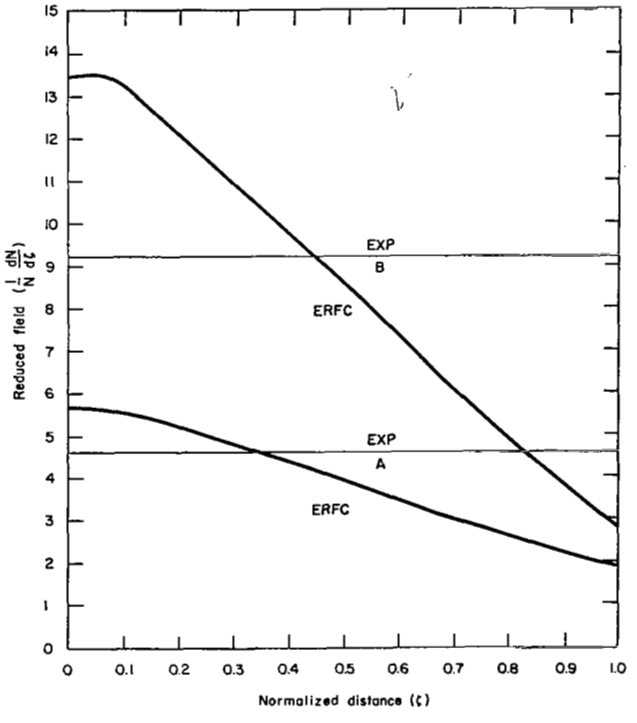


Figure 11. Electric fields (in dimensionless units) for the distributions of Figure 10.

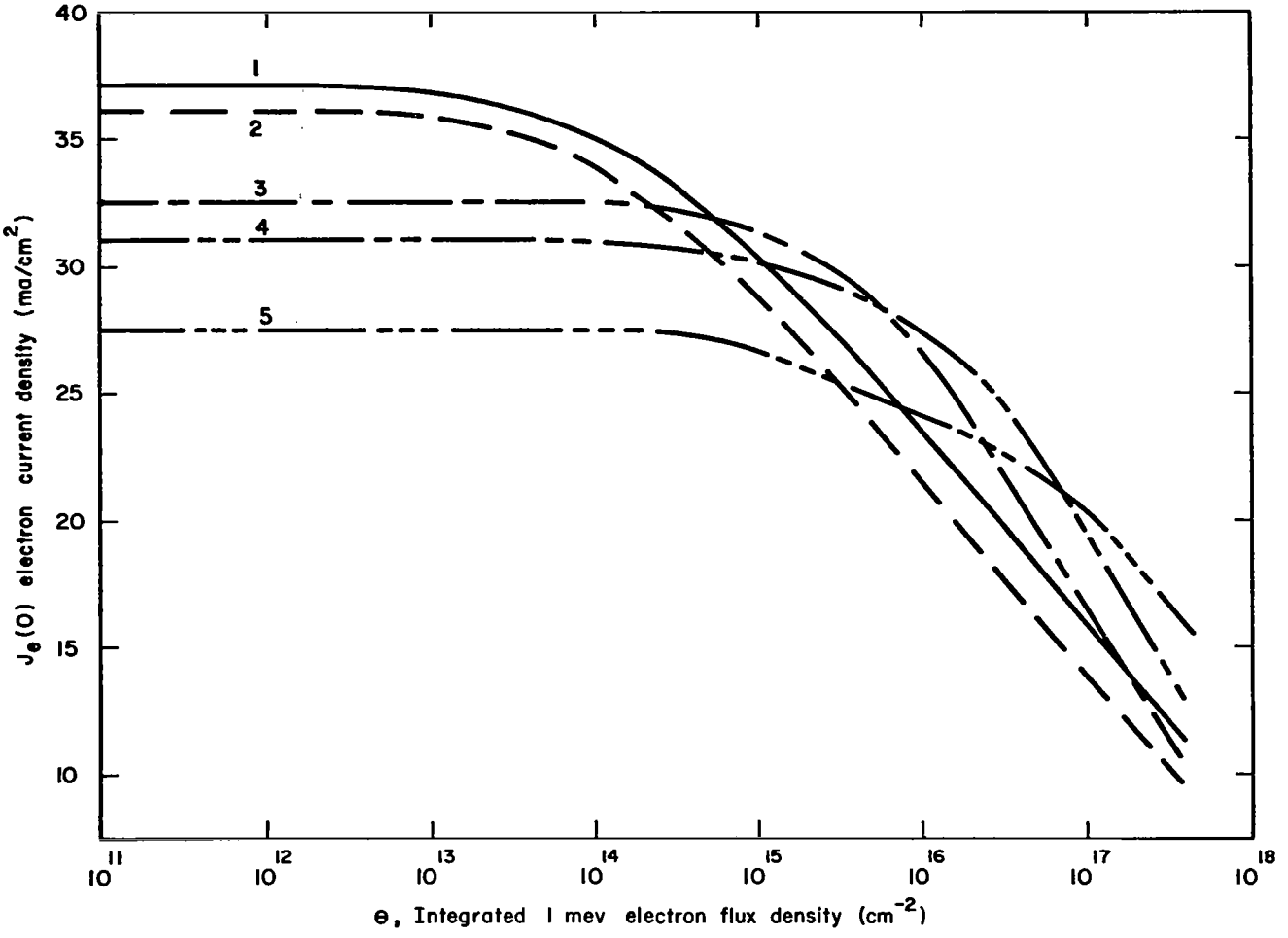


Figure 12. Effect of irradiation by 1 Mev electrons on the short circuit electron current of an n-on-p silicon solar cell. Curve 1: no drift field, $N_A = 10^{16}$ cm$^{-3}$. Curve 2: no drift field, $N_A = 10^{16}$ cm$^{-3}$. Curve 3: 25 micron drift field. Curve 4: 12 micron drift field. Curve 5: 5 micron drift field. In curves 3-5 the drift field is a result of an exponential distribution of acceptors varying from $10^{15}$ cm$^{-3}$ at the junction to $10^{18}$ cm$^{-3}$ in the substrate.

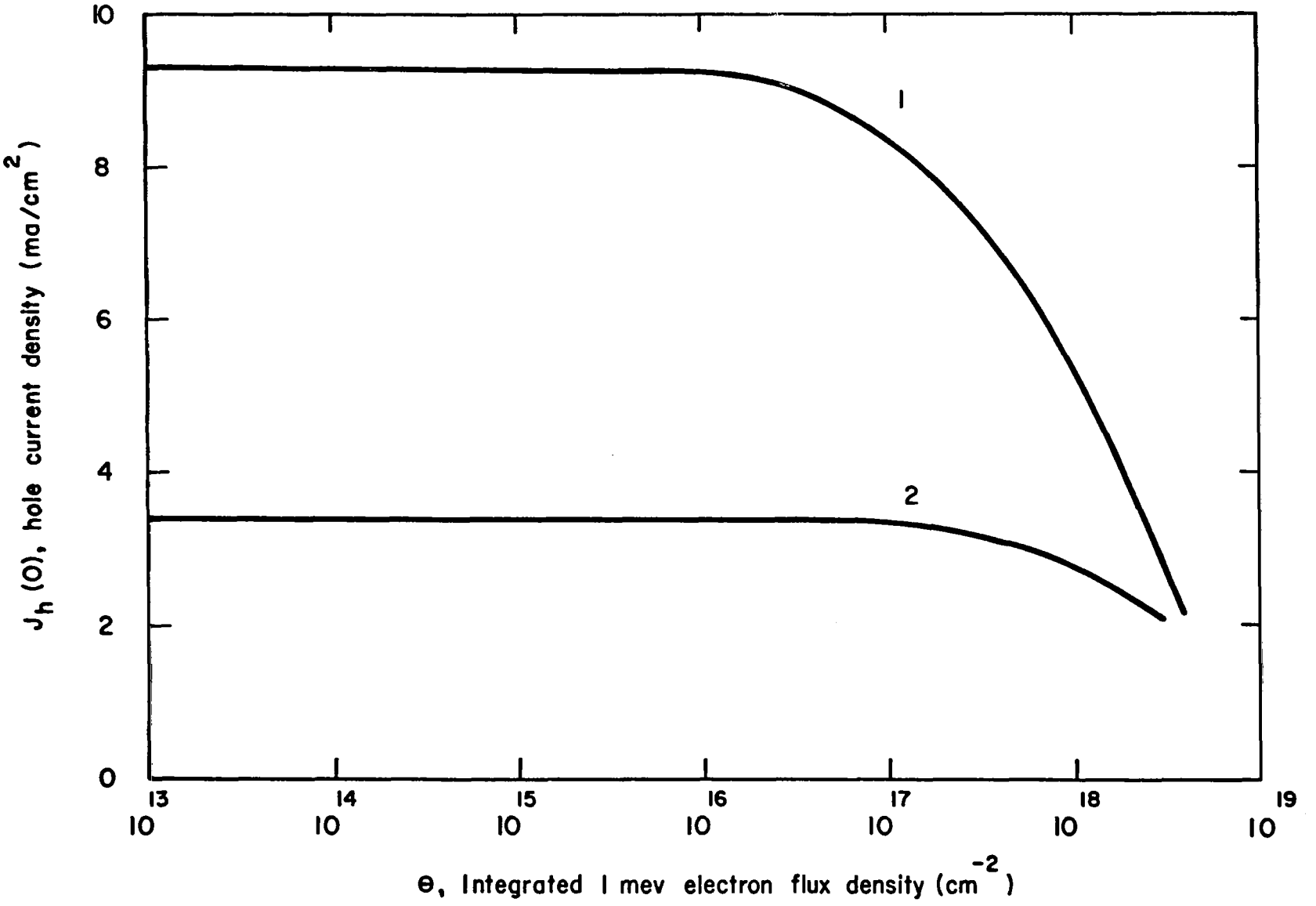


Figure 13. Effect of irradiation by 1 Mev electrons on the short circuit current of an n-on-p silicon solar cell with a diffusion depth of 0.3 microns. Curve 1: zero surface recombination velocity. Curve 2: infinite surface recombination velocity.